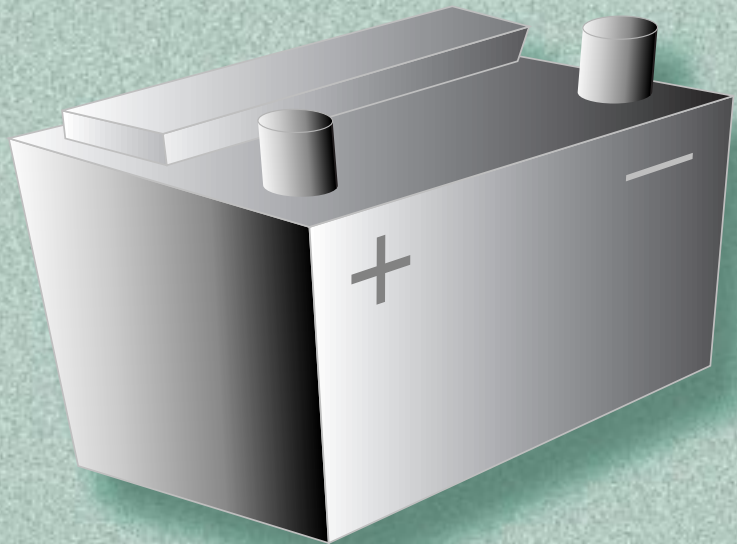


# ADVANCED TECHNOLOGY DEVELOPMENT (HIGH-POWER BATTERY)

2001  
ANNUAL  
PROGRESS  
REPORT



U.S. Department of Energy  
Energy Efficiency and Renewable Energy  
Office of Transportation Technologies

## A C K N O W L E D G E M E N T

We would like to express our sincere appreciation to Sentech, Inc., for its technical contributions in preparing and publishing this report.

In addition, we would like to thank all our program participants for their contributions to the programs and all the authors who prepared the project abstracts that comprise this report.

**U.S. Department of Energy  
Office of Advanced Automotive Technologies  
1000 Independence Avenue, S.W.  
Washington, D.C. 20585-0121**

**FY 2001**

**Progress Report for the Advanced Technology  
Development Program**

**Energy Efficiency and Renewable Energy  
Office of Transportation Technologies  
Office of Advanced Automotive Technologies  
Energy Management Team**

**Raymond A. Sutula      Energy Management Team Leader**

**February 2001**

## TABLE OF CONTENTS

<b>1. INTRODUCTION.....</b>	<b>1</b>
<b>2. ATD PROGRAM OVERVIEW AND FY 2001 HIGHLIGHTS ....</b>	<b>3</b>
<b>3. CELL DEVELOPMENT .....</b>	<b>9</b>
<b>4. DIAGNOSTICS .....</b>	<b>45</b>
<b>5. ELECTROCHEMISTRY IMPROVEMENT .....</b>	<b>65</b>
<b>6. LOW-COST CELL PACKAGING.....</b>	<b>75</b>
<b>7. ADVANCED PROCESS RESEARCH.....</b>	<b>83</b>

# 1. INTRODUCTION

## Advanced Technology Development Program

On behalf of the Department of Energy's Office of Advanced Automotive Technologies (OAAT), I am pleased to introduce the Fiscal Year (FY) 2001 Accomplishments Report for the Advanced Technology Development (ATD) Program. OAAT funds high-risk research and development to provide enabling technologies for fuel efficient and environmentally-friendly light duty vehicles. The ATD Program focuses on high-power battery development in support of a government-industry partnership striving to develop a mid-sized passenger vehicle capable of achieving enhanced fuel economy while adhering to future emissions standards, and maintaining such attributes as affordability, performance, safety, and comfort.

Note that, since its inception, Advanced Battery Activities have supported the government/industry Partnership for a New Generation of Vehicles (PNGV) through its technology research projects. The partnership's goals are being re-evaluated to identify changes that will maximize the potential national petroleum-savings benefit of the emerging advanced technologies. When these goal changes have been defined, OTT will adjust the focus of its technology research programs accordingly.

Initiated in late 1998, the ATD program focuses on finding solutions to barriers that are impeding U.S. battery manufacturers in their efforts to produce and market high-power batteries for use in hybrid electric vehicles (HEV). HEVs - which combine the heat engine and fuel tank of a conventional vehicle with the battery and electric motor of an electric vehicle - offer an attractive alternative to conventional vehicles because they can deliver the extended range and rapid refueling that consumers expect from a conventional vehicle while achieving increased fuel economy and reduced greenhouse gases and criteria pollutants. By providing strong technical direction, management and financial support, OAAT is a leader in supporting the development of high-power battery technology for hybrid electric vehicle applications.

High-power battery technology is a key element to the ultimate success of hybrid electric vehicles. The primary challenges facing the commercialization of high-power battery technology include insufficient calendar life, poor response to abuse scenarios, and high production cost. Over the past two years, the ATD program has continued to focus on these objectives, and has been slightly re-organized in response to reviewer comments and suggestions. The main areas of work are: Gen 2 Cell Development and Evaluation; Diagnostic Evaluations; Electrochemistry Improvement; Low-Cost Packaging, and Advanced Process Research. The program requires that five national laboratories (ANL, BNL, LBNL, INEEL, and SNL) work in close coordination to achieve the objectives of the program. Additional information on the purpose, focus, organization and direction of the ATD program can be found in *Section 1. Background/Overview*.

This report highlights the activities and progress achieved during FY 2001 by the ATD Program. The report is comprised of ten technical project summaries submitted by five national laboratories and two universities and provides an overview of the exciting work being conducted to tackle the technical challenges associated with high power batteries. We are encouraged by the technical progress realized under this dynamic program in FY 2001, and look forward to continued success in FY 2002.

Raymond A. Sutula  
ATD Program Manager  
Office of Advanced Automotive Technologies  
Office of Transportation Technologies  
Department of Energy



## 2. ATD PROGRAM OVERVIEW AND FY 2001 HIGHLIGHTS

### a. Advanced Technology Development (ATD) Program: Purpose, Focus, Organization and Direction

*Vincent Battaglia*

*Argonne National Laboratory, Argonne IL 60439-4837*

*(202) 488-2461; fax (202) 488-2413; e-mail: [batman@anl.gov](mailto:batman@anl.gov)*

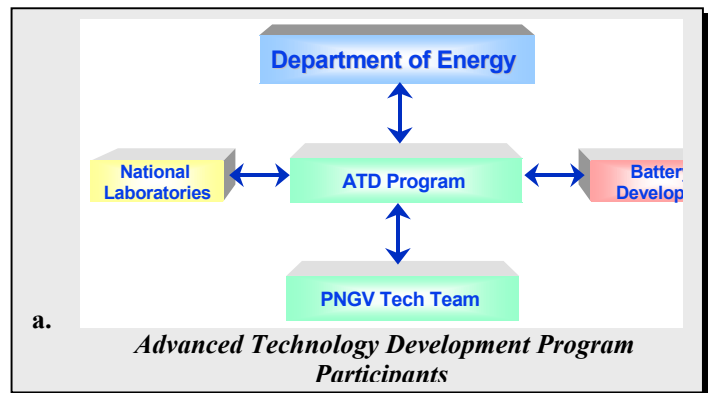
The ATD Program was established to help solve the key technical barriers limiting the development of high-power lithium-ion battery technology for hybrid electric vehicles (HEVs). The program was initiated in late 1998 through the PNGV to focus on solutions to barriers that are impeding US battery manufacturers in their efforts to produce and market high-power lithium-ion HEV batteries. Among other programs, the ATD Program supports the recently announced FreedomCAR Program and has contributed to the success of the PNGV. Although falling short of cost and total miles per gallon targets, this government-industry partnership has made considerable progress towards developing a mid-sized passenger vehicle capable of surpassing current emissions and vehicle mileage standards while maintaining performance, safety, and comfort.

The objectives of the ATD Program are to:

- Determine the root cause of power and capacity fade as a function of calendar time;
- Determine the chemical mechanisms associated with thermal abuse intolerance;
- Narrow the field and refine the diagnostic tools that provide the greatest insight into cell degradation with time and safety-related mechanisms;
- Pursue low-cost alternatives in cell packaging and battery materials' processing; and,
- Facilitate cooperation between battery developers and the laboratories in order to efficiently utilize resources and accelerate the pace to commercialization.

#### ATD Program Organization

The ATD Program was created to assist in the development of an affordable, high-power battery having a fifteen-year life. The program is managed by the Energy Management Team of the Office of Advanced Automotive Technologies (OAAT). Technical guidance to the program has been provided through semi-quarterly meetings with the PNGV Electrochemical Energy Storage Technical Team. Five national laboratories work in a collaborative manner to carry out the research and report their results through monthly reports and quarterly reviews. The PNGV industrial battery contractors attend the review meetings and provide feedback to the labs.



#### Addressing Three Major Technical Barriers

The ATD Program is focused on three major technical barriers confronting high-power battery technology, as follows:

### **Calendar Life**

At present, a 15-year calendar life is required to meet the California emissions standards. Calendar life of lithium-based batteries is estimated to be approximately 6-10 years (although there are encouraging estimates approaching 12 years). Mechanisms resulting in poor calendar life are further exasperated as the temperature of the system increases. This requires additional effort in advanced thermal management and the development of more robust chemistries. To address issues associated with the calendar life of high-power batteries, the ATD Program is:

Developing and validating accelerated life test methods.  
Identifying life-limiting mechanisms.  
Identifying advanced cell components that address these life-limiting mechanisms and extend cell life.

### **Abuse Tolerance**

High power batteries are not intrinsically tolerant of abuse such as short circuits, overcharge, over-discharge, mechanical shock, vibration, crush, or fire exposure. Chemical additives that circumvent smoke and/or fire generation are being designed and evaluated to operate in conjunction with mechanical safeguards. In addition, challenging thermal management requirements faced during stressful periods in a driving cycle need to be addressed. The general approach to safety issues includes:

Specify relevant abuse conditions and desired responses to those conditions, along with standards for abuse testing.

Test, evaluate, and redesign cell and chemistry (developer proprietary information) to ensure abuse tolerance.

Develop detection and management controls for battery state-of-charge, battery temperatures, and electrical faults. Controls at the cell level will include devices for relief of internal pressure buildup and for internal circuit interruption.

Develop *in situ* overcharge protection.

The ATD Program is assisting in this overall effort by investigating the thermal failure modes through comprehensive cell testing and diagnostic efforts. It is anticipated that the detailed thermal runaway mechanisms will be understood and addressed with more optimal materials. This information will be shared with the developers and used to develop cells that are more inherently safe.

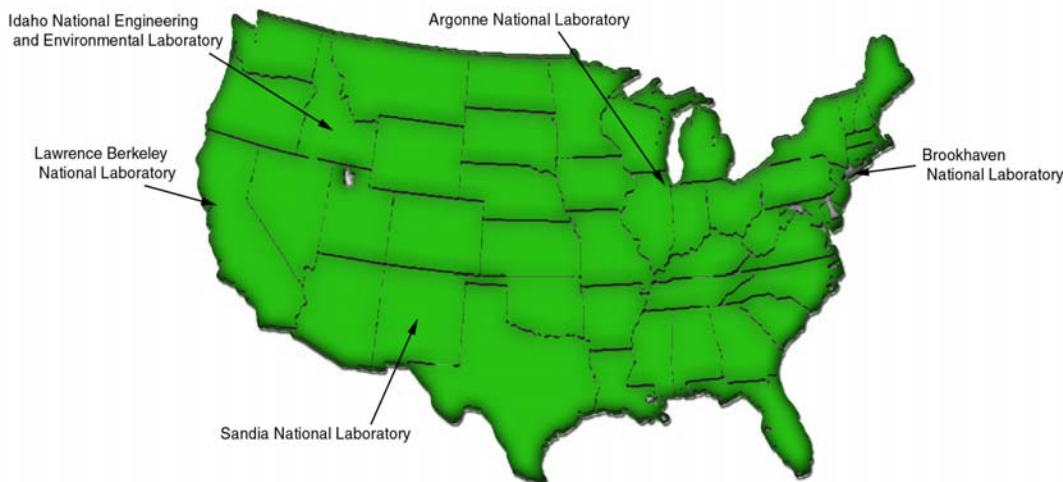
### **Cost**

The current cost of high-power lithium-based cells is prohibitively high on a kW or kWh basis. Multiple strings of cells pose a problem for lithium-based technologies, because they require overcharge and over-discharge protection at the cell level. The main cost drivers being addressed are the high cost of raw materials and materials processing, cell and module packaging cost, and low-cost, failsafe electric and mechanical safety devices. The ATD program is addressing cell cost issues through the following activities:

Evaluating lower cost cell components: electrolytes, anodes, and cathodes.  
Developing low-cost processing methods for producing advanced cell materials.  
Working with potential US suppliers to implement low-cost material production.  
Developing low-cost cell packaging alternatives.

## **ATD Program Participants**

The ATD program requires the close coordination of research and diagnostic efforts of five national laboratories: Argonne National Laboratory, Brookhaven National Laboratory, Idaho National Engineering and Environmental Laboratory, Lawrence Berkeley National Laboratory, and Sandia National Laboratory (BNL, INEEL, LBNL, and SNL). Close communication is maintained with battery developers, car manufacturers, and related corporations (including, among others, Adv. Membrane Systems, Compact Power, Delphi Automotive, Moltech, Quallion, Ford, DaimlerChrysler, and General Motors) to ensure that the issues being investigated within the program will be of direct benefit to the U.S. battery manufacturing community. To make an impact on the cost barriers, the ATD Program has established over a dozen relationships with present and potential battery component vendors. In addition, the ATD Program maintains close ties with other governmental organizations involved in advanced battery research through the Interagency Power Working Group. This ensures that relevant technical issues being addressed and timely solutions being developed are disseminated amongst the other government agencies.



## **Advanced Technology Development Program Participants**

### **Accomplishments in FY 2001**

The major accomplishments for the Advanced Technology Development Program in FY 2001 are presented below, organized by program area:

#### **Gen 1 and 2 Cell Development and Evaluation**

Onset of thermal runaway in Gen 1 cells occurs below 80°C for cells at 100% SOC and initiates at the anode. Impedance rise & power fade occur rapidly early in life and impedance controlled by the positive electrode.

Gen 1 power fade and resistance rise data from the calendar-life studies follow  $t^{1/2}$  kinetics.

Gen 2 cells show comparable impedance at the positive & negative electrodes.

Gen 2 cells showed thermally activated heat output with an average activation energy of 13.2 cal/mole.

Between 55°C and 65°C the magnitude of the heat decay rate increases abruptly.

The relative ASI increase of Gen 2 cells at 55°C is less than that for Gen 1 at 35°C. Baseline Gen 1 cells at 25°C exhibited a fade of 8.63% after 20 weeks of testing and thus will last beyond 300,000 cycles before their scaled-power drops below the goal of 25 kW. The baseline cells at 45°C are fading faster and are projected to complete just above 200,000 cycles before dropping below the PNGV power goal.

### **Gen 1 and 2 Cells: Diagnostic Evaluations**

Soft x-ray XAS detected the presence of LiF (from decomposition of LiPF<sub>6</sub> from the electrolyte) on the surface of cycled Gen 1 and Gen 2 cathodes.

Aged Gen 1 surfaces contain increased concentrations of Ni<sub>2</sub>O<sub>3</sub> or NiO<sub>2</sub>, which are decomposition products of the original LiNi<sub>0.8</sub>Co<sub>0.2</sub>O<sub>2</sub>.

XAS has clearly identified insoluble decomposition products from the electrolyte on the Gen 2 cathode.

These are possible causes of power fade at elevated temperatures.

Evidence that carbon disappears from the cathode surfaces of aged and cycled Gen 2 lithium-ion cells.

The surface composition of particles of cathode active materials taken from tested Gen 2 cells differs from the particle bulk composition, which is uniform

Gas emissions for several species were measured in Gen 2 cells as a function of power fade.

### **Electrochemistry Improvement**

Evaluated eight graphite based materials and found the most promising materials for high power are the Mitsui GDR grade carbon-coated graphite, the Superior Graphite round-edge natural graphite, and the Hitachi boron-doped MAG graphite.

Found that the particle morphology of the Mitsui GDR anode material did not change during the electrode pressing process nor exfoliate in PC electrolyte, both of which are common to most graphite materials.

Developed a new low-cost titanium-doped lithium nickel oxide cathode material (and LiNi<sub>0.95</sub>Ti<sub>0.05</sub>O<sub>2</sub>) and found that it has excellent capacity, power, and calendar life.

Demonstrated that the Tosoh lithium manganese oxide spinel cathode material has good power and safety characteristics, as well as enhanced calendar life, when used with the new Merck LiFAP salt-based electrolytes.

Identified and evaluated new electrolyte systems and electrolyte additives that enhance the safety and performance of lithium ion cells.

## **Low Cost Packaging**

Received and evaluated five different laminate rolls. Determined from these rolls that the polyolefin class of polymers provides good moisture and electrolyte barrier properties.

- Determined that adhesive compatibility with electrolyte is critical.
- Evaluations are underway of four more modified laminate rolls from Rollprint.
- Initiated investigations of organoclay composites with an on-site expert who has novel approach of creating organoclay precursor.

Screened and performed permeation tests on candidate polymer films with the assistance of Mocon Controls, Inc.

Conducted preliminary evaluations of permeation rates and extrapolated to 15 years for the 10 Ah flexible packaging design.

## **Advanced Process Research**

Established collaborations with FMC, OMG, and Fuji to study industrial-scale processes that can be used to manufacture multi-doped lithium nickel oxide positive electrode materials. FMC produced pilot-scale samples and performed manufacturing cost studies on a solid-state process, while OMG and Fuji produced pilot-scale quantities of material using two different solution-based processes.

Established a collaboration with Superior Graphite to develop and characterize a rounded-edge low-cost natural graphite. This material has a reversible capacity density >300 mAh/g, possesses safety characteristics similar to the expensive MCMB synthetic graphite, can be used in 30% PC-based electrolytes (w/o exfoliating), and is projected to cost <\$10/kg.

Established a collaboration with Quallion, LLC, to produce pilot-scale quantities of an advanced PC-based 3-solvent electrolyte system (1.2M LiPF<sub>6</sub>/EC:PC:EMC [3:3:4]). Merck and Ube have both agreed to make larger quantities of this electrolyte, with and without additives.

Used a spreadsheet battery design model to conduct material cost comparisons for the Gen 1, Gen 2, and advanced cell chemistries.

## **Future Directions**

The ATD program will continue to focus on overcoming the main barriers to the successful development and commercialization of high-power lithium-ion batteries. The following modifications to the program are being implemented in FY 2002 to enhance its effectiveness:

An advanced manganese cathode chemistry will be studied in response to reports of much improved stability and enhanced power capabilities.

Diagnostics will be focused on understanding both capacity and power fade associated with the cathode and anode/electrolyte interfaces.

The abuse tolerance efforts are being shifted from characterization toward chemical identification of specific thermal events.

The low-cost cell packaging effort will continue to investigate pouch technology and will more aggressively investigate cost savings techniques with established packaging companies.

## 3. Cell Development

### b. Calorimetric Study of Thermal Performance and Abuse Tolerance in Li Ion Cell Constituents and Cell Hardware

*Pete Roth, Chris Crafts, Rudy Jungst, Dan Doughty*

*Mail Stop 0613, Sandia National Laboratory, Albuquerque, NM 87185*

*Contact: E. P. Roth phone: 505-844-3949 fax: 505-844-6972; e-mail: [eproth@sandia.gov](mailto:eproth@sandia.gov)*

---

#### Objectives

- Identify mechanisms and chemical constituents leading to reduced thermal tolerance, reduced thermal stability, or reduced operational lifetime in Li Ion cells.
- Identify chemical mechanisms resulting in gas generation that lead to cell venting.
- Determine the effects of aging on cell thermal stability.
- Develop a knowledge base of cell thermal properties leading to improved cell designs.
- Determine and document the operational modes that lead to unsafe behavior or thermal runaway in Gen 2 Li-Ion cell hardware.

#### Approach

- Test full size cells by the method of Accelerating Rate Calorimetry (ARC) to determine cell properties leading to cell thermal runaway.
- Measure gas generation in full cells as a function of temperature and cell properties such as state of charge and aging/cycling history.
- Test full size cells under low to moderate temperature by Isothermal Microcalorimetry to measure long-term thermal reaction rates.
- Measure the thermal inter-reactivity of fresh cell solvents, conductive salts, and fresh/aged cell electrodes recovered from disassembled test cells by using Differential Scanning Calorimetry (DSC).
- Prepare larger quantities of Gen 2 electrode materials in various states of charge by cycling large pellets in special full and half-cell fixtures.
- Measure gas-generating reactions and evolved gas species in ARC bomb capsules of electrode materials in electrolyte.
- Determine thermal response of whole cells from measurements of the thermal reactivity and interactions between the cell components leading to improved cell designs.
- Perform and video document short circuit, overcharge, and thermal heating tests on Gen 2 cells to benchmark the unsafe or thermal runaway behaviors seen in Gen 2 Li-Ion hardware.

#### Accomplishments

- Measured thermal runaway behavior of Gen 2 cells as a function of state of charge and aging.
- Determined evolved gas species of Gen 2 cells during thermal runaway and venting.
- Determined decomposition temperature range and evolved gas species of electrolyte components during thermal runaway temperature profile.
- Determined activation energy of self-discharge heat generation reactions by microcalorimetry for Gen 2 cells.

- Determined thermal reaction and decomposition regions for SEI layers, electrolyte, binder and active materials for Gen 2 anode and cathode materials.
- Ran and video recorded short circuit, overcharge test, and heating tests in air on Gen 2 cells at 100% SOC. Also performed heating tests at 60% SOC. Determined acceptable shutdown behavior in short circuit, acceptable vent behavior on overcharge, and vent failure to function in thermal heating tests.

### Future Directions

- Determine evolved gas species at the onset of thermal runaway in Gen 2 cells.
- Determine evolved gas species of Gen 2 anode and cathode materials from cycled Gen 2 cells.
- Determine evolved gas species of Gen 2 anode and cathode materials from T-cell prepared material as a function of state of charge.
- Measure effect of additives for thermal mitigation in Gen 2 variant cells during thermal abuse.
- Develop real-time gas analysis capability to monitor gas evolution of Gen 2 materials during ARC bomb testing.
- Determine cell thermal response and runaway behavior during overcharge.
- Develop real-time gas analysis capability to monitor gas evolution of Gen 2 materials during overcharge and heating tests.
- Develop the capability to continuously demonstrate the flammability or non-flammability of evolved gases during overcharge and thermal heating tests.

### Publications

Crafts, C. C., Borek, T. T., Jungst, R. G., Doughty, D. H., Mowry, C. D., "Development of an Abuse Tolerance Test Protocol with Continuous Gas Monitoring," SAND2000-1734.

Nagasubramanian G., "Electrical Characteristics of 18650 Li-ion cells at low temperature" J. Applied Electrochemistry 31 99-104(2001).

Nagasubramanian G., "Improving the interfacial resistance in lithium cells with additives" J. Power Sources 96 29-32(2001).

---

### Thermal Abuse Characterization:

The use of high-power Li-ion cells in hybrid electric vehicles is determined not only by the electrical performance of the cells but by the inherent safety and stability of the cells under normal and abusive conditions. The thermal response of the cells is determined by the intrinsic thermal reactivity of the cell components and the thermal interactions in the full cell configuration. The purpose of this study is to identify the thermal response of these constituent cell materials, their contribution to the overall cell thermal performance and the effects of aging on this behavior. Calorimetric techniques were used as a sensitive measure of these thermophysical properties.

### ARC Thermal Analysis:

ARC allows determination of adiabatic cell response to increasing temperature and thus measures the onset and development of thermal runaway under controlled conditions. ARC runs were performed to 160°C on Gen 2 cells and compared with previous measurements of Gen 1 and SONY cells. Figure 1 shows that the Gen 2 cell at 100% state of charge (SOC) had greater thermal activity than the Gen 1 cells. The onset of self-generated heating was around 50°C as in Gen 1 cells but the heating rate accelerated with increasing temperature very similar to that in the SONY cells. However, the Gen 2 cells did not show the SEI breakdown reaction at 100°C as was seen in the SONY cells. These results suggest that the Gen 2 cells were not experiencing an anode SEI passivation film growth that was as effective as that in the Gen 1 cells. Voltage measurement of the cells during the ARC run showed that separator melting occurred at 130°C but did not stop the thermal runaway reaction. ARC runs were also performed on Gen 2 cells at 60% SOC. Figure 2 shows the data for two cells, one at 60% and one at 100% SOC) that did not vent during the run and thus represent the inherent thermal response of the cell components. The 60% SOC cell showed lower heating rate than was seen for the 100% SOC cell but the only significant difference was measured above 110°C.

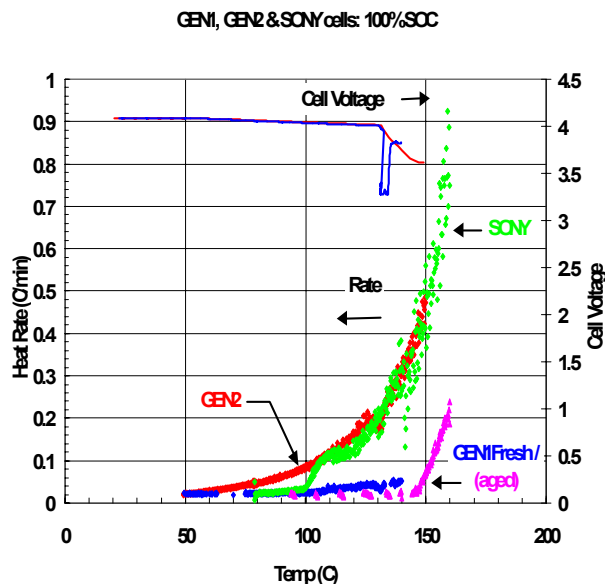


**Figure 1.** ARC run comparisons for Gen 2, Gen 1 and SONY cells.

### ARC/Gas Analysis:

The ARC system was modified this year to allow capture of vented cell gases during the ARC runs. A closed 18650 cell fixture was installed that allowed measurement of cell temperature, cell voltage and total system pressure in a leak tight assembly. Gases were collected at the end of the ARC run and analyzed by gas chromatography (GC). Initially a cell was punctured and placed immediately into the ARC to measure the temperature and pressure of the gas evolution in the cell since not all cells vented during the ARC run. Figure 3 shows that the main evolution of gas began at 125°C and increased linearly up to the maximum run temperature of 160°C. The sudden onset of gas evolution occurred at the same temperature at which cell venting was observed in some of the cells. The gas analysis for this cell showed that CO<sub>2</sub> was the main evolved gas species. Figure 4 shows all the identified gases for this cell along with the gases identified for a vented cell taken at 130°C and 160°C. These cells showed comparably low levels of H<sub>2</sub>, CO, methane and ethylene.

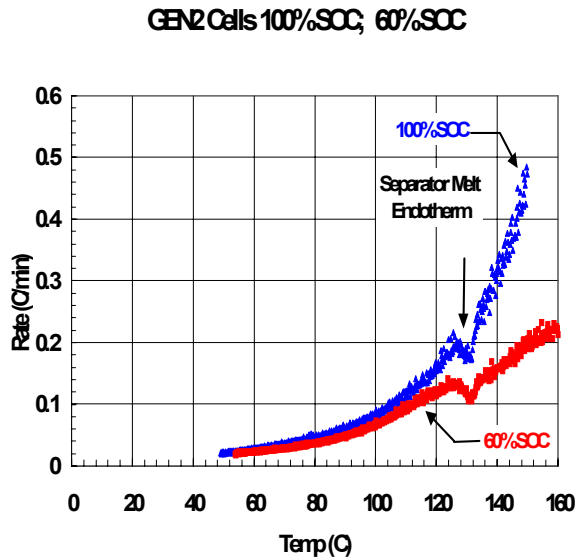


Figure 2. ARC runs of Gen 2 cells at 60% SOC and 100% SOC.

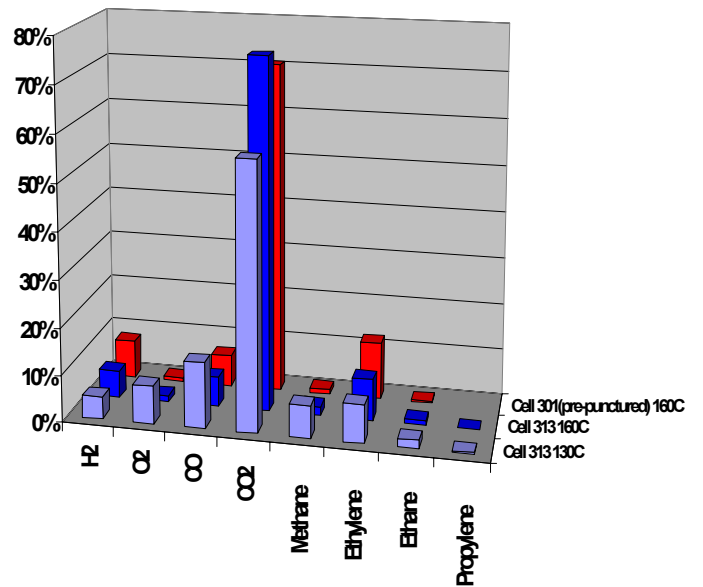


Figure 4. GC gas analysis data of vented and pre-punctured Gen 2 cells from ARC runs.

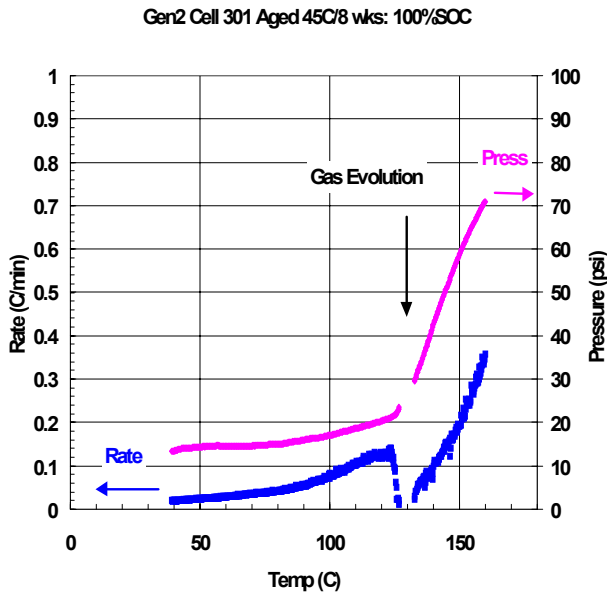
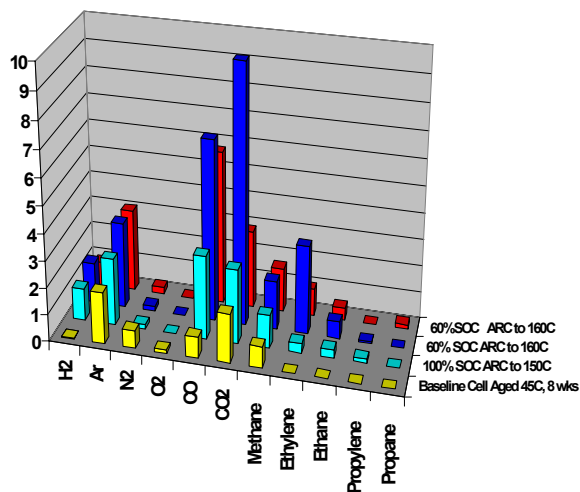


Figure 3. ARC run of pre-punctured aged Gen 2 cell with gas collection.

Unvented cells from the ARC were punctured in a special fixture that allowed direct sampling of the cell gases by the GC. These evolved gas species were compared to the gases from a baseline cell, which had been aged but not thermally abused. The baseline cell showed primarily CO<sub>2</sub>, CO and methane. The cells run in the ARC to high temperatures (160°C) showed new generation of H<sub>2</sub> and increased levels of CO<sub>2</sub>, CO and ethylene as shown in Figure 5. The CO generation occurred primarily in the 130°C to 160°C region based on comparison to the gases seen for the 130°C vented cell. Calculations made from the pressure increase in the calibrated gas collection system showed that the total evolved gas volume ranged from 15 ml to 30 ml.

ml of evolved



**Figure 5.** GC gas analysis data of punctured Gen 2 cells from ARC runs compared with baseline cell.

Gas evolution results from reactions of the cell electrodes and the cell electrolyte. The gas evolution attributable to electrolyte breakdown was determined by performing ARC bomb capsule runs of the Gen 2 solvent and electrolytes. The ARC system was modified to allow not only measurement of the total pressure increase during the ARC run but also to allow gas collection during or after the run. Figure 6 shows the ARC bomb pressure and exothermic heat rate data for the solvent (EC:EMC) and electrolyte (EC:EMC/LiPF<sub>6</sub>). The solvent showed little exothermic behavior or gas generation up to 300°C. Slight decomposition was seen around 225°C. The addition of the salt to the solvent resulted in greatly increased gas generation and exothermic reaction. Additional gas evolution was seen starting at 140°C followed by a sharp exotherm at 185°C. GC analysis of these evolved gases showed that the solvent gases were largely CO<sub>2</sub> with small amounts of methane and ethylene. The addition of the LiPF<sub>6</sub> salt resulted in new generation of H<sub>2</sub> and ethylene. These results are shown in Figure 7. These measurements show that the CO generation seen in the full cells does not result from direct electrolyte decomposition.

**Cell Aging Effects:**

The effects of aging at elevated temperatures were measured by performing ARC runs of thermally aged Gen 2 cells. A total of 12 cells were aged at 45°C/80% SOC for 8 weeks. RPTs were performed at 4 weeks and 8 weeks to measure power fade. The aging test was terminated when 15% capacity fade was reached, which is about half the allowed power fade. Initial ARC runs were performed on the aged cells at 100% SOC and compared to unaged cells. Figure 8 shows that the aged cells have lower heat rate than the unaged cells, as was also seen for the Gen 1 and SONY cells. Passivation of the anode by the SEI diminishes the electrolyte reduction by the lithiated carbon.

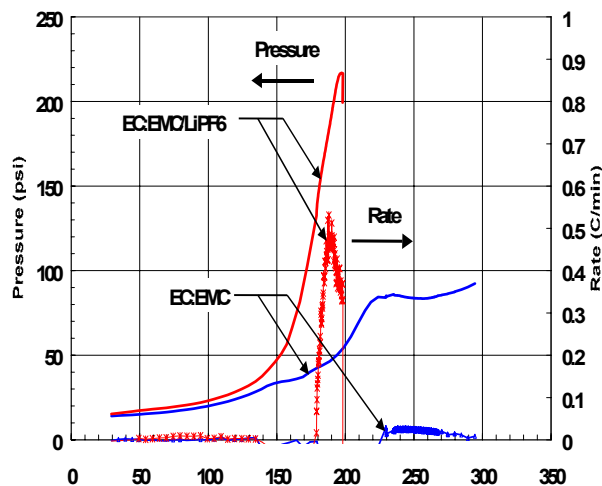


**Figure 6.** ARC bomb runs of Gen 2 solvent and electrolyte.

**Microcalorimetry Analysis:**

Microcalorimetry measurements were performed on two Gen 2 cells at several states of charge to determine the self-discharge heating rate and activation energy. The cells were held at temperature for only a little over 24 hours to minimize any aging effects in the cells. The heat output and the heat rate of decay after

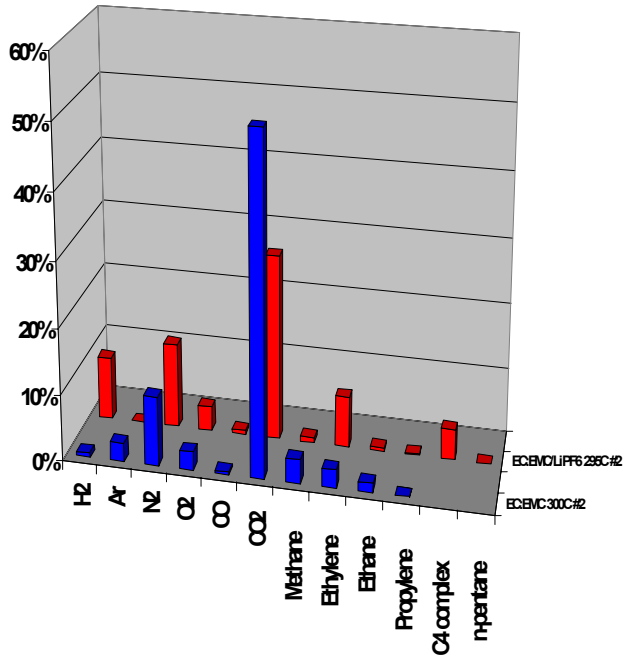


Figure 7. GC gas analysis of decomposition gases of Gen 2 solvent and electrolyte.

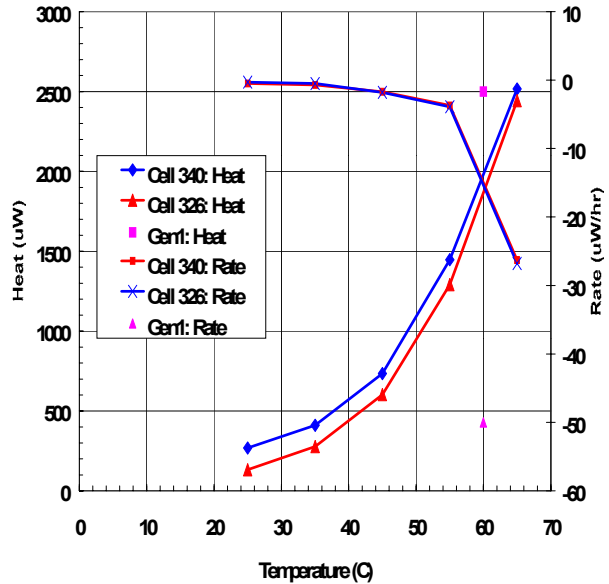


Figure 9. Microcalorimetry of Gen 2 cells as a function of SOC showing heat output and heat decay rate.

equilibration were determined for each temperature. The cells were all measured at 80% SOC. Figure 9 shows this data for the Gen 2 cells as well as a comparison to a Gen 1 cell measured at 60°C/90% SOC. The Gen 2 cells showed comparable heat output to the Gen 1 cells but the rate of decrease of the generated heat was much lower indicating that the Gen 2 cells were not passivating as well as the Gen 1 cells. An Arrhenius plot of the heat output is shown in Figure 10. The cells clearly showed thermally activated heat output with an average activation energy of 13.2 cal/mole. Between 55°C and 65°C the magnitude of the heat decay rate increased abruptly suggesting changes in the kinetics of the passivating reactions. The electrical performance of the cells has also shown abrupt changes in this temperature range.

Gen2 Cells: 100%SOC Fresh/Aged

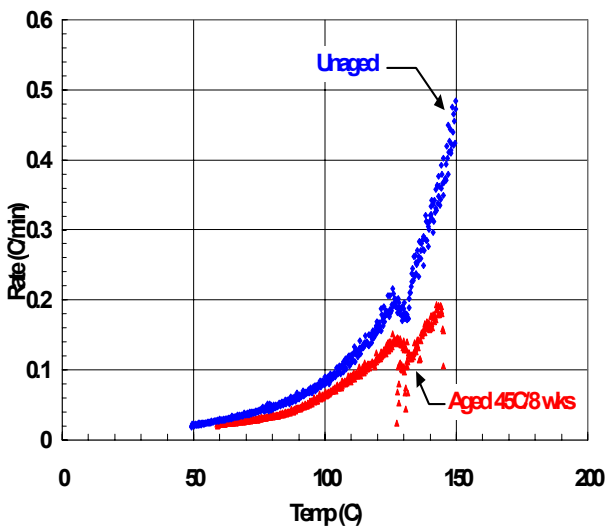


Figure 8. ARC run of Gen 2 fresh and aged cells.

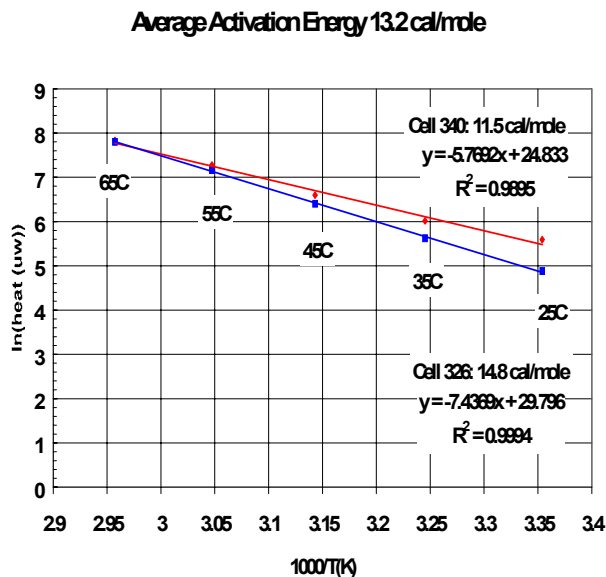


Figure 10. Arrhenius plot of Gen 2 microcalorimetry data.

**DSC Analysis:**

Differential scanning calorimetry (DSC) was performed on Gen 2 electrode materials up to 400 °C in sealed Al pans. Electrodes cut from Gen 2 anode and cathode sheets were cycled in a T-cell against Li using Gen 2 electrolyte and placed in a known state of charge. The thermal signatures of these materials were compared to similar measurements of Gen 1 materials and used to identify heat generation mechanisms observed by ARC runs of full cells and cell components. Figure 11 shows typical data for DSC measurement of Gen 2 and Gen 1 anodes in the fully lithiated (charged) state. The Gen 2 anode showed greater thermal output in the 50 °C to 175 °C range and did not show the abrupt SEI breakdown reaction as seen for the Gen 1 anode material. This data is consistent with the ARC results obtained for the full cells. These results are consistent with the differences in the anode carbon materials. The Gen 1 cell used MCMB carbon that has small spherical particles and can be easily passivated with an SEI layer. The Gen 2 carbon active material was MAG10, which has flaky edges and is less spherical. Our data (ARC, DSC and microcal) indicate that these particles do not form an effective passivating layer and allow continued reaction of the lithiated carbon with the electrolyte. These reactions begin

as low as 50 °C and constitute the initial source of heat output leading to thermal runaway.

DSC measurements of the cathode material ( $\text{Li}_x\text{Ni}_{0.8}\text{Co}_{0.15}\text{Al}_{0.05}\text{O}_2$ ) are shown in Figure 12 along with the corresponding Gen 1 material ( $\text{Li}_x\text{Ni}_{0.85}\text{Co}_{0.15}\text{O}_2$ ) data. The Gen 2 cathode material showed lower heat evolution and higher onset

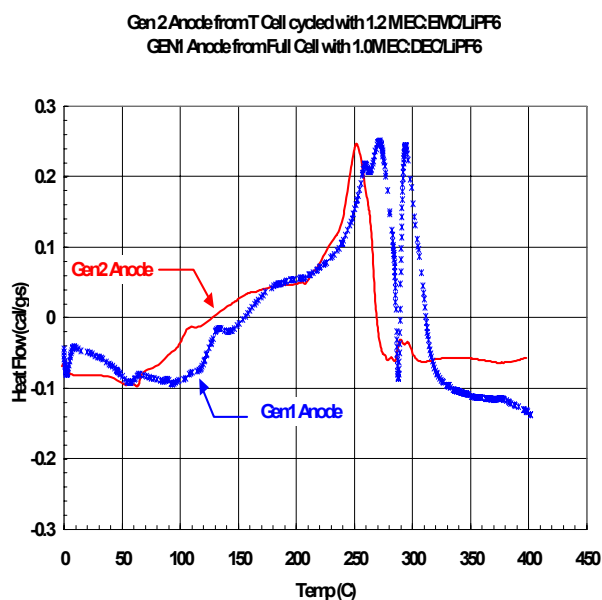


Figure 11. DSC data of charged (lithiated) Gen 2 and Gen 1 anodes in electrolyte.

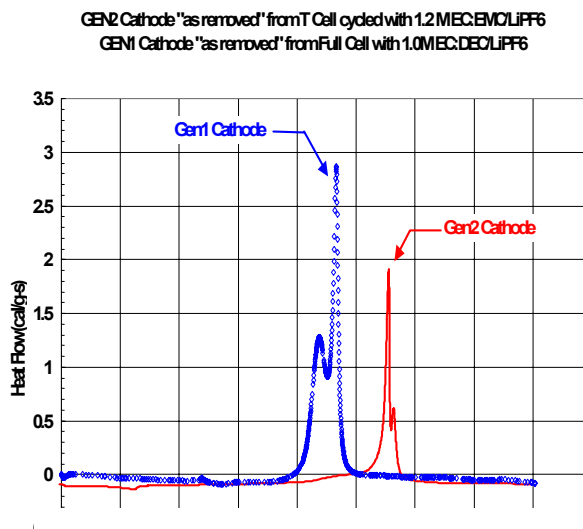
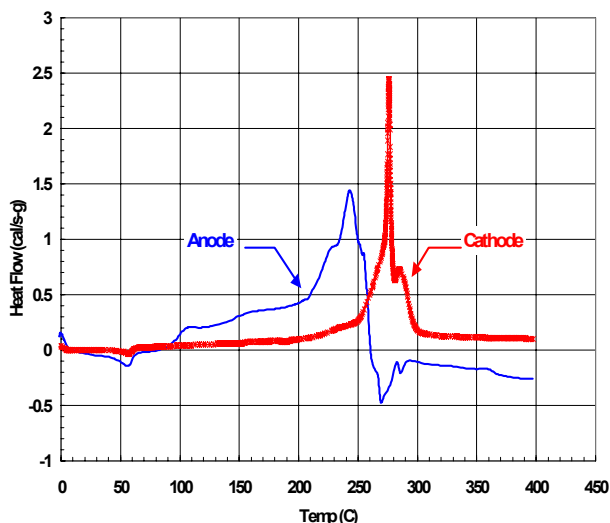


Figure 12. DSC data of charged (delithiated) Gen 2 and Gen 1 cathodes in electrolyte.

temperature compared to the Gen 1 material. The Gen 2 cathode material leads to greater thermal stability for these cells at high temperature but does not affect the onset of thermal runaway. Figure 13 shows a comparison of the heat output of the Gen 2 anode and cathode materials where it is clearly evident that the anode material is the initial source of heat output in the cell.



**Figure 13.** Comparison of DSC data of Gen 2 anodes and cathodes in charged state.

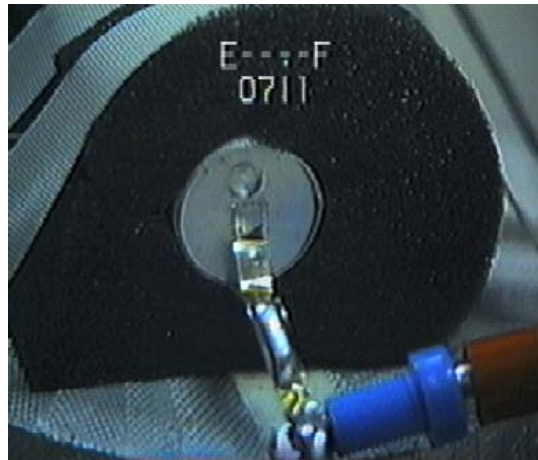
### **Safety Testing on Gen 2 Hardware:**

Safety tests on Gen 2 hardware showed Gen 2 chemistry to behave in a similar fashion to Gen 1. The Gen 2 cells showed differences in these tests not due to the chemistry, but due to the considerable difference in cell hardware. Gen 1 used conventional steel 18650 drawn tube/crimp seal hardware while Gen 2 hardware was custom made of aluminum with welded closures. Gen 2 cells showed better leak tightness, and appeared to be a better experimental hardware design. However, in thermal block heating tests, Gen 2 cell machined vents did not open, and did not successfully protect the cell case from damage.

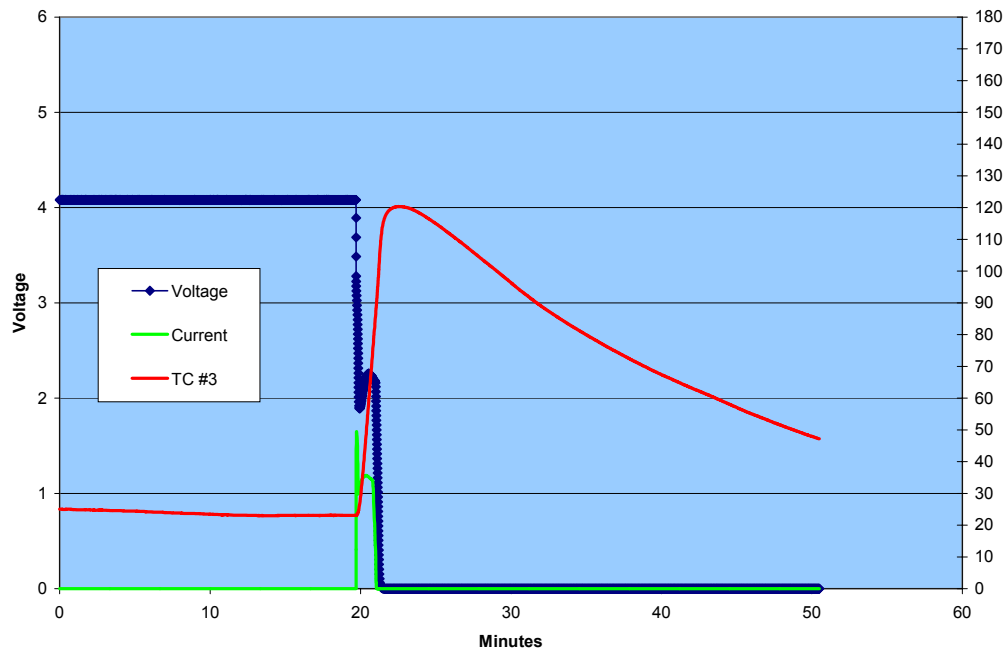
Two cells at 100% SOC were each separately short-circuited through a 0.050 Ohm load. Figures

14 and 15 show the typical result. The cell's high current was apparently cut off by the response of the cell roll's shut-down separator, leaving the cell vent unopened and the resulting cell safe and leak free. Two cells at 100% SOC were each overcharged separately at a 5C rate. In both cases the cell vent opened successfully to save the cell hardware from overpressurization. The cell interior appeared to be very hot and glowed orange, but the can remained intact as can be seen in the sequence shown in Figures 16-20.

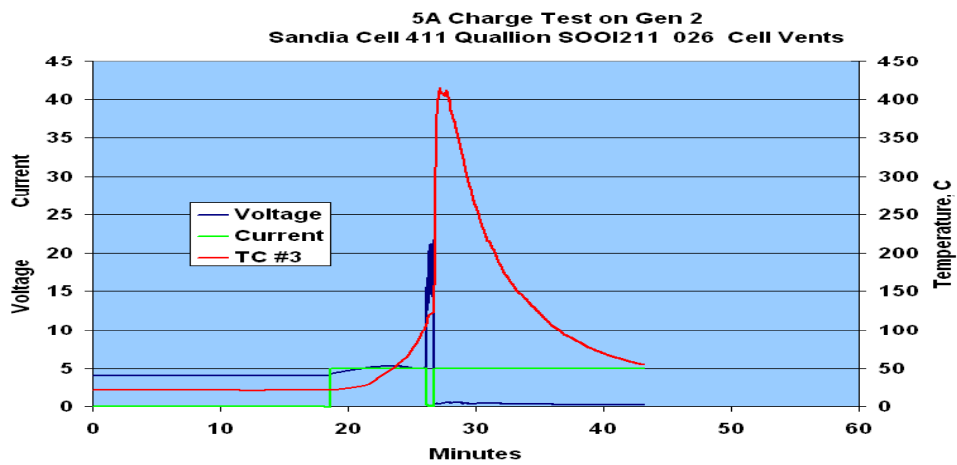
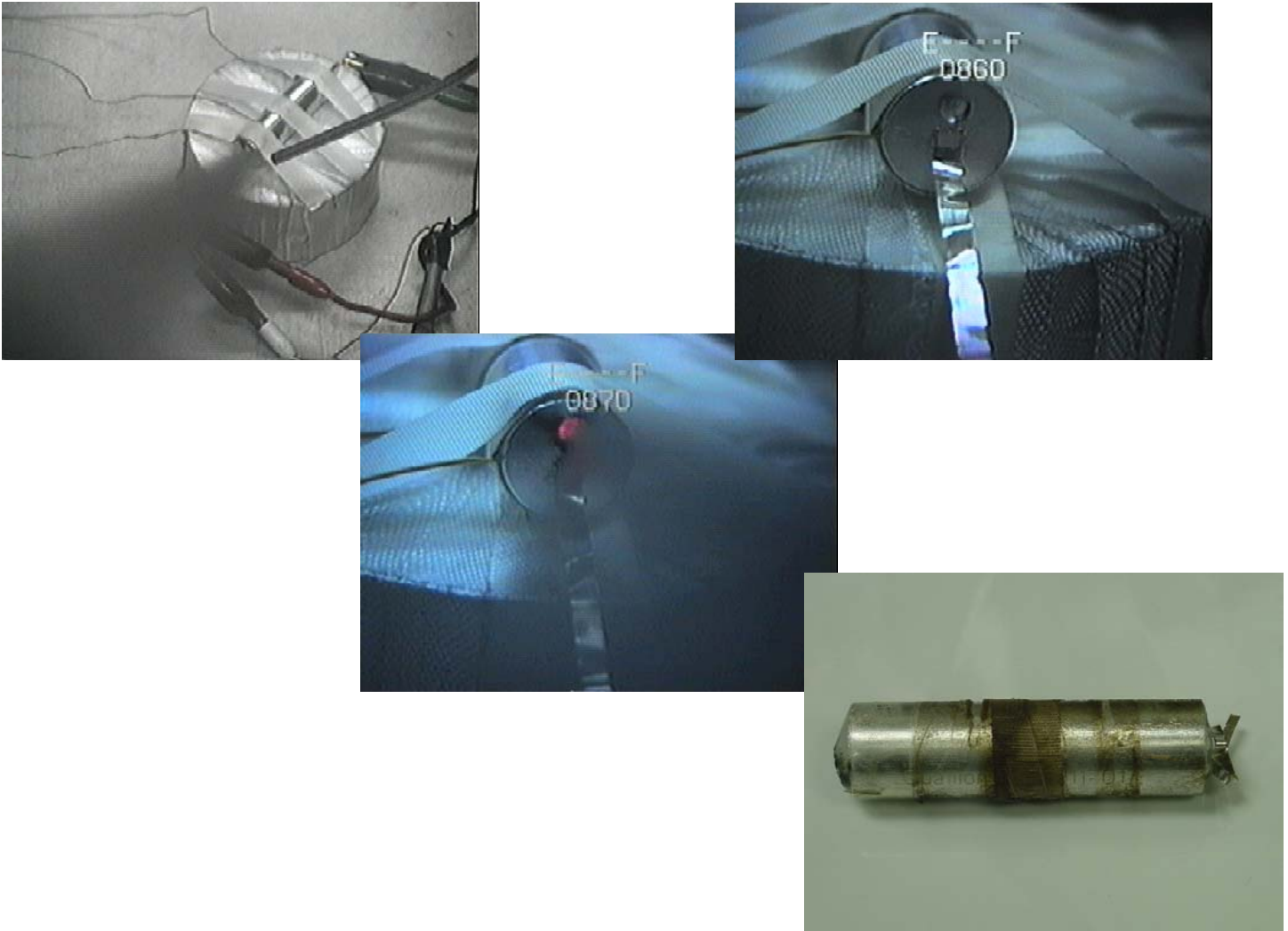
Two cells at 100% SOC and two cells at 60% SOC have been run in heating tests to 200°C. In these tests, two cells vented, saving the respective cans, and two cells did not, causing the can lid to fail and the roll to eject. There was a result each way, at each SOC. It appears that in instances where there was can, seal, or vent damage which could cause the cell to leak prematurely, then the cell did leak prematurely, and the cell was eventually observed to vent through the machined vent, and the can was saved from overpressure. In the other two, normal, cases where there was no premature leakage, the machined vent never opened, and the case and roll were destroyed by overpressure. It is this result for the 100% SOC case that is shown in Figures 21 and 22.



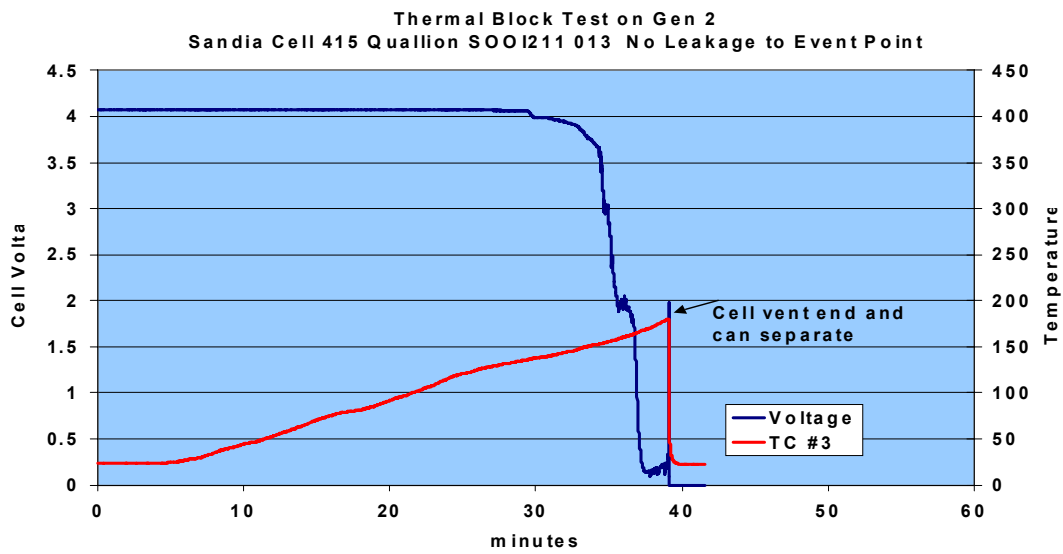
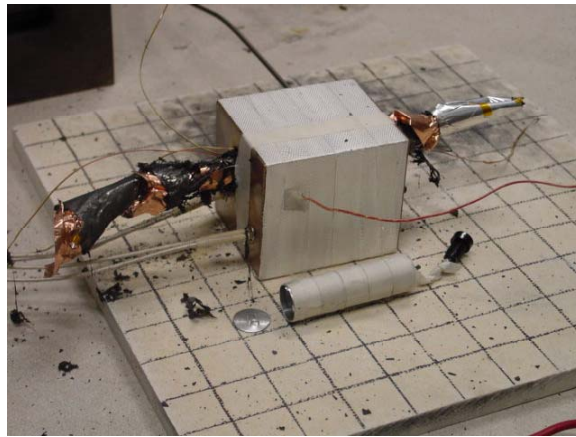
0.050 Ohm Short Circuit on Gen 2  
Sandia Cell 412 Quallion SOO1211 023 No Venting, Reinforced Leads



Figures 14 and 15. Observed Successful Cell Non- Venting during Short Circuit



**Figures 16-20.** Observed Successful Cell Vent during 5C Overcharge Test



**Figures 21 and 22.** Observed Unsuccessful Cell Vent during Heat Test of Cell at 100% SOC to 200°C.

## c. Gen 1 and Gen 2 Accelerated Life Testing

*Ira Bloom and Scott Jones*

*Argonne National Laboratory, Argonne, IL 60439-4837*

*(630) 252-4516; fax (630) 252-4176; e-mail: [bloom@cmt.anl.gov](mailto:bloom@cmt.anl.gov)*

*Chet Motloch, Roger Richardson, Jon Christophersen and Randy Wright*

*Idaho National Engineering and Environmental Laboratory, Idaho Falls, ID 83415-3830*

*(208) 526-0643; fax (208) 526-0969; e-mail: [motlch@inel.gov](mailto:motlch@inel.gov)*

*Rudy Jungst, Herb Case, Terry Unkelhaeuser, and Dan Doughty*

*Sandia National Laboratory, Albuquerque, NM 87185-0613*

*(505) 844-1103; fax: (505) 844-6972; e-mail: [rgjungs@sandia.gov](mailto:rgjungs@sandia.gov)*

---

### Objectives

- Determine the effect of elevated temperature and state-of-charge on the calendar and cycle life of ATD Gen 1 Li-ion cells to be able to project calendar life at ambient temperature
- Determine the effect of changes in cell chemistry on the calendar life of ATD Gen 2 baseline cells at elevated temperatures

### Approach

- Gen 1: Populate a test matrix with cells using selected temperature and state-of-charge conditions. The temperatures used are 40, 50, 60 and 70°C; the states-of-charge are 40, 60 and 80%. Send cells to the diagnostics labs either after 8–12 weeks of testing or after the end-of-test criterion has been met.
  - Collect all the calendar- and cycle-life HPPC<sup>1</sup> data and model the changes in resistance and power order to project life times at 25°C
- Gen 2: Populate a test matrix with cells using selected temperature and state-of-charge conditions. The temperatures used are 45 and 55°C for the baseline and 45°C for the variant cells; the state-of-charge is 60%. For the 55°C cells, send cells to the diagnostics labs after characterization, after 1 month, and thereafter whenever the power fade increment is greater or equal to 5%. Send cells to diagnostics labs when cell reaches 30% power fade, past 30% or after the end-of-test criterion has been met.

### Accomplishments

- Gen 1: All testing has been completed and the HPPC data from ANL, INEEL and SNL have been collected. The resistance rise and discharge power fade data have been modeled using Arrhenius and time-dependent kinetics. The power fade and resistance rise data from the calendar-life studies follow (time)<sup>0.5</sup> kinetics, which may be attributed to SEI layer formation and growth. The cycle-life data are more complex and has a strong state-of-charge dependence. A journal paper has been written and published.
- Gen 2: The baseline cells have been characterized and put on calendar test at 45 and at 55°C. After removing cells at selected intervals, there are 5 cells left at 55°C and 2 at 45°C. The Variant C (improved cathode) cells have also been characterized and are on calendar-life test at 45°C.

### Future Directions

- Finish testing Gen 2 baseline and Variant C cells
- Finish analyzing and modeling cell performance data

## Publications

An Accelerated Calendar Life and Cycle Life Study of Li-Ion Cells, I. Bloom, B.W. Cole, J.J. Sohn, S.A. Jones, E.G. Polzin, V.S. Battaglia, G.L. Henriksen, C. Motloch,

R. Richardson, T. Unkelhaeuser, D. Ingersoll, and H. Case, *Journal of Power Sources* 101 (2001) pp 238-247.

---

## Introduction

The goal for the first part of the project is to develop an understanding of the effect of accelerated calendar-life testing on the performance of ATD Gen 1 Li-ion cells. For the second part, the goal is to understand the effect of changes in cell chemistry on the accelerated calendar-life testing on the performance of ATD Gen 2 baseline and variant Li-ion cells. The results of this testing will be used to project the performance and life of these cells at ambient temperature.

### Gen 1

During the third phase<sup>2</sup> of this project, the three test labs, ANL, SNL and INEEL, finished testing the Gen 1 cells and combined their results. The accelerated calendar-life testing for the ATD program consisted of exposing 18650 cells to the conditions as shown in the test matrix (see Table 1). The cycle-life matrix consisted of temperatures similar to those given in Table, but used only 60 and 80% SOC. Three cycle-life profiles were used, based on the amount of cell capacity removed ( $\Delta$ SOC) per profile, 3, 6, and 9%.

**Table 1.** Cell distribution for calendar-life testing. Each lab abbreviation represents 3 cells.

SOC, %	Temperature, °C			
	40	50	60	70
40	ANL	ANL	ANL	ANL
60	ANL INEEL	ANL INEEL	ANL INEEL	ANL INEEL
80	INEEL SNL	INEEL SNL	INEEL SNL	INEEL SNL

The data for the analyses came from the HPPC-M test performed during periodic RPTs. RPTs were performed every 4 weeks for those cells at 40, 50, and 60°C and every 2 weeks for the cells at 70°C.

## Gen 2

Seventeen baseline cells were received at ANL and characterized in terms of C/25 discharge and charge curves, C/1 capacity, electrochemical impedance spectroscopy (EIS), and HPPC-L. The cells were tested at 60% SOC and at 45 and 55°C. The performance of the cells was measured every four weeks. Cells were removed from the 55°C test after characterization, 4 weeks at temperature, and after an increment of 5% power loss up to 30% loss and one with more than 30% loss.

## Summary Of Studies

### Gen 1

The changes from initial values (see Fig. 1 for an example of HPPC-M data) were calculated on a cell-by-cell basis. These values were then averaged before modeling. The change from the initial values was fit using an Arrhenius and time-dependent equation:<sup>3</sup>

$$Q = A \exp(-E_a/RT) t^z,$$

where Q = %change in ASI or power, A=pre-exponential factor,  $E_a$ =activation energy, R=gas constant, T=absolute temperature, t=time and z=exponent of time. It should be noted that the data from the 9% $\Delta$ SOC cells could not be fit with a reasonable regression coefficient and were excluded from the remaining data interpretation. The values of the exponent of time, z, are given in Tables 2 and 3 for calendar and cycle life, respectively.

**Table 2.** Values of “z” from Calendar-Life Model

%SOC		ASI Increase	Power Fade
40	value	0.52	0.44
	std error	0.05	0.06
60	value	0.51	0.46
	std error	0.06	0.18
80	value	0.61	0.46
	std error	0.14	0.15

The values of “z” provide clues to the mechanisms of ASI increase and power fade. If z in (time)<sup>z</sup> is 0.5, then power or ASI change follow one-dimensional kinetics. Thin-film growth has been described as following this kinetic law. In the cell, a possible thin film is the SEI layer.

**Table 3.** Values of “z” from Cycle-Life Model

%SOC	%ΔSOC		ASI Increase	Power Fade
60	3	Value	0.54	0.25
		std error	0.09	0.00
	6	Value	0.11	0.08
		std error	0.08	0.07
80	3	Value	0.57	0.19
		std error	0.12	0.14
	6	Value	0.15	0.14
		std error	0.10	0.07

From all calendar-life data, z is approximately 0.5 (within experimental error) for both ASI increase and power fade.

From cycle-life data, z is ~0.5 for ASI increase at 3% ΔSOC, but z decreases to ~0.1 for the 6% ΔSOC data. The values of z for power fade also change between 3 and 6% ΔSOC, 0.25 to 0.15. The low value of z indicates different mechanism(s) may be present. Some possibilities are the dissolution and reforming of SEI layer, the PVDF binder reacting with electrodes and LiPF<sub>6</sub> in the electrolyte reacting with electrodes and/or electrolyte.

A comparison of the calculated values for ASI increase for calendar and cycle life is given in Fig. 2. It shows that cycling causes the ASI to increase faster than calendar time. Fig. 2 also shows an

unexpected result; after some time, the rate of ASI increase in the 6% ΔSOC cells is less than that of the 3% cells.

## Gen 2

Fixed voltages define all the states-of-charge. These voltages were determined by performing a C/25-rate discharge at 25°C on a group of baseline cells at ANL. These discharges were between the voltage limits of 4.1 and 3.0 V. The voltage, at 25°C, for 60% SOC is 3.723V. INEEL performed the C/25 discharge curve for the Variant C cells. The voltage that corresponds to 60% SOC is 3.741V.

After 2.5h, the cells were heated to the target temperatures and the voltages allowed to drift. The cells were then potentiostated at the new equilibrium voltage and held there for 4 weeks.

RPTs were performed after the soak periods and the cells were cooled to 25°C. Some of RPTs consisted of a C/1 discharge and the HPPC-L test (a partial RPT). Others received a full RPT consisting of the partial RPT plus the C/25 charge and discharge and EIS. Comparing the results from all the RPTs indicated the changes in cell performance. Cells were removed after characterization, 4 weeks under test, and thereafter after 5% incremental power fade to ~30%.

Additional information was gathered during the soak periods. ANL performed the special calendar test, which consists of using a single 3C discharge and charge pulse to determine resistance changes on a daily basis.

Typical HPPC-L data showing resistance rise and power fade are given in Figs. 3 and 4, respectively. It should be noted that the values in Fig. 4 for available energy and power have been multiplied by battery scaling factor of 553. In both figures, there are changes with time.

Changes in the interfacial processes were seen in the EIS measurements (see Fig. 5). From the figure, the real impedance ( $Z_{\text{real}}$ ) has increased significantly with time.

In the literature, the incremental capacity curve ( $d[\text{Ah}]/dV$ ) provides a method to determine lithium ordering or co-ordination in the electrode and how it changes.<sup>4</sup> Discretely differentiating the C/25 charge and discharge curves yields Fig. 6. As can be seen, there are changes in the curves occurring at low cell voltages (low SOCs), indicating that the ordering of  $\text{Li}^+$  ions in the electrodes has changed with time.

Using the model derived for the calendar life of Gen 1 cells, the relative ASI increase was calculated for the Gen 2 test temperatures, 45 and 55°C. These curves are given in Fig. 7 along with some ASI increase data gained from Gen 2. Fig. 7 shows that the rate of increase for Gen 2 cells is much less than that for Gen 1. In fact, the rate of increase for Gen 2 at 55°C is less than that for Gen 1 at 35°C.

Fifteen of the Variant C cells arrived at ANL in August. Five of them had unacceptably low open-circuit voltages (e.g., 0.8–1.8 V). Variant-C characterization testing of the remaining ten cells began on 9/10/01. The average characterization data for these cells are listed below.

- Measured static capacity 830 mAh.
- PNGV power is 33.88 kW at 300 Wh
- Calculated BSF is 626

These cells are now on calendar test at 45°C.

## **References**

1. For a description of the HPPC test, see “PNGV Test Plan for Advanced Technology Development Gen 2 Lithium-Ion Cells,” EHV-TP-121, Revisions 1 through 6
2. The other phases of the program have been described in: C. Motloch, I. Bloom, D. Ingersoll, H. Case, H. Haskins, V. Battaglia, and T. Unkelhaeuser, Advanced Technology Development, 1999 Annual Progress Report, Energy Management Team, U.S. DOE, Office of Advanced Automotive Technologies, March 2000, pp. 12, 18, and 21ff.
3. I. Bloom, B. W. Cole, J. J. Sohn, S. A. Jones, E. G. Polzin, V. S. Battaglia, G. L. Henriksen, C. Motloch, R. Richardson, T. Unkelhaeuser, D.

Ingersoll, and H. L. Case, J. Power Sources 101 (2001) pp 238-247.

4. A. H. Thompson, J. Electrochem. Soc., 126 (1979), pp.608 to 616.

## d. Overview of ATD Cell Performance and Life Evaluations

*Chet Motloch, Jon Christophersen, Randy Wright, Roger Richardson, Chinh Ho, David Glenn, Kevin Gering, Tim Murphy*

*Idaho National Engineering and Environmental Laboratory, Idaho Falls, ID 83415-3830  
(208) 526-0643; fax: (208) 526-0969; e-mail: [motlch@inel.gov](mailto:motlch@inel.gov)*

*Ira Bloom, Scott Jones, Vince Battaglia, Gary Henriksen*

*Argonne National Laboratory, Argonne, IL 60439-4837  
(630) 252-4516; fax: (630) 252-4176; e-mail: [bloom@cmt.anl.gov](mailto:bloom@cmt.anl.gov)*

*Rudy Jungst, Herb Case, Terry Unkelhaeuser, Dan Doughty*

*Sandia National Laboratory, Albuquerque, NM 87185-0613  
(505) 844-1103; fax: (505) 844-6972; e-mail: [rgjungs@sandia.gov](mailto:rgjungs@sandia.gov)*

---

### Objectives

- Help identify and quantify the factors responsible for power fade through data analysis of aged cells
- Provide aged cells to diagnostics laboratories
- Provide analyzed performance data to enable correlations against diagnostic results and facilitate selection of most useful tools
- Develop aging protocols and explore new tests, analyses, and modeling methodologies related to calendar and cycle life and provide results to battery developers and other laboratories

### Approach

- Develop a standardized test plan and analytical methodologies for calendar-life and cycle-life testing of ATD Gen 2 lithium-ion cells
- Perform Gen 2 characterization, cycle-life, and calendar-life testing, and analyze data based upon the PNGV Battery Test Manual, Revision 3 to help identify factors that limit cell life
- Perform independent, but coordinated, performance testing at INEEL, ANL, and SNL:
  - INEEL has been tasked with test plan development, cycle-life testing, and life modeling
  - ANL has been tasked with calendar-life testing and life modeling
  - SNL has been tasked with Accelerated Life Testing methodology development and life modeling
- Measure the Gen 2 baseline performance and evaluate subsequent electrochemistry improvements of the variant cells
- Correlate capacity fade, resistance and AC impedance growth, power fade, and changes in differential capacity against calendar life
- Develop and utilize a new end-of-test criteria designed to provide diagnostics laboratories with aged cells at specified intervals based upon power fade

### Accomplishments

- Completed performance testing, data analyses, life modeling, and reporting regarding Gen 1 lithium-ion cells
- Helped develop and implement a standardized electrochemical impedance spectroscopy methodology for Gen 2 testing

- Helped develop and implement a new standardized C<sub>1</sub>/25 differential capacity testing and analysis methodology for Gen 2
- Began testing Gen 2 baseline cells in January 2001
- Began testing Gen 2 Variant C cells in August 2001
- Shipped aged Gen 2 cells to diagnostics laboratories at specified intervals
- Completed performance analysis of all available Gen 2 characterization and cycle-life data

### Future Directions

- Complete cycle-life testing and data analyses for the Gen 2 baseline and variant cells
- Continue to coordinate testing at INEEL, ANL, and SNL and resolve testing related issues
- Continue to supply aged cells to diagnostics labs at specified intervals
- Develop phenomenological hypotheses to explain performance degradation and power fade
- Correlate testing results with diagnostic results
- Continue to develop predictive models for calendar life and cycle life

### Publications

Issued "PNGV Test Plan for Advanced Technology Development Gen 2 Lithium-Ion Cells," EHV-TP-121, Revisions 1 through 6

Issued "Cycle-Life Studies of Advanced Technology Development Program Gen 1 Lithium-Ion Batteries," DOE/ID-10845, April 2001

Issued "Calendar-Life Studies of Advanced Technology Development Program Gen 1 Lithium-Ion Batteries," DOE/ID-10844, March 2001

Issued "DOE Advanced Technology Development Program for Lithium-Ion Batteries: INEEL Gen 1 Final Report," INEEL/EXT-2001-00417, September 2001

A major objective of the Advanced Technology Development (ATD) testing program is to characterize the performance and determine the cycle-life and calendar-life behavior of lithium-ion cells. The purpose of this study is to help identify factors that limit cell life and to provide aged cells to the diagnostics laboratories. This performance testing and aging of the ATD cells has been performed at three U.S. Department of Energy Laboratories: Idaho National Engineering and Environmental Laboratory (INEEL), Argonne National Laboratory (ANL), and Sandia National Laboratory (SNL). ATD Gen 1 performance results have been reported in References 1 through 5.

For Gen 2, the cells are again 18650 size and have specifications developed by ANL for the ATD Program, but were manufactured by Quallion Corporation. ATD Gen 2 cells include baseline cells

and up to three variants of the baseline chemistry. Variant A cells have a TBD flame-retardant electrolyte additive. Variant B cells have a TBD aqueous binder. Variant C cell cathodes are doped with 10% aluminum. The specific chemistries of the baseline and variant cells are discussed elsewhere in this report. To date, the baseline and Variant C cells have been delivered to the laboratories and are undergoing performance testing. This testing is based upon the Power Assist performance and life test procedures that have been developed for the Partnership for a New Generation of Vehicles (PNGV) Program (Reference 6).

In addition to the change in the cell chemistry from Gen 1 to Gen 2, several testing changes have also been implemented. Lessons learned from the Gen 1 phase of the ATD program have been incorporated into the Gen 2 test plan. These include improvements in the methodology for

electrochemical impedance spectroscopy and the use of thermal blocks as originally proposed by SNL to minimize temperature transients during testing. Also, to the extent possible, standard PNGV Power Assist testing protocols and analytical methodologies have been utilized which enable comparison of Gen 2 cell performance against the PNGV hybrid electric vehicle energy storage system goals. Also, a  $C_1/25$  discharge and recharge test has been implemented which provides near-equilibrium performance data from which differential capacity may be calculated. Further, the Gen 2 test matrix has been revised. The matrix reduces the number of test conditions while assigning more cells to each of the remaining conditions in order to provide more information for statistical validation of data. Lastly, the assignment of tests amongst the three labs has been changed in order to reduce duplication while at the same time providing some overlap for validation

Table 1 shows the ratings and test limits for the Gen 2 cells. Values for the variant cells are the same as for the baseline cells, except where noted. Some of the information for the Variant A and for the Variant B cells remains to be determined (TBD). The baseline cell rated capacity is 1.0 Ah; the nominal capacity is 0.979 Ah; and the nominal weight is 38.8 g. The corresponding values for the Variant C cells are 0.8 Ah, 0.826 Ah, and 38.3 g, respectively. All tests are scaled to PNGV Power Assist goals using a Battery Size Factor of 553 for the baseline cells and 651 for the Variant C cells. The operating temperature range is  $-20^{\circ}\text{C}$  to  $+60^{\circ}\text{C}$  for all cells. The minimum discharge voltage is 3.0 V under all conditions. The maximum charge voltage is 4.1 V for a continuous current and 4.3 V for up to a 10-second pulse. The maximum discharge currents are 2.0 A continuous, and 8.0 A for up to an 18-second pulse. The maximum charge currents are 1.0 A continuous, and 8.0 A for up to a

of methodologies. To this end, INEEL has been tasked with cycle-life testing; ANL has been tasked with calendar-life testing; and SNL has been tasked with accelerated life testing. The INEEL test matrix and testing is described further below. ANL's and SNL's testing are described elsewhere in this report.

All of these changes have been incorporated into the Gen 2 test plan to help ensure coordinated testing amongst the three test laboratories (Reference 7). The test plan defines the purpose for testing and identifies test equipment requirements, prerequisites, cell ratings and limitations, and safety concerns. It defines the tests to be performed and the data acquisition requirements. It describes the anticipated results and prescribes the disposition of the cells at the completion of testing. Revisions to the test plan are made as necessary, and as new information is learned.

10-second pulse. Figure 1 shows a photograph of seven typical Gen 2 baseline cells with their cabling mounted in an aluminum thermal block. Cells were shimmed as necessary using aluminum foil to provide good thermal conductivity between the cells and the block.

**Table 1.** ATD Gen 2 Cell Ratings and Test Limits

<b>Ratings</b>	<b>Baseline</b>	<b>Variant A</b>	<b>Variant B</b>	<b>Variant C</b>
C <sub>1</sub> /1 rated capacity (Ah)	1.0	TBD	TBD	0.8
C <sub>1</sub> /1 nominal capacity (Ah)	0.979	TBD	TBD	0.826
Cell nominal weight (g)	38.8	TBD	TBD	38.3
PNGV application	Power Assist	Same	Same	Same
Battery Size Factor	553	TBD	TBD	651
Temperatures:				
Operating range	-20°C to +60°C	Same	Same	Same
Maximum during discharge	+60°C			
Maximum during charge	+40°C			
Storage	+10°C - ±3°C			
Voltage Limits				
Minimum discharge voltage (V)	3.0, continuous 3.0, up to 18-s pulse	Same	Same	Same
Maximum charge voltage (V)	4.1, continuous 4.3, up to 10-s pulse	Same	Same	Same
Current Limits				
Maximum discharge current (A)	2.0, continuous 8.0, up to 18-s pulse	Same	Same	Same
Maximum charge current (A)	1.0, continuous 8.0, up to 10-s pulse	Same	Same	Same

Following receipt inspection, characterization tests were performed on all the cells. These tests included full-range C<sub>1</sub>/1 and C<sub>1</sub>/25 static capacity measurements; electrochemical impedance spectroscopy (EIS) at 60% state-of-charge (SOC); and Hybrid Pulse Power Characterization at a 5C rate. These same four tests also constitute what are

called Reference Performance Tests (RPT's). The RPT's were conducted at 25°C every four weeks during life testing and form the bases for determining capacity fade and power fade. All testing was performed under controlled conditions using programmable testers and environmental chambers. All characterization testing and RPT's were performed at 25°C. All of these are standard PNGV tests and are described in detail in Reference 6.

For ATD, the OCV is used to define the SOC of the cell regardless of age or degradation. In contrast, depth-of-discharge (DOD) is defined as the fraction of rated capacity removed relative to a fully-charged cell. To facilitate performing tests at specified SOC's, an open circuit voltage (OCV) versus SOC curve was developed based upon the average of the C<sub>1</sub>/25 discharge test results during characterization testing.

### **Gen 2 Cell Life Testing: Cycle Life**

The ATD Gen 2 cycle-life testing, which is being performed at the INEEL, is conducted at 60% SOC and utilizes the PNGV 25 Wh Power Assist Life Test Profile. The pulse profile is scaled using the Battery Size Factor of 553 for the baseline cells and 651 for the Variant C cells. Determination of the Battery Size Factor is based upon initial HPPC test results and utilizes the scaling methodology defined in Reference 6. Life testing is being performed at two temperatures, with 15 baseline cells tested at 25°C and 15 cells at 45°C. All variant cells are being tested at 45°C. The higher temperature was selected to accelerate aging without unduly stressing the cells. The lower temperature was selected to enable projection of life at the standard PNGV cell operating temperature. Just prior to beginning life cycling, an Operating Set Point Stability Test is performed at the appropriate aging temperature and SOC. Its purpose is to fine tune the cycle-life test profile such that a charge-balanced profile is used and that cycling is performed under stable cell conditions.

Cycling performance and aging results for the Gen 2 baseline cells and the Variant C cells are presented below. These include C<sub>1</sub>/1 and C<sub>1</sub>/25 static capacity, C<sub>1</sub>/25 differential capacity, EIS

Nyquist plots, available energy, PNGV power fade, and aging performance summaries. Testing continues until one or more of the end-of-test criterion is met. These criteria are: completion of the specified life interval; inability to successfully perform a test; or as directed by the DOE Program Manager or the DOE Technical Contact. To date, the baseline cells have completed 20 weeks of cycle-life testing (approximately 168,000 PNGV Power Assist cycles) and the Variant C cells have completed 4 weeks of testing (approximately 33,600 PNGV Power Assist cycles).

Figure 2 shows the  $C_1/1$  static capacity test results for 30 ATD Gen 2 baseline cells every four weeks starting from characterization and ending at 20 weeks of cycle-life testing. Fifteen cells each were aged at 25°C and 45°C. The initial average capacity for the 15 baseline cells at 25°C was  $0.981 \pm 0.013$  Ah and after 20 weeks it had dropped to  $0.926 \pm 0.008$  Ah. Similarly, the initial average capacity for the 45°C cells was  $0.976 \pm 0.006$  Ah and had dropped to  $0.900 \pm 0.008$  Ah after 20 weeks of cycling. The figure shows that the cells were all initially fairly well matched and that the capacity fade was fairly uniform at each temperature with the highest fade at the higher temperature, as expected. The gaps in the data are a result of periodically taking selected cells off test and sending them to the diagnostics labs for destructive examination. The details of the diagnostic examinations are found elsewhere in this report.

Figure 3 shows similar information for the 15 Variant C cells at characterization and after four weeks of cycling at 45°C. The initial average capacity for these 15 cells was  $0.826 \pm 0.016$  Ah and after 4 weeks it had dropped to  $0.812 \pm 0.017$  Ah. The Variant C cells had a lower capacity than the baseline and also exhibited a slightly larger, but still small, statistical variation. The figure shows that these cells also were all initially fairly well matched and that the capacity fade was fairly uniform.

Figure 4 shows the  $C_1/25$  static capacity test results for 30 ATD Gen 2 baseline cells every four weeks starting from characterization and ending at 20 weeks of cycle-life testing. Here, the gaps in the data are a result of a combination of periodically taking selected cells off test and sending them to the

diagnostics labs for destructive examination, as well as the fact that initially, fewer cells underwent the  $C_1/25$  test at each RPT. The initial average capacity for the 15 baseline cells at 25°C was  $1.075 \pm 0.014$  Ah and after 20 weeks it had dropped to  $1.019 \pm 0.011$  Ah. Similarly, the initial capacity of the 45°C cells was  $1.074 \pm 0.013$  Ah and had dropped to  $0.965 \pm 0.113$  Ah after 20 weeks. The data again show that the cells were all fairly uniform and that the capacity at the  $C_1/25$  rate was higher than that of the  $C_1/1$  rate, as expected. The  $C_1/25$  data are also used to construct the differential capacity curves, which are discussed below.

Figure 5 shows the corresponding  $C_1/25$  capacity information for the 15 Variant C cells at characterization and after four weeks. The initial average capacity for these 15 cells was  $0.976 \pm 0.028$  Ah and after 4 weeks it had dropped to  $0.952 \pm 0.028$  Ah. Again these results are consistent with those described above.

Further inspection of the data reveals the following. The capacity fade rate for the cells at 25°C is the lowest (2.8 mAh/wk) and the capacity fade rates for the baseline and Variant C cells at 45°C are higher and similar to each other (3.8 mAh/wk and 3.5 mAh/wk, respectively). The corresponding  $C_1/25$  capacity fade rates are 2.8 mAh/wk for the 25°C baseline cells, 5.5 mAh/wk for the 45°C baseline cells, and 6.0 mAh/wk for the 45°C Variant C cells. Interestingly, the  $C_1/25$  fade rate is higher than the  $C_1/1$  fade rate at 45°C, but the two are about equal at 25°C.

Figures 6 and 7 show the  $C_1/25$  differential capacity curves for a representative ATD baseline cell aged at 45°C at successive RPT's over 20 weeks and a representative Variant C cell also aged at 45°C but for only four weeks, respectively. Each curve is normalized to the cell's group average capacity at characterization. It can be seen in both figures that as the cells age the magnitude of the peaks decreases and their locations shift. The locations are thought to be related to specific intercalation sites within the anode and/or cathode. The integrated-area under each peak is equal to the capacity added or discharged over the associated voltage interval. Thus, a decreasing peak indicates an increasing amount of work required to add or remove capacity over that voltage interval. It is believed that this

may be related to changes in the solid electrolyte interface (SEI) layer. Peaks at approximately 3.37, 3.60, and 3.90 V may be fruitful areas for diagnostic evaluation. Interestingly, there is no corresponding discharge peak at 3.37 V for the Variant C cell shown in Figure 7.

Figures 8 and 9 show the Nyquist plots for the same two cells that were used in Figures 6 and 7. As the figures show, the real impedance of the cells increases with aging. It is believed that this increase is related to growth of the SEI layer. By comparing the minima of the curves, it is seen that the Variant C cell shows slightly higher real impedance (0.019 ohms) at characterization compared to the baseline cell (0.017 ohms). However, the real impedance of the Variant C cell after four weeks has grown to 0.024 ohms compared to only 0.019 ohms for the baseline cell. Thus, because of the higher resistance growth rate, one expects that the Variant C cells suffer a higher power fade than the baseline cells. This indeed is the case as follows below.

Figures 10, 11, and 12 show representative BSF-scaled available energy versus BSF-scaled discharge power curves at successive RPT's for a 25°C baseline cell, a 45°C baseline cell, and a 45°C Variant C cell, respectively. (Figures 11 and 12 show data from the same two cells discussed above.)

initial average scaled-power was  $32.51 \pm 0.73$  kW and dropped to  $26.60 \pm 0.58$  kW after 20 weeks. For the Variant C cells at 45°C, the initial average scaled-power was  $32.57 \pm 1.06$  kW and dropped to  $28.23 \pm 1.07$  kW after only four weeks. As with the much faster rate than any of the baseline cells. This is consistent with the Nyquist plot results discussed earlier. Note that this information is also used to calculate power fade and may be useful for life modeling. All of the information from the above results is summarized in Table 2.

The power fade of the baseline and Variant C cells is shown in Figures 15 and 16. The average power fade after 20 weeks of cycling for the baseline cells at 25°C is  $8.63 \pm 0.59\%$ . Similarly, for the baseline cells at 45°C, the average power fade after 20 weeks is  $17.85 \pm 0.70\%$ . Likewise, for the Variant C cells at 45°C, the average power fade after only 4 weeks is  $13.42 \pm 0.76\%$ . Clearly, the power fade increases with time and temperature and the Variant C cells have a fade rate much greater than

In accordance with standard PNGV practice, the cycle-life tests were initially scaled to provide a 30% margin beyond the PNGV discharge power goal of 25 kW and the energy goal of 300 Wh. The 30% margin was selected to accommodate a reasonable amount of cell degradation during life testing. As seen in the figures, the available energy curves move monotonically to the left as the cells are cycled. As long as the available energy curves stay to the right of the cross over point of the 25 kW power line and the 300 Wh line, the cells are able to simultaneously meet the PNGV power and energy goals. As the cells age, pairs are removed from test at predetermined intervals based on the changes in the cell power. These cells are then sent to the diagnostics labs.

Figures 13 and 14 show the change in PNGV power at the 300 Wh line for the baseline and Variant C cells at successive RPT's. The average scaled-power of the 25°C baseline cells was  $32.51 \pm 0.72$  kW and dropped to  $29.68 \pm 0.70$  kW after 20 weeks of life cycling. Similarly, for the baseline cells at 45°C, the capacity curves, these figures show that all the cells were initially fairly well matched. Also, the baseline cells are losing power at a faster rate at 45°C compared to 25°C. Lastly, the Variant C cells are losing power at the baseline cells. All of the information from the above results is summarized in Table 2.

**Table 2.** Summary of ATD Gen 2 Baseline Cell and Variant C Cell Performance.

Cell Description	Cycle Temp. (°C)	Weeks	Initial C <sub>1</sub> /1 Capacity (Ah ±σ)	Present C <sub>1</sub> /1 Capacity (Ah ±σ)	Initial C <sub>1</sub> /25 Capacity (Ah ±σ)	Present C <sub>1</sub> /25 Capacity (Ah ±σ)	Initial Power (kW ±σ)	Present Power (kW ±σ)	Power Fade (% ±σ)
Baseline	25	20	0.981 0.013	0.926 0.008	1.075 0.014	1.019 0.011	32.51 0.72	29.68 0.70	8.63 0.59
Baseline	45	20	0.976 0.006	0.900 0.008	1.074 0.013	0.965 0.013	32.51 0.73	26.60 0.58	17.85 0.70
Variant C	45	4	0.826 0.016	0.812 0.017	0.976 0.028	0.952 0.028	32.57 1.06	28.23 1.07	13.42 0.76

### **Conclusions:**

INEEL has completed 20 weeks of baseline cell cycle-life testing and 4 weeks of Variant C cell testing. All cells have shown to be fairly well balanced at the beginning of testing and are exhibiting fairly consistent behavior as they are aged. The capacity fade rates are all fairly small. Between groups, the 45°C cells show a higher capacity fade rate than the cells at 25°C, and the C<sub>1</sub>/25 capacity is fading faster than the C<sub>1</sub>/1 capacity at 45°C, but not at 25°C.

The power fade is highest at the higher temperatures. The baseline cells at 25°C have only shown a fade of 8.63% after 20 weeks of testing and are likely to complete well beyond the PNGV Power Assist goal of 300,000 cycles before their scaled-power drops below the PNGV goal of 25 kW. The baseline cells at 45°C are fading faster and are projected to complete just above 200,000 cycles before dropping below the PNGV power goal. Lastly, the power of the Variant C cells is dropping rapidly. Unless their rate of degradation decreases substantially (as was seen with the baseline cells), they are projected to complete only about 60,000 cycles before they decrease below the PNGV power goal.

Importantly, measurements of the capacity and power and changes to these two parameters with aging have been investigated using several techniques with self-consistent results. The differential capacity results are consistent with the C<sub>1</sub>/1 and C<sub>1</sub>/25 static capacity results, and the Nyquist results are consistent with the PNGV power fade results. Each technique provides unique details that may be valuable for better understanding cell degradation mechanisms.

### **References**

1. Raymond A. Sutula et al., "FY 1999 Progress Report for the Advanced Technology Development Program," U.S. Department of Energy, Office of Advanced Automotive Technologies, March 2000.
2. Raymond A. Sutula et al., "FY 2000 Progress Report for the Advanced Technology Development Program," U.S. Department of Energy, Office of Advanced Automotive Technologies, December 2000.
3. Randy B. Wright and Chester G. Motloch, "Calendar-Life Studies of Advanced Technology Development Program Gen 1 Lithium-Ion Batteries," DOE/ID-10844, March 2001

4. Randy B. Wright and Chester G. Motloch, "Cycle-Life Studies of Advanced Technology Development Program Gen 1 Lithium-Ion Batteries," DOE/ID-10845, April 2001
5. Jon P. Christophersen et al., "DOE Advanced Technology Development Program for Lithium-Ion Batteries: INEEL Gen 1 Final Report," INEEL/EXT-2001-00417, September 2001
6. "PNGV Battery Test Manual, Revision 3," Idaho National Engineering and Environmental Laboratory, DOE/ID-10597, February 2001.
7. "PNGV Test Plan for Advanced Technology Development Gen 2 Lithium-Ion Cells," Idaho National Engineering and Environmental Laboratory, EHV-TP-121, Rev. 6, October 5, 2001.

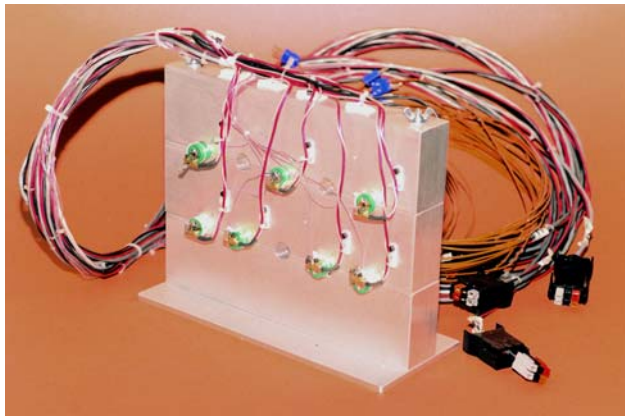


**Figure 1.** Seven typical ATD Gen 2 cells and cabling mounted in an aluminum thermal block.

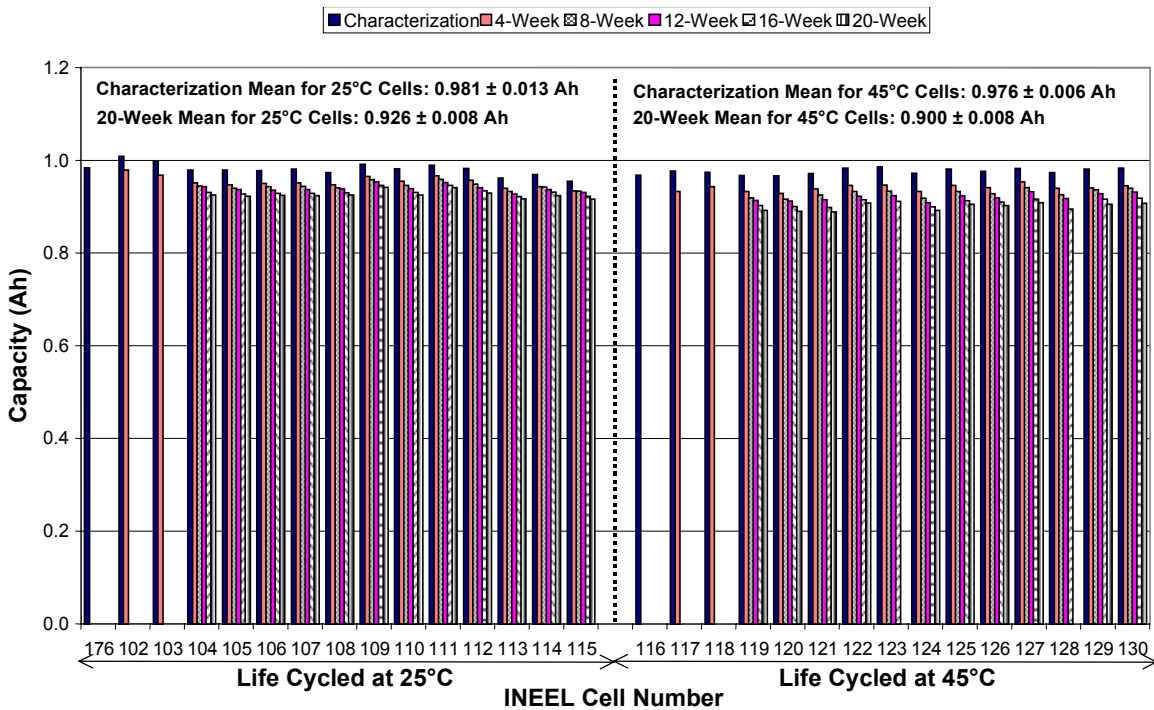


**Figure 2.**  $C_1/1$  static capacity for 30 ATD Gen 2 baseline cells.

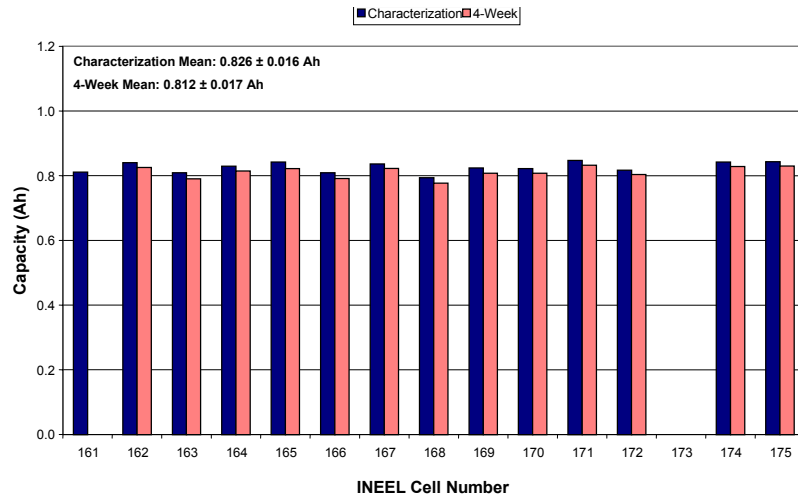


Figure 3.  $C_1/1$  static capacity for 15 ATD Gen 2 Variant C cells

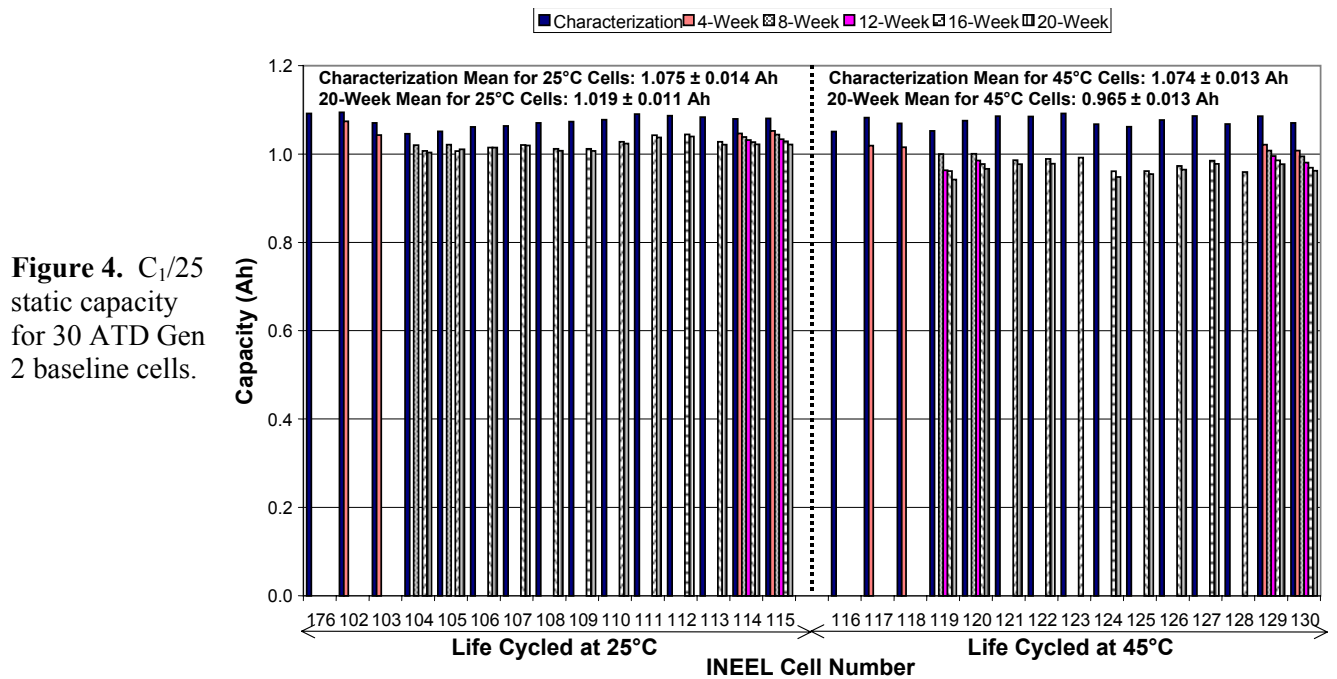


Figure 4.  $C_1/25$  static capacity for 30 ATD Gen 2 baseline cells.

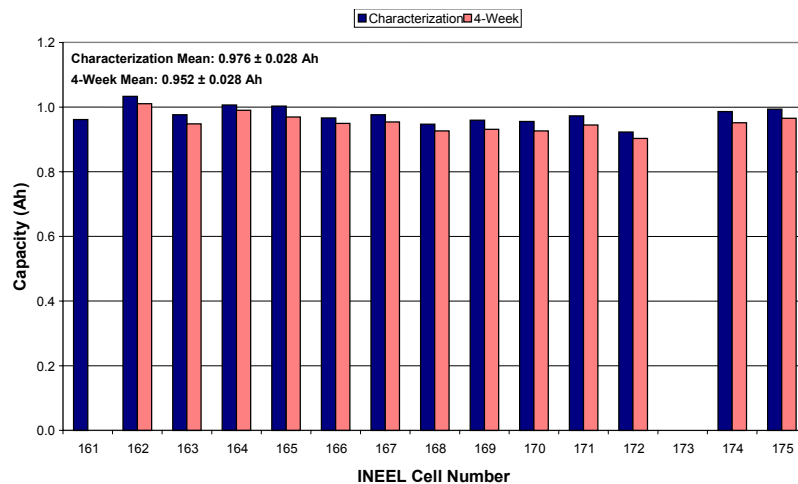


Figure 5.  $C_1/25$  static capacity for 15 ATD Gen 2 Variant C cells.

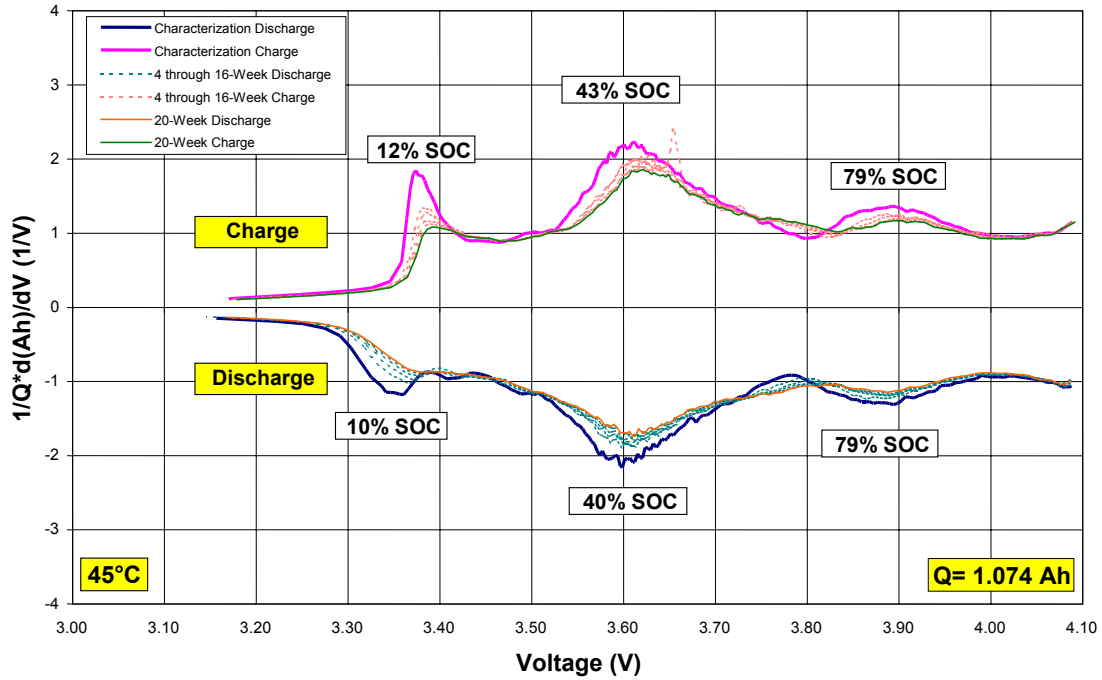


Figure 6. Differential capacity for a representative ATD Gen 2 baseline cell aged at 45°C

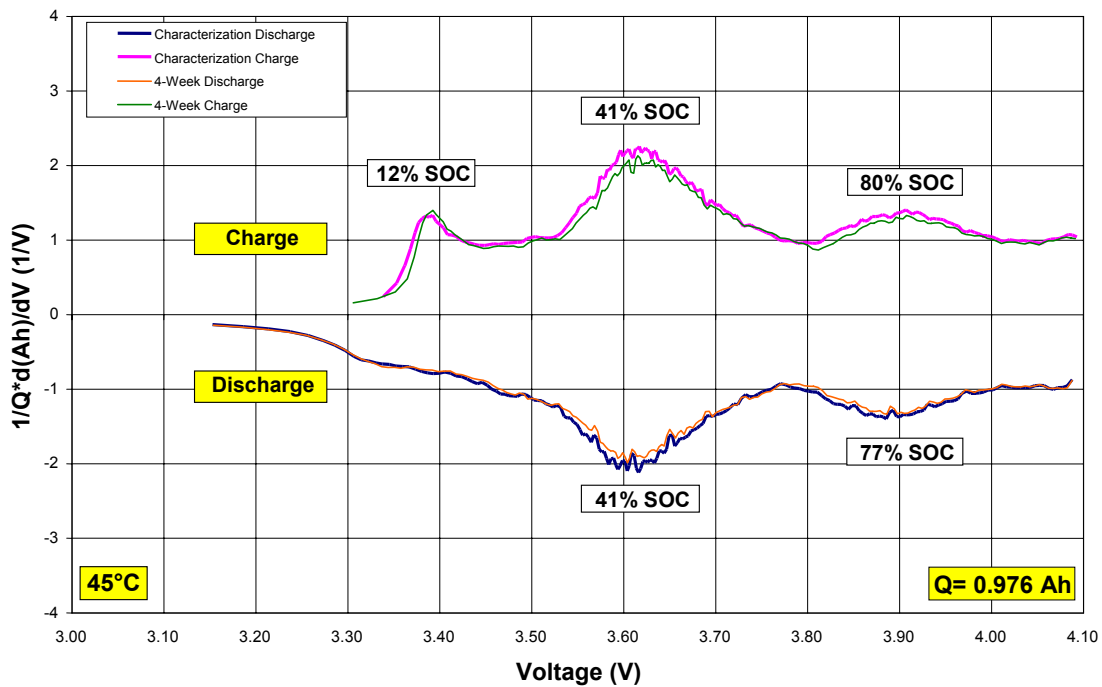


Figure 7. Differential capacity for a representative ATD Gen 2 Variant C cell aged at 45°C

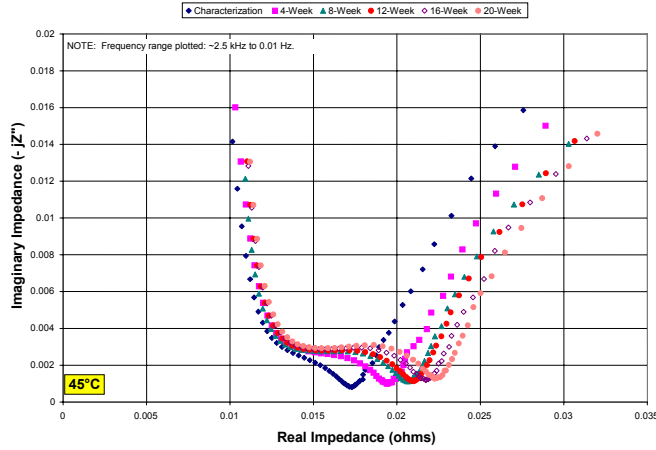


Figure 8. Nyquist plot for a representative ATD Gen 2 baseline cell aged at 45°C

Figure 9 Nyquist plot for a representative ATD Gen 2 variant C cell aged at 45°C

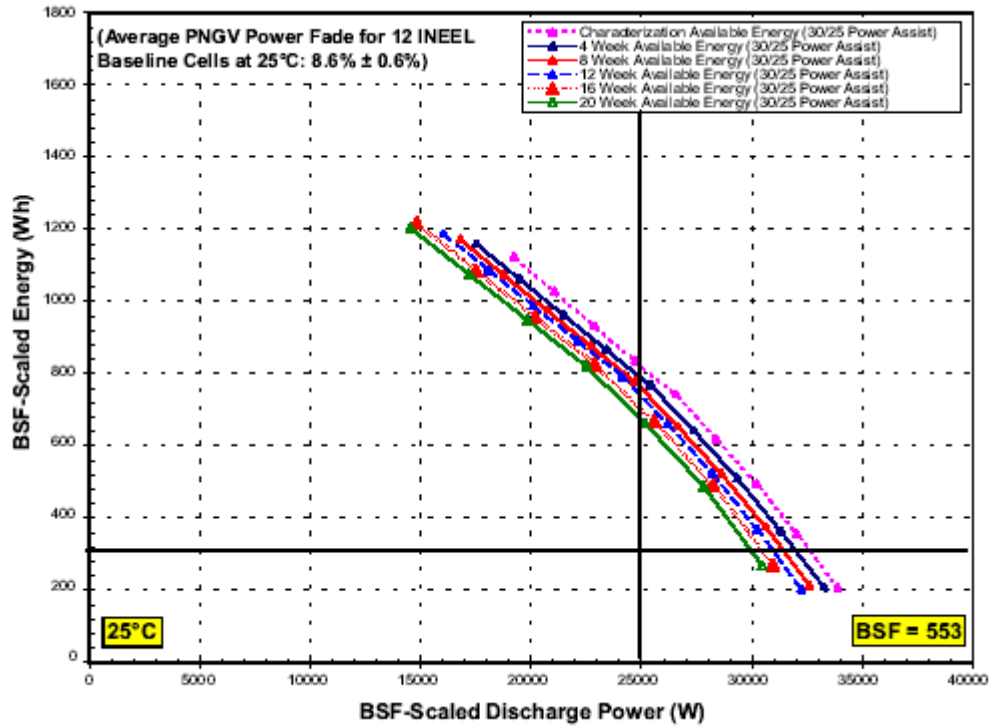
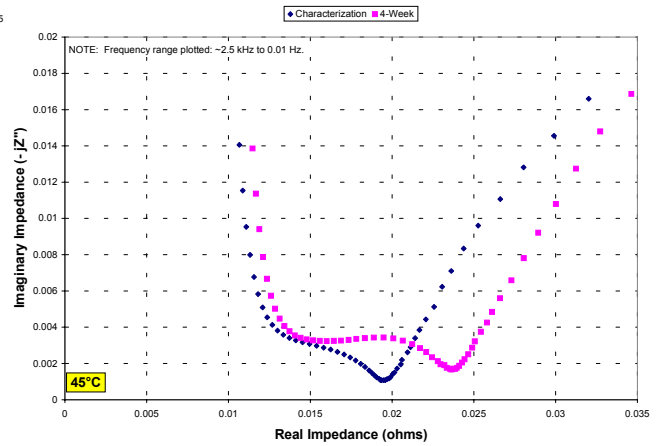


Figure 10. Available energy for a representative ATD Gen 2 baseline cell at 25°C

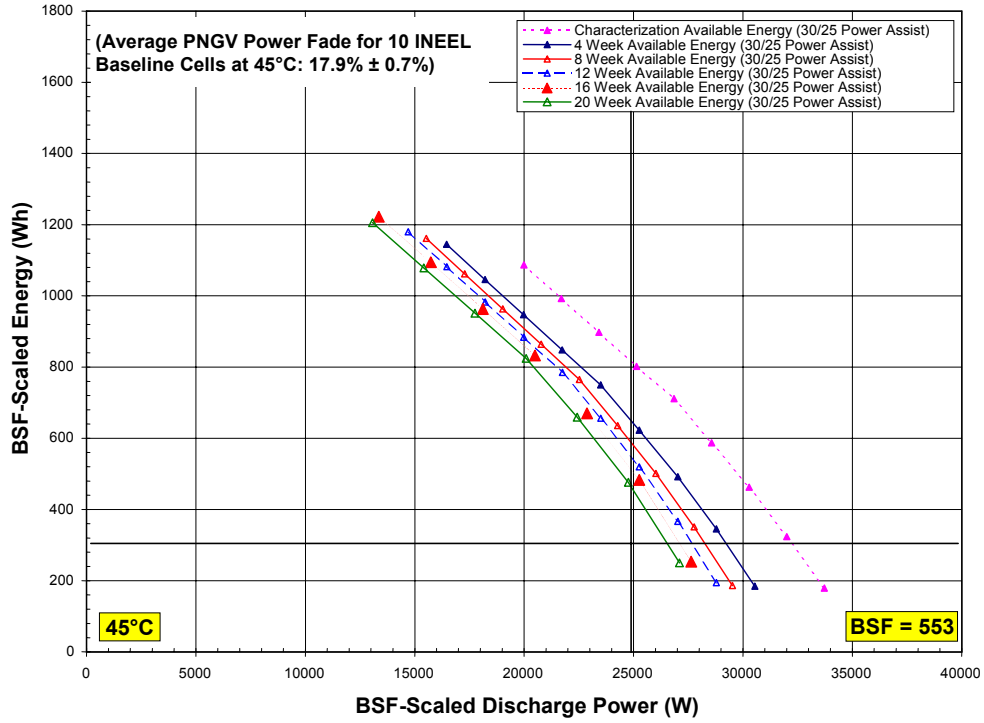


Figure 11. Available energy for a representative ATD Gen 2 baseline cell at 45°C

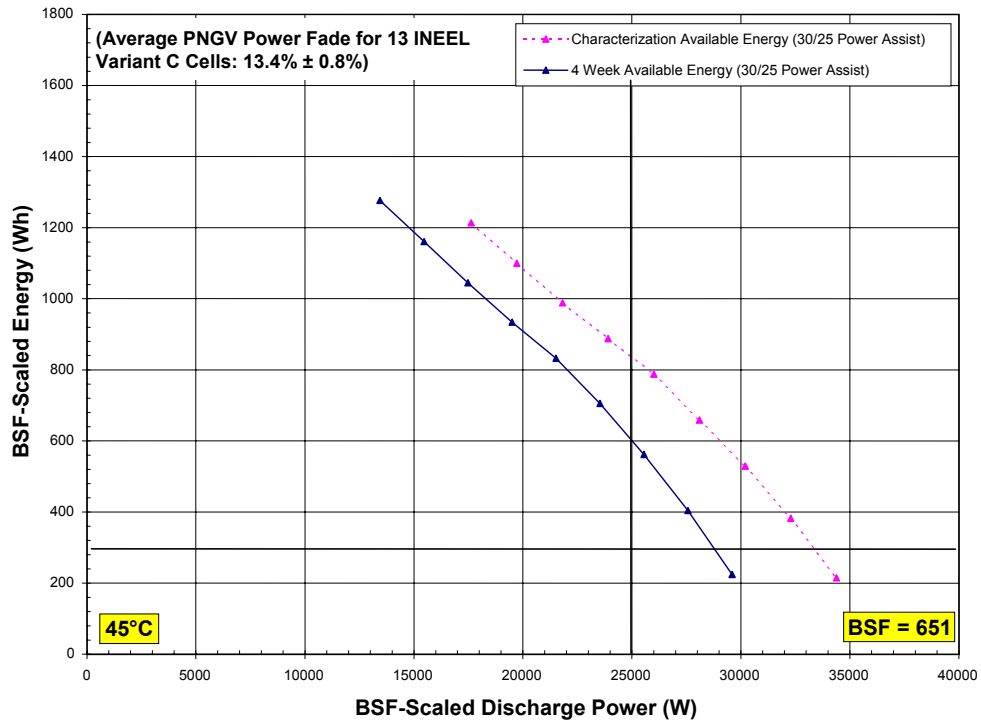


Figure 12. Available energy for a representative ATD Gen Variant C cell at 45°C

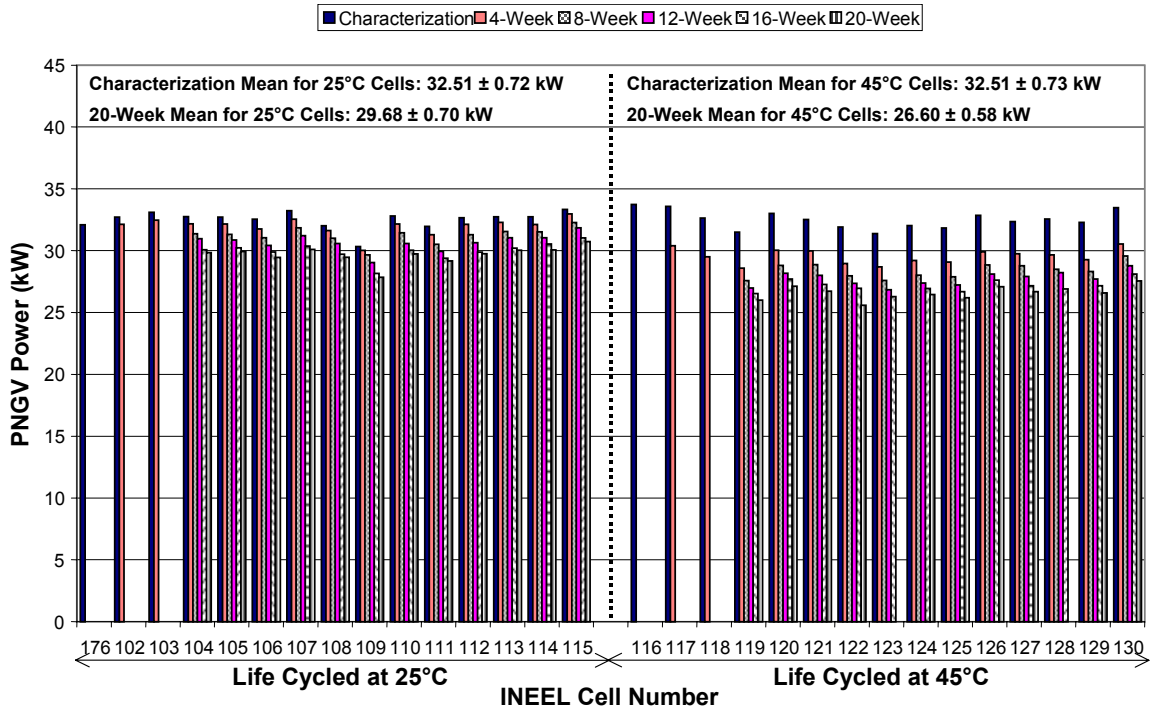


Figure 13. PNGV power at 300 Wh for 30 ATD Gen2 baseline cells

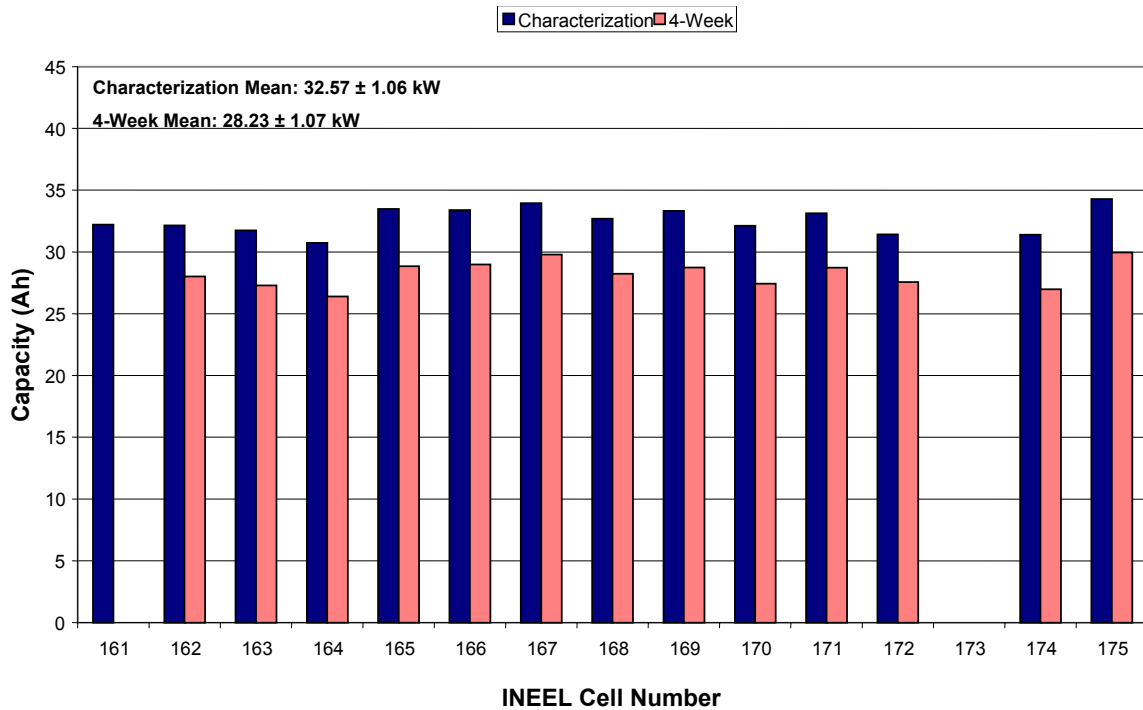


Figure 14. PNGV power at 300 Wh for 15 ATD Gen 2 Variant C cells.

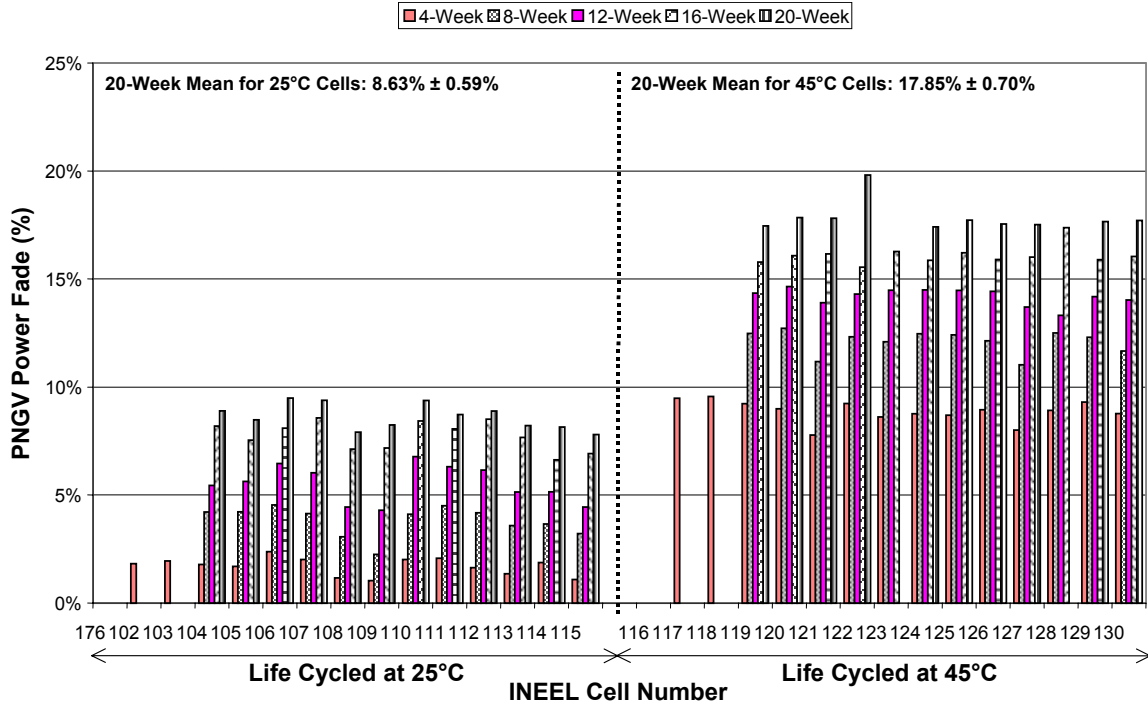


Figure 15. PNGV power fade for 30 ATD Gen 2 baseline cells.

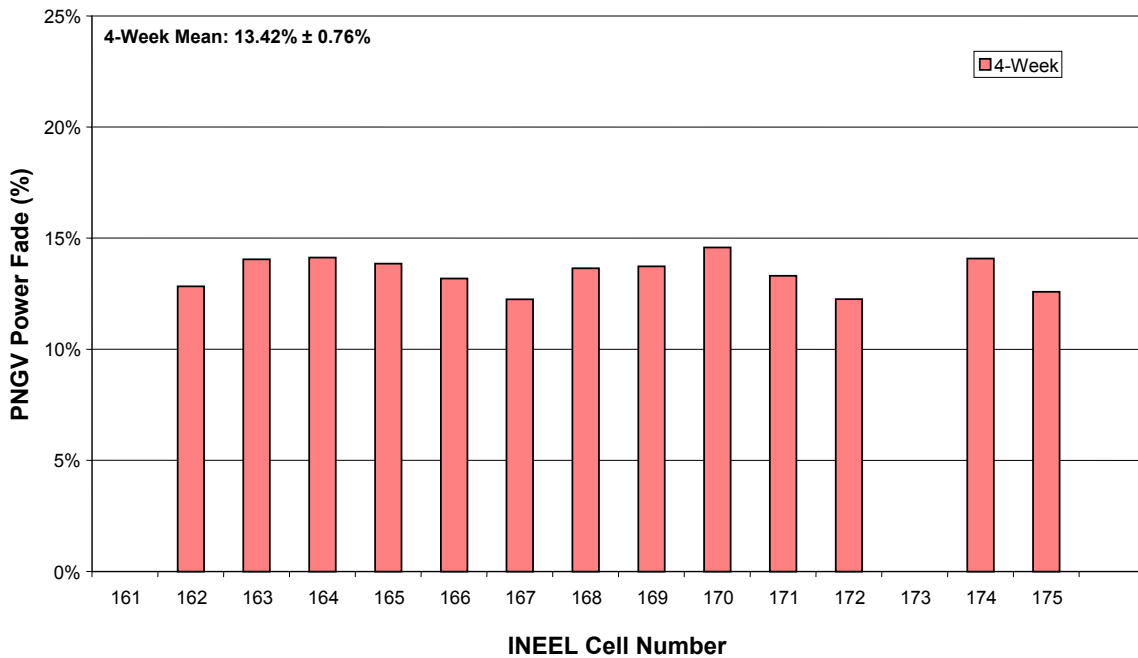


Figure 16. PNGV power fade for 15 ATD Gen 2 Variant C cells

## **d. ACCELERATED LIFE TESTS AND LIFE PREDICTION**

### **Calendar/Cycle Life**

## **e. ACCELERATED LIFE TESTS TO DEVELOP MODEL OF BATTERY LIFE PREDICTION**

*Rudolph G. Jungst, Ganesan Nagasubramanian, Herbert L. Case, Terry Unkelhaeuser, Angel Urbina, Thomas L. Paez, Ed Thomas, Bor Yann Liaw, and Daniel H. Doughy*  
MS 0613, Sandia National Laboratories, P. O. Box 5800, Albuquerque, NM 87185  
Contact: D. H. Doughy, (505) 845-8105; fax (505) 844-6972; e-mail: [dhdough@sandia.gov](mailto:dhdough@sandia.gov)

---

### **Objectives**

- Develop an accelerated aging test protocol for the Advanced Technology Development (ATD) Program.
- Study degradation mechanisms for high-power battery chemistries being developed for use in hybrid electric vehicles. Use diagnostic techniques such as electrochemical impedance spectroscopy (EIS) to investigate the interface properties of the cell to assist diagnosis of the degradation mechanism.
- Develop an analytical and numerical model to describe the battery performance and enable calendar life prediction of high power hybrid electric vehicle lithium-ion batteries.

### **Approach**

- Perform accelerated life tests on 18650-size lithium-ion cells with a large set of test conditions in a matrix covering temperature, aging time, cycling profiles, and state of charge (SOC) variations to suffice the protocol development.
- Combine empirical and mechanistic approaches to correlate the test results, including EIS data, with variation of the test conditions to identify possible degradation mechanisms for power capability and capacity loss and incorporate the mechanisms in the prediction of life performance.
- Use a connectionist normalized linear spline (CNLS) artificial neural network (ANN) to relate variations of impedance and capacity to power fade to aid the identification of degradation mechanism and to develop a numerical model for calendar life prediction.

### **Accomplishments**

- Designed statistically robust test matrices to cover both calendar and screening test conditions, therefore all temperature, state of charge and cycling effects can be captured in the analyses and the development of the calendar life prediction model.
- Completed two aging cycles and data evaluations, showing some successful indications of accelerated fading effects and allowing an initial estimation of the fading rate and correlations with test conditions and EIS data for mechanistic study.
- Developed the ANN framework for data analysis and correlation of fading with test conditions and EIS data.

### **Future Directions**

- Continue long term tests for empirical life prediction. Incorporate diagnostic EIS techniques to identify and characterize degradation mechanism.
  - Complete the development of numerical prediction and correlation tools using the ANN approach. Improve data correlation techniques in the numerical approach.
  - Investigate the origin of the fading mechanisms. Work with other ATD labs to determine the origin of power fade and capacity loss. Analyze samples from the accelerated life test matrix at the ATD diagnostics labs to broaden understanding of the degradation mechanisms to improve life prediction capabilities through a mechanistic approach.
-

To develop an accelerated aging test protocol, the performance of 18650-size lithium-ion cells is being evaluated under a range of accelerated aging conditions. The performance characteristics that are pertinent to the analysis are power capability and capacity. The calendar-aging matrix for these experiments is shown in Figure 1. This matrix focuses on two aging condition parameters, temperature and SOC. The cells are stored open circuit except for a single daily discharge pulse in order to track resistance changes. Figure 2 shows the increasing resistance over the first 4 weeks of aging calculated from the pulse per day data. A separate screening experiment investigating the effect of different discharge pulse profiles and frequencies to be applied during the aging as an additional accelerating factor is also under way. Features of the calendar aging matrix include a designed experiment plan that can be analyzed statistically, and use of SOC and temperature values that cover the range of expected use, thereby avoiding long extrapolations of measured power fade rates to make predictions at nominal use conditions. A minimum of three levels has been chosen for each acceleration parameter so that nonlinear effects and interactions can be assessed. To assess the power capability and capacity changes as the cells aged, at four-week intervals we return the cells to 25°C and conduct a series of performance tests to determine how much fade has occurred. These tests include discharge capacity measurements to a 3.0-V cutoff at C/1 and C/25 rates, a pulse power capability measurement at 25°C and 0°C, and AC impedance measurements at 100% and 60% SOC (both conducted at 25°C). The pulse power capability metric is obtained by discharging and charging the cell at 10% SOC intervals from 90% to 10%. A plot of power versus energy removed can be constructed from this data for both the discharge and charge (representing regenerative breaking) pulses. Figure 3 shows such a plot for a typical cell. The difference between the two curves yields power versus available energy, which can be

SOC	Temp. (°C)			
	25	35	45	55
60%	3	3	3	3
80%	3	3	3	5
100%	3	3	5	5

Figure 1. Distribution of cells in the calendar aging matrix.

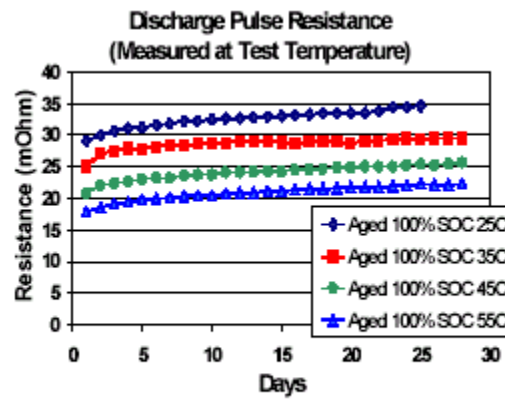
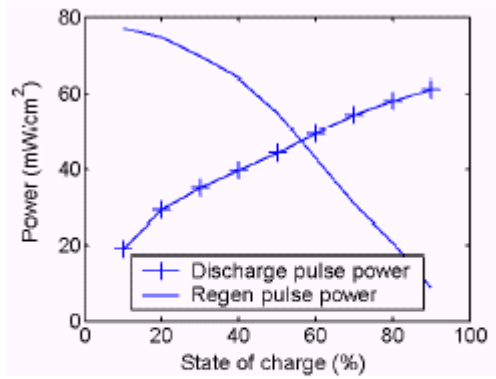


Figure 2. One pulse/day cell resistance.



**Figure 3.** Example showing pulse capability of a Li-ion cell defined in terms of curves established during discharge and regenerative charge of the cell at different SOC's.

tracked over time by comparing with the PNGV 300 Wh energy requirement.

An important aspect of the accelerated life tests is to unequivocally determine the fading effects in the early stage of aging so fading effects can be assessed sooner rather than later. To achieve this, we often need to properly gauge the measurement conditions, so adequate measurements of the aging behaviors are accomplished. To illustrate the point, the power fade data from fresh to 4 weeks are shown in Figure 4 for measurements both at 25°C and at 0°C. The 0°C tests were instituted because it was anticipated that small increases in cell resistance during low-temperature aging might be more readily observed at that test temperature. Figure 4 shows that the fade is indeed higher at 0°C, particularly for cells aged at 60% SOC, although the difference is most pronounced at the higher cell aging temperatures. Power fade is extremely small at 25°C, and the expected trends may become visible only after much longer aging times than 4 weeks.



**Figure 4.** Power fade after 4 weeks of aging at 25, 35, 45, or 55°C.

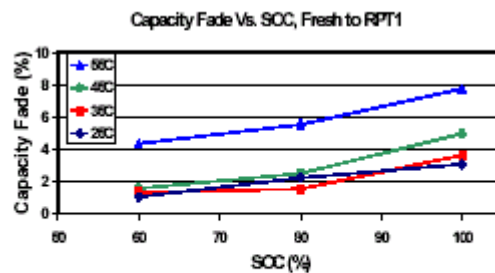
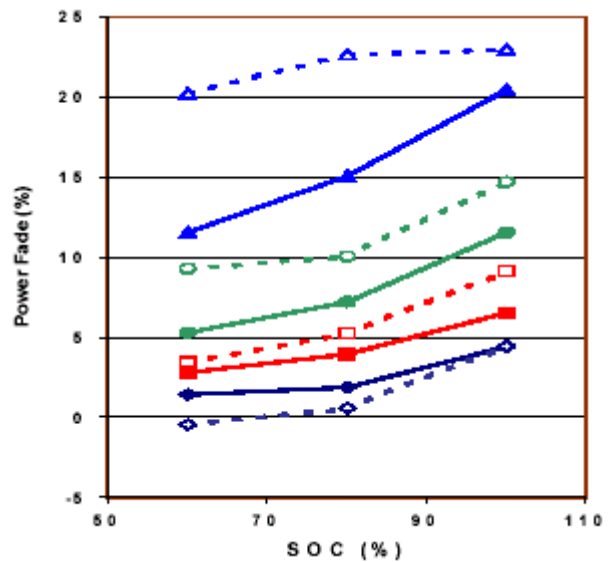


**Figure 5.** Capacity fade after 4 weeks aging.

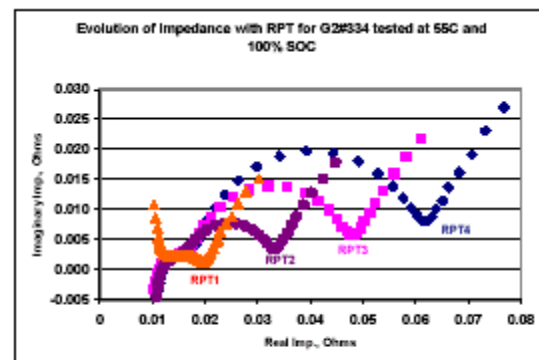
Cells exposed for 4 weeks to temperatures up to 55°C at three states-of-charge (60, 80, and 100%) show power fades as high as 20% and capacity losses of up to 8%. This coincides with a significant interfacial impedance increase in the cell. Figures 4 and 5 compare the power capability and capacity

under various aging conditions after the first 4-week aging period. Capacity fade at a C/1 discharge rate is most noticeable for cells aged at 55°C. The larger capacity fade observed at 100% SOC compared to 60% SOC (see Figure 5) parallels the dependence of power fade on SOC. In relative terms, capacity fade is smaller than power fade in that the maximum fade after 4 weeks is only about 8%. Capacity losses at 25, 35, and 45°C were all similar within measurement accuracy.

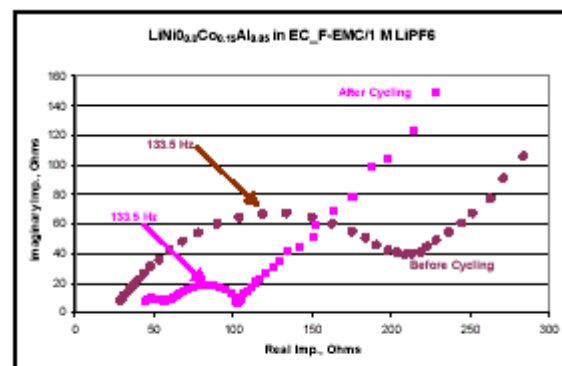
The final cell characteristic tracked during aging was AC impedance. A Nyquist plot of impedance results measured at 100% SOC after 4 weeks of aging at 55°C and at three SOC is given in Figure 6. The un-labeled curves on the left of the graph are the impedance results for the un-aged cells. The remaining groups of labeled curves show the dispersion of the aging effect from SOC. Impedance measurements were also carried out at 60% SOC on the same samples and these generally showed lower impedance and less change after aging. There is again a strong dependence on SOC with those aged at 100% showing the greatest amount of change. Banding of results by SOC is clearly emerging in Figure 6. Figure 7 shows the interfacial impedance growing with aging time in a typical cell. The growth of the impedance after aging is primarily in the interfacial impedance loop, as indicated by the semi-circle in the Nyquist plots. The interfacial impedance loop has been assigned to the cathode in an earlier generation of the cell that had a very similar chemistry.

Figure 8 shows further evidence to distinguish the SEI contribution from the charge transfer impedance. A virgin T-cell (cathode half-cell) stored immediately at 0°C without experiencing any aging condition showed a noticeable impedance loop with a peak at 133.5 Hz when measured in a 3-electrode experiment at 0°C. This cell should not have any significant SEI layer. A second T-cell was aged and cycled 5 times at 35°C and then brought down to 0°C for impedance measurements. Some SEI layer would be expected to form as a result of cycling and aging. The resulting complex impedance curve showed another loop with a higher peak frequency (5 kHz) in addition to the 133.5 Hz loop. The higher frequency loop is typically assigned to the growth of the SEI layer, while the loop peaked at 133.5 Hz is assumed to be the one corresponding to the charge transfer impedance.

To further analyze the fading results and develop a mathematical model and capability to predict battery calendar life, we employed a connectionist-normalized linear spline (CNLS) artificial neural network (ANN) to relate inputs of impedance and capacity to power fade. It has been found that the dimension of the impedance data can be reduced through use of data reduction techniques such as singular value decomposition. Transforming the data to a space of standard normal variables prior



**Figure 7.** Evolution of impedance with RPT for Gen2 #334 aged at 100% SOC and 55°C. Impedance was collected at 100% SOC.



**Figure 8.** Nyquist plots for cells with different history. The impedance values were measured at 0°C.

to training the ANN parameters also results in a data representation that is more easily modeled. The model has negligible bias and a low standard error compared to the span of the power fade data. Mathematical models of physical systems are constructed to facilitate our understanding of mechanisms that lead to specific responses and to enable response predictions. They are constructed in two basic frameworks: deductive (or

phenomenological) and inductive (or data-based). When possible, models are built in the phenomenological framework to reflect our understanding of the fundamental mechanisms underlying complex phenomena, but it is often difficult to obtain satisfactory simulations using this approach. An alternative is the inductive model. These models are parametric frameworks with databased training of the parameters that seek to simulate input/output relations as interpolations among measured data. They do so through adjustment of their parameters.

Artificial neural networks are frameworks for creating inductive mappings. We use an ANN for the inductive modeling of input/output relations in lithium-ion electrochemical cells. The output is a measure of power fade in lithium-ion cells. Cell capacity is used directly as an input along with a metric of cell impedance.

Because successful model construction in inductive frameworks requires that models be parsimonious, redundancy in input information needs to be reduced as much as possible. Further, model accuracy is improved when we map inputs from a well-distributed input space. Therefore, we also consider the use of transformations that expand measured data into well-behaved spaces. We use the singular value decomposition (SVD) and Rosenblatt transform to accomplish these goals. We choose to use the CNLS network here, because it is particularly well suited to the current application. It is an ANN of the radial basis function type with the following form:

$$g(\mathbf{x}) \cong y = \frac{\sum_{j=1}^N A_j \left\{ \frac{1}{\|\mathbf{x} - \mathbf{c}_j\|} \right\} w(\mathbf{x}, \mathbf{c}_j, \beta)}{\sum_{j=1}^N w(\mathbf{x}, \mathbf{c}_j, \beta)} \quad -\infty < \mathbf{x} < \infty$$

The quantity  $y$  is the ANN output, and  $g(\mathbf{x})$  is the function it seeks to approximate. It does so using the radial basis functions  $\frac{1}{\|\mathbf{x} - \mathbf{c}_j\|}$ ,  $w(\mathbf{x}, \mathbf{c}_j, \beta)$ , which are dependent on location in input space,  $\mathbf{x}$ , center locations  $\mathbf{c}_j$ , and widths  $\beta$ .  $A$  is a  $1 \times n$  row vector of parameters corresponding to the coefficients in the Taylor series expansion of  $g(\mathbf{x})$

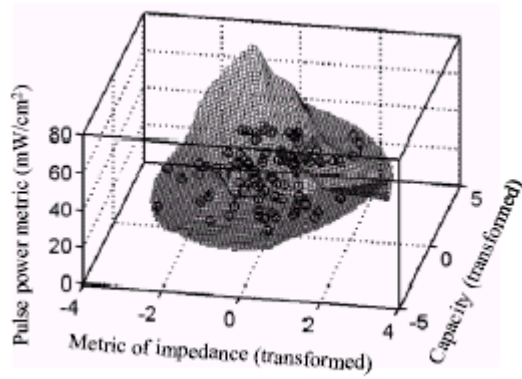
at the center location  $\mathbf{c}_j$ . These are the parameters of the CNLS net and can be identified or “trained” using any of a number of schemes. The basic idea behind the CNLS net is that it approximates a function with linear surfaces in various regions of the function, then splines the approximations together. In the current application, we train the parameters using weighted least squares where the weighting function is the same radial basis function used in the ANN.

The following examples illustrate the use of ANN tools to predict power fade of lithium-ion cells. We first train an ANN to simulate the input/output characteristics of the 18650 lithium-ion cell performance. Given the impedance estimate for a cell and its capacity, we train the ANN tool to predict a metric of the cell’s power fade. The CNLS net is trained using exemplars of two inputs: cell capacity and the real part of the first column in the compatibility matrix of the SVD of the impedance. These two inputs are transformed into a space that is approximately uncorrelated and normalized using the Rosenblatt transform before the ANN training.

Figure 9 shows a trained CNLS network that correlates the pulse power metric with impedance and capacity data, transformed by the SVD and Rosenblatt transform. The pulse power capability of the cell is measured by discharge and charge at 10% increments from 90% to 10% state-of-charge (SOC), as shown in Figure 3. The metric used to track power fade was the power meeting the 300-Wh PNGV available energy requirement. The trained surface that represents the power fade correlating the impedance and capacity metrics resulted in a sample mean of the errors of the order of  $-0.0145$  with sample standard deviation of  $2.416$ . The pulse power capability values span a range of approximately  $50 \text{ mW/cm}^2$ . The former result leads to the conclusion that model bias is negligible. Model standard error is approximately five percent of the span of the data.

Our intent is to use this type of approach for cell life predictions under conditions of temperature and SOC that are within the range of experimental data. The model will also be capable of predicting cell performance at various stages of life under different conditions. The data reduction tools will continue to be applied to expand complex

phenomena into separate components and to determine and interpret complex behavior mechanisms so that life prediction can cover a wide spectrum of use conditions.





## 4. Diagnostics

### a. Diagnostic Evaluations of Gen 1 and Gen 2 Cells and Cell Components

*Khalil Amine, Daniel Abraham, Jun Liu, Chun-hua Chen, Michael Stoll, Yoo-Eup Hyung and Gary Henriksen*

*Argonne National Laboratory, Argonne, IL 60439*

*(630) 252-3838; fax: (630) 252-4176; e-mail: [amine@cmt.anl.gov](mailto:amine@cmt.anl.gov)*

*Rick Haasch and Scott MacLaren*

*Center for Microanalysis of Materials, University of Illinois at Urbana-Champaign*

*(217) 265-4065; email: [haasch@uiuc.edu](mailto:haasch@uiuc.edu)*

---

#### Objectives

- Continue development of diagnostic techniques to identify and elucidate parameters that cause capacity and power fade in Gen 1 and Gen 2 cells.
- Apply these techniques to cell components to identify the most effective techniques for cell performance analysis.
- Determine mechanisms of power fade from data obtained by ANL and other participating laboratories.

#### Approach

- Quantitative analysis of gases generated in 18650 Gen 1 and Gen 2 cells during formation cycling and accelerated aging tests (elevated temperature calendar-life and cycle-life tests).
- Qualitative and quantitative analysis of electrolyte composition changes during accelerated aging tests.
- Reference electrode and electrochemical impedance spectroscopy (EIS) measurements to determine relative contributions of the positive and negative electrodes to cell impedance.
- Surface and bulk characterization of electrode materials by various microscopy and spectroscopy techniques to identify the best techniques for studying chemical, physical, and structural changes in electrode materials resulting from accelerated aging tests.
- Examination of current collector and separator materials to determine changes that result from accelerated aging tests.

#### Accomplishments

- Identified and quantified the gases generated in Gen 1 and Gen 2 cells. The experimental fixture that was designed to collect gases from Gen 1 cells was modified to accommodate Gen 2 cell design.
- Developed experimental protocols to identify and quantify electrolyte components in Gen 1 and Gen 2 cells by high performance liquid chromatography (HPLC).
- Determined, via reference electrode and EIS measurements, that the positive electrode is the main contributor to impedance rise in Gen 1 cells. Initial results from Gen 2 cells indicate that the impedance of the negative electrode is comparable to that of the positive electrode.
- Identified surface species on positive electrodes from Gen 1 and Gen 2 cells by scanning electron microscopy (SEM) and X-ray photoelectron spectroscopy (XPS).

- Evaluated pitting characteristics of the Al current collector and investigated its effects on cell impedance rise.
- Determined, via SEM examination and electrochemical studies, that the separator is unlikely to cause significant impedance rise in Gen 1 cells.

### Future Studies

- Continue development of diagnostic tools that will enable
  - determination of surface layer thickness on positive and negative electrodes
  - characterization of oxide particles in the positive electrodes to determine differences in surface and bulk properties.
  - characterization of the negative electrodes
- Identify battery components responsible for capacity and power fade in Gen 2 cells.
- Formulate mechanisms to explain capacity and power fade in Gen 1 and Gen 2 cells.
- Compare diagnostic data from Gen 1 and Gen 2 cells to determine reasons for the superior stability of the Gen 2 cells during accelerated aging.

### Publications

Factors Responsible for Impedance Rise in High Power Lithium Ion Batteries, K. Amine, C.H. Chen, J. Liu, M. Hammond, A. Jansen, D. Dees, I. Bloom, D. Vissers, G. Henriksen, *J. Power Sources* 97-98: 684-687, (2001).

Symmetric Cell Approach and Impedance Spectroscopy of High Power Lithium-Ion Batteries, C.H. Chen, J. Liu, K. Amine, *J. Power Sources*, 96 (2): 321-328 (2001).

Symmetric Cell Approach Towards Simplified Study of Cathode and Anode Behavior in Lithium Ion Batteries, C. Chen, Jun Liu, and K. Amine, *Electrochem. Commn.* 3 (1): 44-47 (2001).

Solid Electrolyte Interface Formation on Lithium-Ion Electrodes, Y. Wang, X. Guo, S. Greenbaum, J. Liu, and K. Amine, *Electrochemical and Solid-State Letters*, 4 (6) A68-A70 (2001).

Change of Conductivity with Salt Content, Solvent Composition, and Temperature for Electrolyte of LiPF<sub>6</sub> in Ethylene Carbonate-Ethyl Methyl Carbonate, M. S. Ding, K. Xu, S. S. Zhang, K. Amine, G. L. Henriksen, and T. R. Jow, *J. Electrochem. Soc.*, 148(10), 1, (2001).

### Introduction

The aim of the diagnostics effort is to develop a thorough understanding of the phenomena that limit the performance and calendar life of lithium-ion cells that employ the Gen 1 and Gen 2 chemistry. The ANL approach includes (1) understanding electrode-electrolyte reactions that result in gas generation and electrolyte composition changes, (2) identifying the cell components

responsible for impedance rise during accelerated aging, and (3) characterization of electrode and separator materials to determine changes (if any) that occur during electrochemical cycling and long-term storage at elevated temperatures.

## Gas Generation and Electrolyte Changes in Gen 2 Cells

The cell puncture and gas collection fixture, developed by ANL to collect and quantify the gases generated in Gen 1 cells, was modified to collect gases from Gen 2 cells. The gases collected were analyzed by a gas chromatography-mass spectroscopy (GC-MS) technique. The total volume of gases generated in Gen 2 cells was small (~3 ml). Most of this volume was generated during the formation process, and included gases such as CO<sub>2</sub>, CO, CH<sub>4</sub>, C<sub>2</sub>H<sub>6</sub>, C<sub>2</sub>H<sub>4</sub> and a small amount of C<sub>2</sub>H<sub>2</sub>; these gases are associated with electrolyte reduction and formation of the solid-electrolyte interface (SEI) layer at the negative electrode. Upon accelerated aging of Gen 2 cells, the gas volumes showed a small (~1 ml) initial increase and then leveled off. The gas compositions in the cells also show some initial changes. A typical example for calendar life cells that were aged at 55°C (see Fig. 1) shows that the concentrations of CO<sub>2</sub> and CH<sub>4</sub> in the cells decrease, whereas the concentrations of CO, C<sub>2</sub>H<sub>6</sub> and C<sub>2</sub>H<sub>4</sub> increase. The gas compositions do not change significantly after the initial period, which suggests an equilibrium of gas-producing reactions in the cells. Furthermore, these observations suggest that, after the initial period, the power fade mechanisms are not directly associated with continued gas generation.

The initial electrolyte formulation for Gen 2 cells was 1.2 M LiPF<sub>6</sub> in 3:7 weight ratio EC:EMC. After the formation process, the electrolyte contained seven identifiable alkyl- and dialkyl-carbonate species, produced from transesterification reactions of the starting alkyl carbonates and their reaction products. The compounds were identified as EC, DMC, EMC, DEC and the three dialkyl-2,5-dioxahexanecarboxylates, dimethyl-, ethylmethyl-, and diethyl-2,5-dioxahexanecarboxylate (DMDOHC, EMDOHC, and DEDOHC, respectively). Analysis of electrolyte samples from cells subjected to accelerated aging tests showed

that the bulk electrolyte composition was only marginally different from cells that had undergone only the formation cycles. Representative data from a calendar life cell, tested at 55° C for 20 weeks, are shown in Figure 2. The overall changes in bulk electrolyte composition after accelerated aging are small and probably not responsible for the power fade observed in the cells.

## Micro-reference Electrode Studies

ANL established a micro-reference electrode technique to study the relative contributions of the positive and negative electrodes to cell impedance. The reference electrode was a tin-plated copper wire, insulated by a 3 μm polyurethane enamel, which prevented mixed potentials along the length of the wire. For cell assembly, the insulating enamel was stripped from the wire tip, and the reference electrode was placed between two separator membranes that electrically insulated it from the positive and negative electrodes. After cell assembly, the tin plated wire tip was charged with lithium from the negative electrode, using a negligibly small quantity of active lithium (~200 μA min). The cell was then subjected to HPPC cycling. Area specific impedance (ASI) values for the cathode and anode were calculated, based on the potential change at each electrode relative to the LiSn reference electrode, resulting from the current pulse. For Gen 1 cells, the bulk of the impedance rise was determined to be associated with the positive electrode. Furthermore, electrochemical impedance spectroscopy (EIS) studies on symmetric cells showed that the impedance rise could be attributed to charge transfer resistance at the interface between the liquid electrolyte and the positive electrode surface. For Gen 2 cells, initial results show that the negative electrode contribution to impedance rise is comparable to that of the positive electrode. Typical data from a Gen 2 control cell (that underwent only formation cycles) and from a cell that was cycle-life tested at 45°C, 60% SOC for 4 weeks are shown in Figs. 3a and 3b, respectively. For both cells, the impedance values associated with the

negative electrode are comparable to those associated with the positive electrode.

### Characterization of Electrode Materials

Electrode materials from Gen 1 and Gen 2 cells were examined to identify the surface layers that contribute to cell impedance. Micrographs from laminates of the positive electrode samples, that had no exposure to electrolyte, clearly show the separate active metal oxide material, graphite, acetylene black, and the PVDF binder (for example, see Fig. 4). On positive electrode samples taken from control cells (formation cycles only), surface layers were observed on the oxide particles. In addition to these layers, particulate-type features were observed on oxide particles from cells that were subjected to accelerated aging (see Fig. 5). These features were more pronounced in samples that were tested for longer durations and/or at higher temperatures. Similar features were not observed on the surface of the graphite negative electrodes, which indicates that the particulate matter resulted from localized reactions at the metal oxide surface.

In our study of the Gen 1 cells, X-ray photoelectron spectroscopy (XPS) spectra were obtained from  $\text{LiNi}_{0.8}\text{Co}_{0.2}\text{O}_2$  powder, fresh positive and negative electrode laminates, and on laminates from cells that were subjected to electrochemical cycling. Spectra from a fresh (uncycled) positive electrode laminate are shown in Fig. 6. The C1s spectrum contains contributions from graphite, acetylene black and PVdF ( $(\text{CF}_2\text{CH}_2)_x^-$ ). The F1s spectrum shows a strong peak at 687.6 eV that is from the PVdF binder, and a weak peak at 684.7 eV from a LiF impurity. The Li1s peak contains contributions from LiF,  $\text{Li}_2\text{CO}_3$  and  $\text{LiNi}_{0.8}\text{Co}_{0.2}\text{O}_2$  that cannot be resolved. The O1s data has peaks at 529.6 eV and 531.6 eV, from the oxide and carbonate, respectively. The weak Co  $2p_{3/2}$  peak at 779.7 eV is from the  $\text{Co}^{3+}$  in  $\text{LiNi}_{0.8}\text{Co}_{0.2}\text{O}_2$ . The binding energy of the major Ni  $2p_{3/2}$  peak (at 854.7 eV) is closer to the expected binding energy for  $\text{Ni}^{2+}$ ;

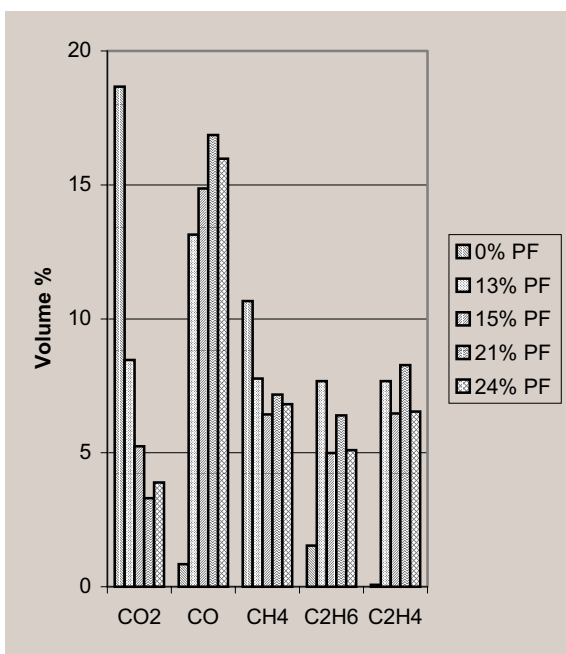
however, it appears likely that areas containing both  $\text{Ni}^{2+}$  and  $\text{Ni}^{3+}$  are present on the oxide surface.

On positive electrode samples from the control cell (formation cycles only) and aged cells, additional surface films were observed. In the O1s spectra, the  $\text{LiNi}_{0.8}\text{Co}_{0.2}\text{O}_2$  signal was relatively strong for the fresh sample but the intensity of this peak was either much lower or absent for samples taken from the cells aged at elevated temperatures (see Fig. 7). This decrease in peak intensity indicates the presence of a surface film on the  $\text{LiNi}_{0.8}\text{Co}_{0.2}\text{O}_2$  particles that is thicker for the samples aged at the higher temperatures. The absence of peak intensity for the 60°C and 70°C samples suggests that the surface film is thicker than the escape depth of photoelectrons originating from  $\text{LiNi}_{0.8}\text{Co}_{0.2}\text{O}_2$ . In contrast, the graphite peak at 284.5 eV in the C1s spectra (Fig. 7) is strong even for the aged samples. This difference between the graphite and  $\text{LiNi}_{0.8}\text{Co}_{0.2}\text{O}_2$  peak intensities suggests that the  $\text{LiNi}_{0.8}\text{Co}_{0.2}\text{O}_2$  particles are preferentially covered by the surface species.

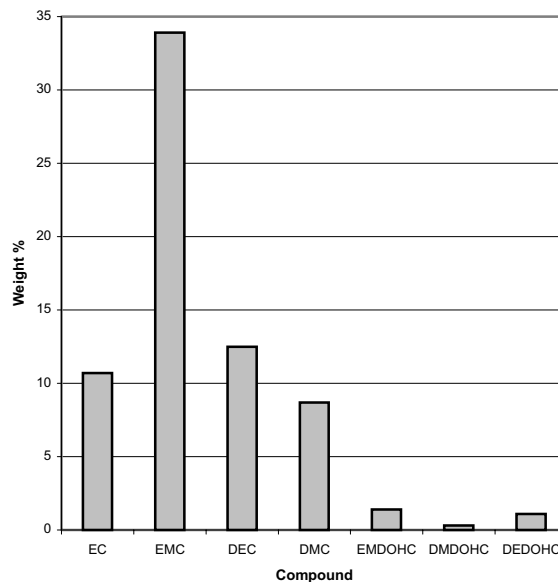
The XPS data also show the presence of  $\text{LiF}$ ,  $\text{Li}_x\text{PF}_y^-$  and  $\text{Li}_x\text{PF}_y\text{O}_z^-$  type compounds in both the control and aged samples (see Fig. 8). Degradation of cell performance is often attributed to the presence of these compounds on the electrode surface. However, the mere presence of LiF cannot be responsible for the observed cell power fade because it is also present on the positive electrodes removed from the control cell (0% power fade). In a similar manner, cell power fade cannot be attributed merely to the existence of surface polymeric compounds because these species are also observed in the control samples. Initial indications are that phase segregation at the oxide particle surface may be a major factor in the impedance rise at the cathode, as observed in both the Gen 1 and Gen 2 cells.

### Future Work

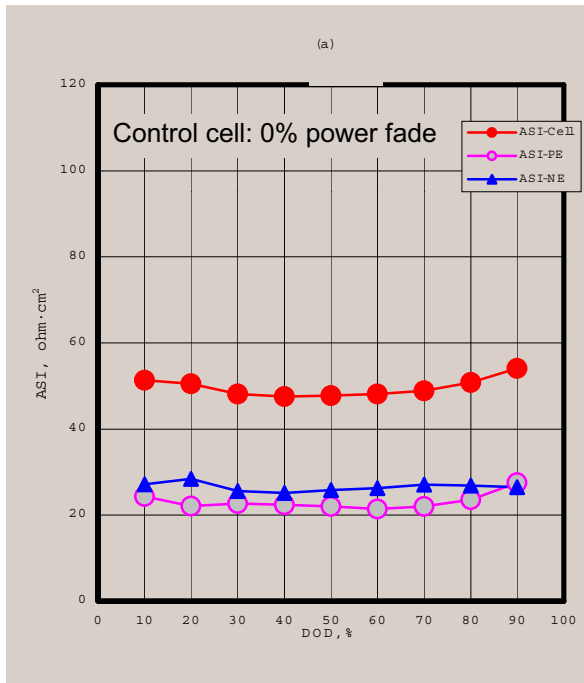
Diagnostic studies of Gen 2 cells will continue in order to identify and understand the mechanisms that control cell performance and life. Changes in the bulk structure and surface structure of  $\text{LiNi}_x\text{Co}_y\text{Al}_z\text{O}_2$  particles will be studied by techniques such as transmission electron microscopy (TEM). The thickness of electrode surface layers will be measured by sputter-depth profiling during XPS and SIMS (secondary ion mass spectrometry) experiments. Characterization of the negative electrode will be expanded to include techniques such as SEM and XPS to elucidate the role of this electrode in the capacity and power fade processes.



**Figure 1.** Gas analysis data from Gen 2 cells. Other gas components, including O<sub>2</sub>, N<sub>2</sub>, and Ar, are excluded from the figure for clarity. The 0% Power fade (PF) data is from a cell that underwent only formation cycles. All other cells were calendar-life tested at 55°C, 60% SOC for various durations.



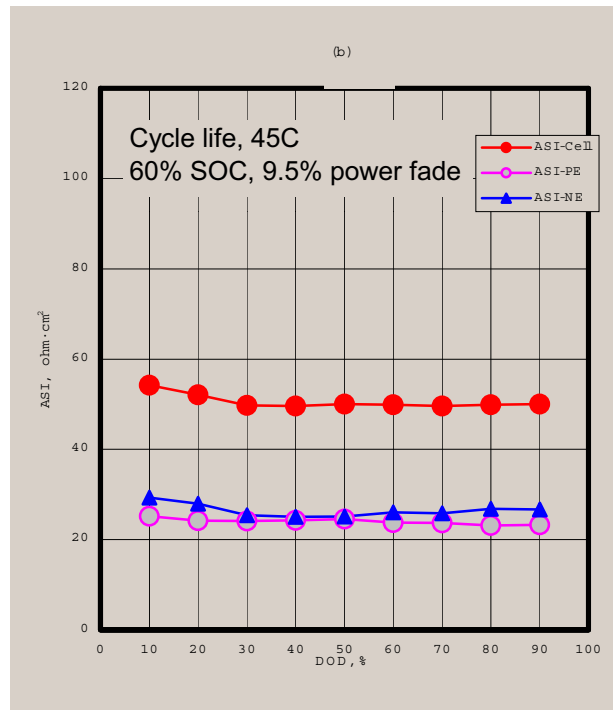
**Figure 2.** High-performance liquid chromatography data from a Gen 2 calendar life cell that was held at 55°C and 60% SOC for 20 weeks. Note that the starting electrolyte contained only two solvent species, EC and EMC, at a weight ratio of 3:7.



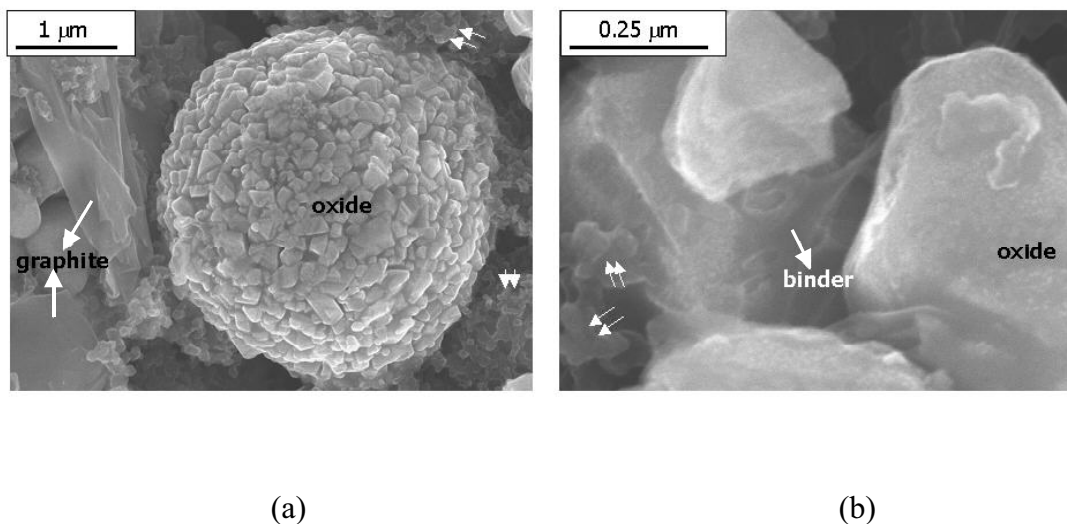
**Figure 3.** Micro-reference electrode data from Gen 2 cells that showed (a) 0% power fade (formation cycles only), and (b) 9.5% power fade at 45°C, 60% SOC. In both cases, the impedance of the negative electrode is comparable to that of the positive electrode.

(a)

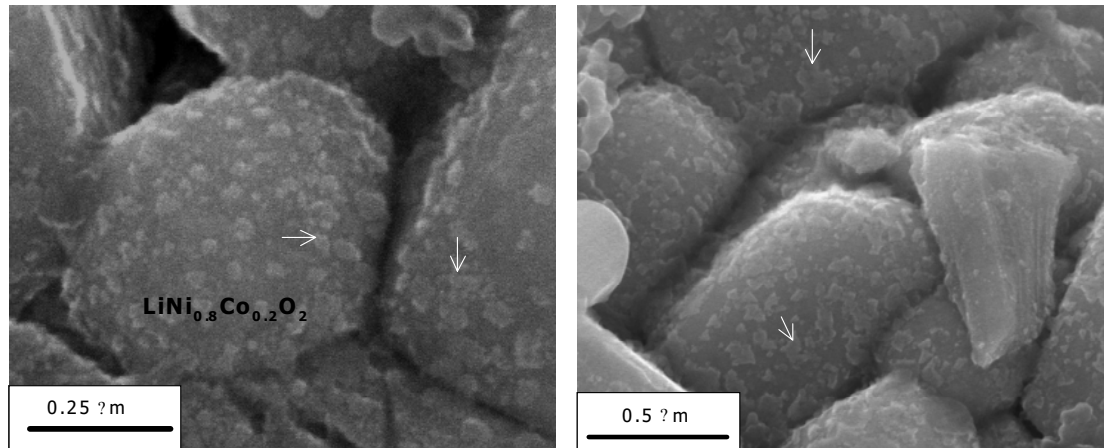
(b)



**Figure 4.** Typical micrographs from a positive laminate showing (a) oxide, graphite and acetylene black (marked by double arrows), and (b) PVdF binder.



**Figure 5.** Particulate-type features (marked by arrows) observed on surfaces of oxide particles in positive electrodes from (a) 40°C, 60% SOC calendar-life Gen 1 cell, (b) 70°C, 60% SOC cycle tested Gen 1 cell.



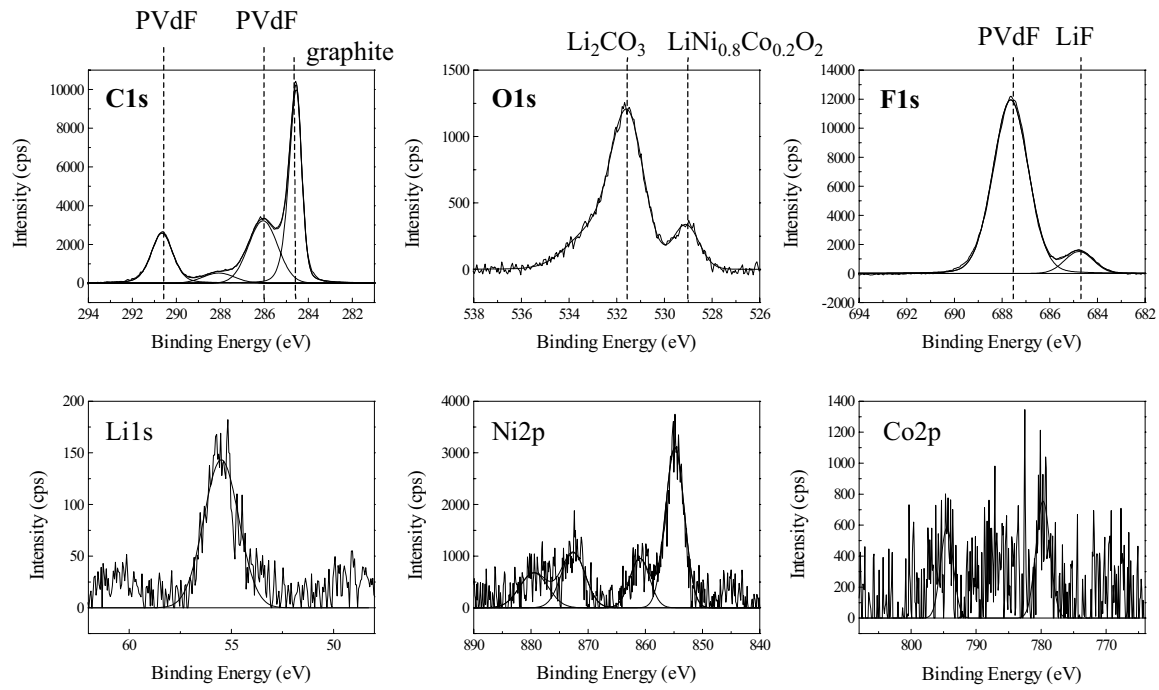


**Figure 6** C1s, O1s, F1s, Li1s, Ni2p and Co2p XPS spectra for a fresh (uncycled)  $\text{LiNi}_{0.8}\text{Co}_{0.2}\text{O}_2$  cathode laminate.

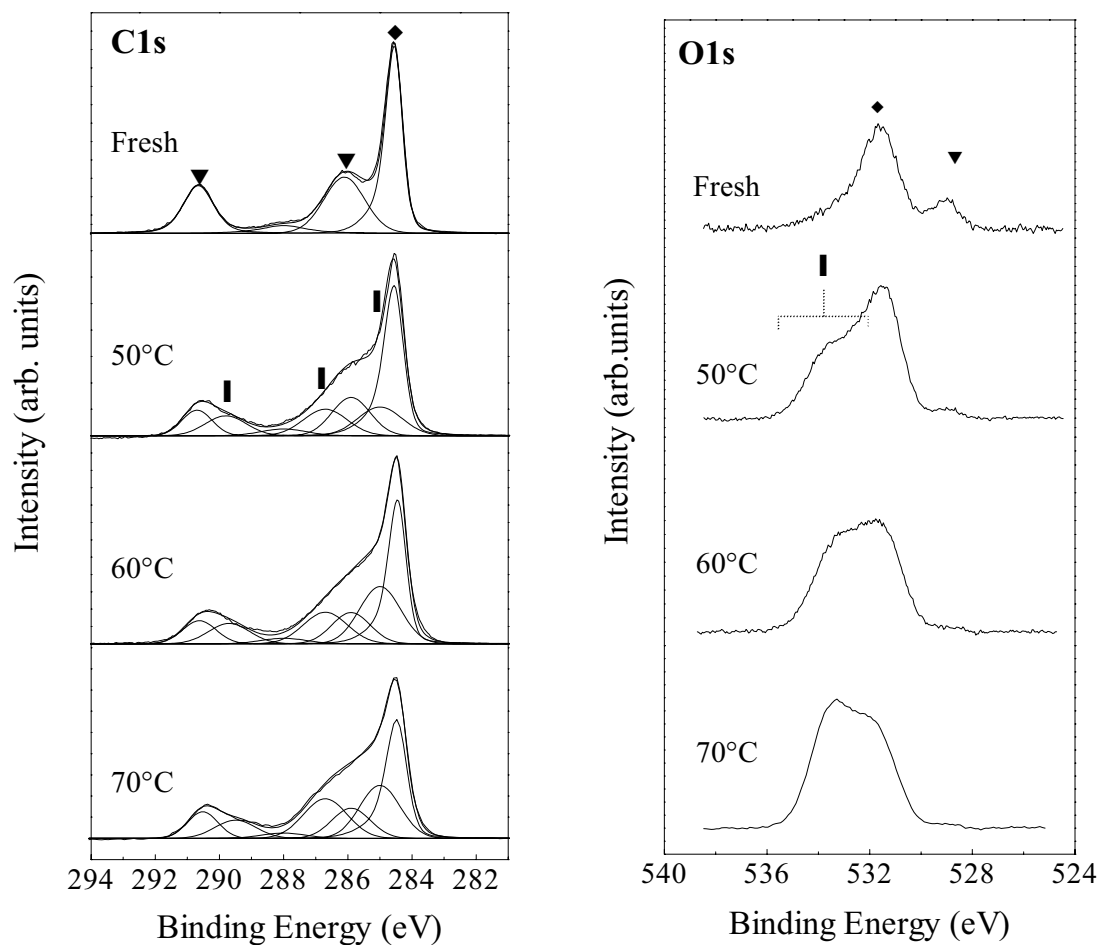


**Figure 7** C1s and O1s XPS spectra for fresh and calendar-life tested  $\text{LiNi}_{0.8}\text{Co}_{0.2}\text{O}_2$  cathode samples. Tested samples were stored at 50, 60 and 70°C at 60%SOC. In the C1s spectra, the marked positions are PVdF (▼), graphite (◆), and surface layer species (|). In the O1s spectra, the marked positions are  $\text{LiNi}_{0.8}\text{Co}_{0.2}\text{O}_2$  (▼),  $\text{Li}_2\text{CO}_3$  (◆), and surface layer species (|).

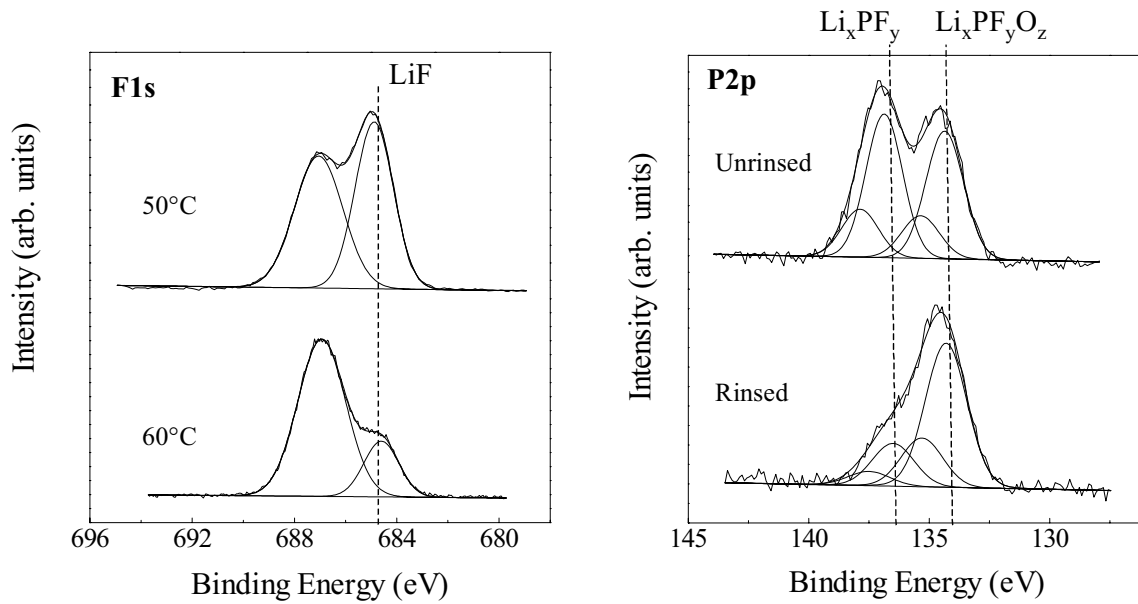


**Figure 8** F1s and P2p XPS spectra for calendar-life  $\text{LiNi}_{0.8}\text{Co}_{0.2}\text{O}_2$  cathode samples, tested at 50 and 60°C at 60% SOC. The F1s spectra show LiF peaks, and the P2p spectra show  $\text{Li}_x\text{PF}_y$  and  $\text{Li}_x\text{PF}_y\text{O}_z$  species. The relative proportion of these compounds is altered by test temperature, and by rinsing in solvents like DEC.

## b. The Development of Diagnostic Techniques for Examining Cathode Structural Degradation

James McBreen, M. Balasubramanian, X. Q. Yang, and X. Sun

Bldg. 555 Brookhaven National Laboratory, , P.O. Box 5000, Upton, NY 11973-5000

Phone: (631)344-4513, fax. (631)344-5815; email [jmcbreen@bnl.gov](mailto:jmcbreen@bnl.gov)

---

### Objective

- Determine the nature of the degradation processes that cause increase in impedance of electrodes in high power lithium-ion cells

### Approach

- Apply techniques that can identify and characterize changes in the bulk and surface of electrodes from cycled and abused cells. A combination of high-resolution *in situ* x-ray diffraction (XRD) and x-ray absorption spectroscopy (XAS) is used to characterize the bulk. Soft x-ray XAS is used to characterize the surface.
- Supplement x-ray work with electrochemical characterization, including EIS.

### Accomplishments

- Soft x-ray XAS detected the presence of LiF on the surface of cycled Gen 1 and Gen 2 cathodes.
- XAS at the P K edge detected the presence of insoluble P species in cycled Gen 1 and Gen 2 cathodes.

### Future Directions

- Soft x-ray XAS at O and F K-edges and at the L-edges of Ni and Co
- XAS studies at the P K-edge to identify P containing decomposition products from the electrolyte
- Studies to identify the contribution of these decomposition products to the impedance increase and power fade

### Publications

- *In Situ* X-Ray Diffraction and X-Ray Absorption Studies of High-Rate Lithium-Ion Batteries, M. Balasubramanian, X Sun, X. Q. Yang, and, J. McBreen, *J. Power Sources*, 92, 1 (2001).
  - *In Situ* X-Ray Absorption Studies of a High-Rate LiNi<sub>0.85</sub>Co<sub>0.15</sub>O<sub>2</sub> Cathode Material, M. Balasubramanian, X Sun, X. Q. Yang, and, J. McBreen, *J. Electrochem. Soc.*, 147, 2903 (2000).
  - Studies of High-Rate Lithium Batteries Using Synchrotron Techniques, M. Balasubramanian, X. Sun, X. Q. Yang and J. McBreen, Proc. Symp. on Rechargeable Lithium Batteries, K. M. Abraham, E. S. Takeuchi, and M. Doyle, Eds. PV 2000-21, 198th Meeting of The Electrochemical Society, Phoenix, Arizona, October 22-27, 2000.
-

Extensive XRD and XAS work in FY 2000 did not detect any changes in the bulk structure of the cathodes from cycled and abused Gen 1 cells. This indicated that the power loss was due to some surface phenomenon. Accordingly, in FY 2001, techniques with surface sensitivity were applied to study the problem. The technique used was soft x-ray XAS at Beam Line U7A at NSLS. The soft x-rays covered a range of 500 to 1000 eV. This encompasses the K edges of O and F and the  $L_3$  and  $L_2$  edges of the elements from Cr to Ni. Two detection methods with different sampling depths were used. One was fluorescence with a sampling depth of  $1000 \pm 2000$  Å. The other was electron yield with a sampling depth of 50 Å. Figure 1 shows XAS spectra in the soft x-ray region for a fresh Gen 1 cathode and a Gen 1 cathode that had been cycled at elevated temperature. XAS at the F K-edge

demonstrates the presence of poly(vinylidene fluoride) (PVdF) in as prepared electrodes. In addition to PVdF LiF was found on the surface of cycled electrodes. Fitting of the F K edge XAS data indicated that the amount of F associated with LiF and PVdF was comparable. The results also indicate that the PVdF in the cycled electrodes is largely intact and that the LiF comes from decomposition of  $\text{LiPF}_6$  from the electrolyte. Soft x-ray XAS also indicate Fe contamination of cycled cathodes. The Fe could come from corrosion of the Al current collectors or the cell can. More recently XAS was done on electrodes from cycled Gen 2 cells in both the electron yield and fluorescent mode. The results indicate that LiF penetrates into the electrode structure. This may indicate pore plugging which could contribute to the impedance rise. The results suggest that soft x-ray XAS is a valuable surface chemistry tool in the study of SEI (surface

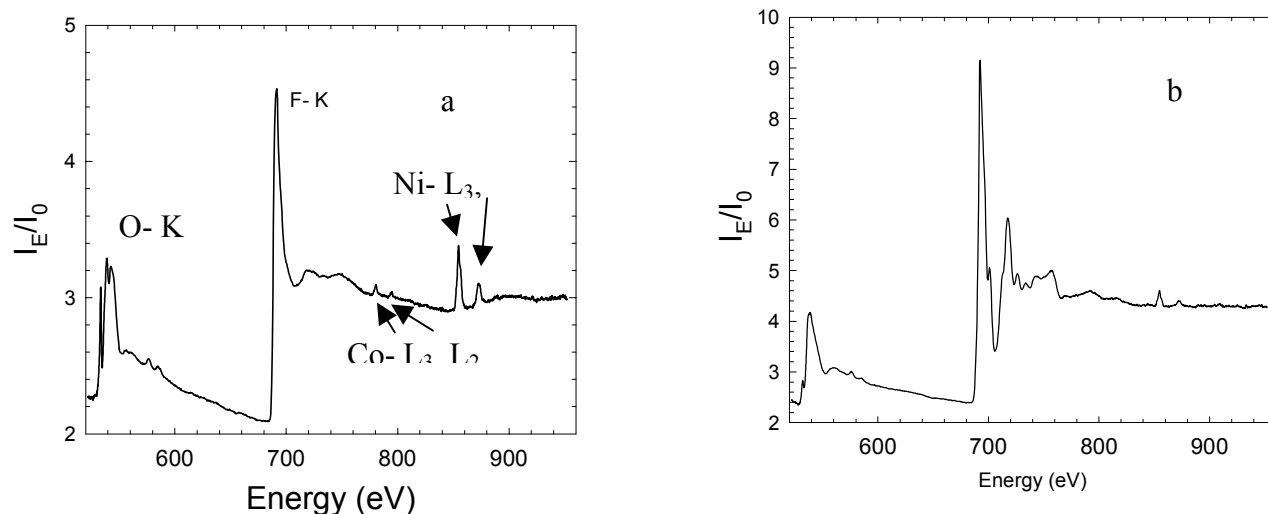


**Figure 1.** Soft x-ray XAS, in the electron yield mode, for (a) an as prepared Gen 1 electrode and (b) for a cycled electrode. Note the major changes at the F K edge in the region of 700  $\pm$  800 eV. Figure 1 (a) indicates the sources of the various features of the spectra.

XAS was also done at the P K edge on Gen 1 calendar life cathodes from ANL and on Gen 2 cycle life cells, from INEEL. The latter were washed in DME to remove residual  $\text{LiPF}_6$ . The results are shown in Figures 2 and 3. Figure 2 also shows a spectrum obtained for  $\text{Na}_3\text{PO}_4$ . P K-edge XAS indicates the presence of insoluble P compounds in cycled Gen-2 cathodes. There are at least two P containing decomposition products present. One of them may be  $\text{Li}_3\text{PO}_4$ , with the amount depending on the temperature of cell operation. Further interpretation of the P XAS spectra requires data on more standard compounds. Therefore, XAS at the F and P K-edges clearly identifies insoluble decomposition products from the electrolyte on the cathode. These are possible causes of power fade in cells at elevated temperatures. So far no inorganic decomposition product from the cathode active material has been identified.

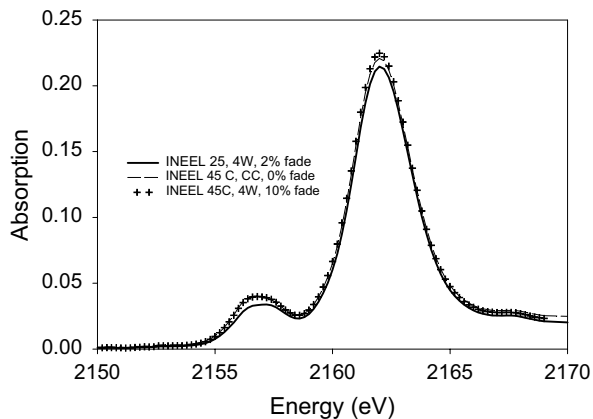


**Figure 2.** P K edge XAS for  $\text{Na}_3\text{PO}_4$  and for cathodes from ANL Gen 1 calendar life cells. The temperature ( $^{\circ}\text{C}$ ) and the test time (weeks) are indicated on the Figure.

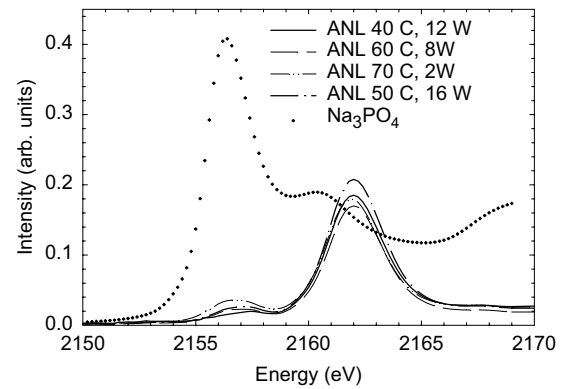


**Figure 3.** P k edge XAS for cathodes from INEEL cycle life cells. Cathodes were washed in DME to remove residual  $\text{LiPF}_6$ . The temperature ( $^{\circ}\text{C}$ ), the cycling time (weeks) and percentage power fade are indicated on the Figure. CC indicates no cycling.

### **c. Advanced Diagnostic Techniques for Characterizing Electrode Surfaces and Processes**

*Frank McLarnon, Robert KostECKI, Laura Norin, Philip Ross, Sherry Zhang, Kim Kinoshita, Xiangyun Song, John Kerr, James Pugh, and Steven Sloop*  
90-1142, Lawrence Berkeley National Laboratory, Berkeley CA 94720  
(510) 486-4636; fax: (510) 486-4260; e-mail: [frmcLarnon@lbl.gov](mailto:frmcLarnon@lbl.gov)

---

#### **Objectives**

- Use advanced diagnostic techniques to determine electrode structural, morphological, and surface changes that lead to cell performance degradation as it is cycled or aged.
- Study solid electrolyte interphase (SEI) formation and dissolution as cells are cycled or aged, and determine its effect on cell power and capacity loss.
- Identify electrolyte reactivity trends in lithium-ion cells with respect to cell history.

#### **Approach**

- Use atomic force microscopy, Raman microscopy, and other techniques to detect and characterize surface processes which contribute to cell deterioration.
- Use infrared spectroscopy and x-ray photoelectron spectroscopy to provide detailed chemical analyses of electrode surfaces.
- Use high-resolution transmission electron microscopy and energy dispersive x-ray analysis to determine changes of electrode crystallographic structure, particle morphology, and elemental composition which accompany cell cycling and aging.
- Use solvent extraction, gas chromatography, and thermal analysis to characterize lithium-ion cell components, and carry out control experiments to facilitate data interpretation.

#### **Accomplishments**

- Discovered that carbon disappears from the cathode surfaces of aged and cycled Gen 2 lithium-ion cells.
- Achieved good understanding of the chemical composition of the SEI on both anodes and cathodes of Gen 2 cells.
- Determined that the surface composition of particles of cathode active materials taken from tested Gen 2 cells differs from the particle bulk composition, which is uniform.
- Identified ethylene carbonate as an unstable component in the presence of Lewis acid salts (PF<sub>6</sub>, BF<sub>4</sub>) that leads to the formation of polymeric material (PEO or polycarbonate ethers) and the generation of CO<sub>2</sub> gas.
- Identified the presence of oxalate in Gen 1 and Gen 2 cells that may be responsible for self-discharge and production of CO.

#### **Future Directions**

- Continue systematic spectroscopic and microscopic studies of aged and cycled cells to correlate changes of electrode surface and structural characteristics with cell performance degradation.
- Correlate SEI composition with cell performance.
- Use quantitative techniques to determine reaction product distributions as a function of cell history, and use this data to develop models of cell performance and to predict cycle and calendar life

- Continue studies to identify cell reaction products and carry out control experiments to further enhance mechanistic understanding.

High-resolution Raman microscopy measurements at various locations on the surfaces of cathodes taken from tested Gen 1 cells revealed strong intensity variation of the sub-peaks which contribute to the overall “oxide” peak at  $520\text{ cm}^{-1}$ . These results not only provide clear evidence for significant spatial variations of the chemical composition and structure of  $\text{LiNi}_{0.8}\text{Co}_{0.2}\text{O}_2$  on the cathode surface but also confirm our earlier AFM and Raman observations of surface phase segregation. A series of Raman measurements on reference nickel and cobalt oxides was carried out to determine the origins of sub-peaks in the micro Raman spectra. We determined that tested cathode surfaces exhibit increased concentrations of  $\text{Ni}_2\text{O}_3$  or  $\text{NiO}_2$ , which are decomposition products of the original  $\text{LiNi}_{0.8}\text{Co}_{0.2}\text{O}_2$ . However, the exact stoichiometries of these new nickel oxide phase could not be determined because all higher-valent ( $n \geq 3$ ) nickel oxides are isostructural and display identical vibrational spectra. Raman microscopy spectra of tested Gen 2 cathodes displayed features typical for a partially charged electrode, *i.e.*, the cathode surface state of charge (SOC) is non-uniform and generally higher than expected for a cathode nominally poised to 0% SOC. AFM images of cathodes from tested cells showed no evidence of new oxide phase formation, suggesting improved surface stability of  $\text{LiNi}_{0.8}\text{Co}_{0.15}\text{Al}_{0.05}\text{O}_2$  compared to  $\text{LiNi}_{0.8}\text{Co}_{0.2}\text{O}_2$ . Thousands of micro-Raman spectra of Gen 2 cathodes recorded at 0.7 micron lateral resolution were converted to color-coded Raman image maps to illustrate how the surface composition [relative amounts of  $\text{LiNi}_{0.8}\text{Co}_{0.15}\text{Al}_{0.05}\text{O}_2$ , graphite, and acetylene black] varies over a  $40 \times 60$  micron area of a typical electrode (Fig. 1). The Raman image map for the aged cathode exhibits several sites of bare active material with no carbon deposit, in marked contrast to the Raman image maps of a single-sided cathode and a fresh cathode, both of which are almost completely covered with carbon black and graphite. The apparent disappearance of carbon from the cathode surface during testing therefore correlates with cell power loss; however, additional data from

Gen 2 cells with greater power fade are required to firmly establish such a correlation.

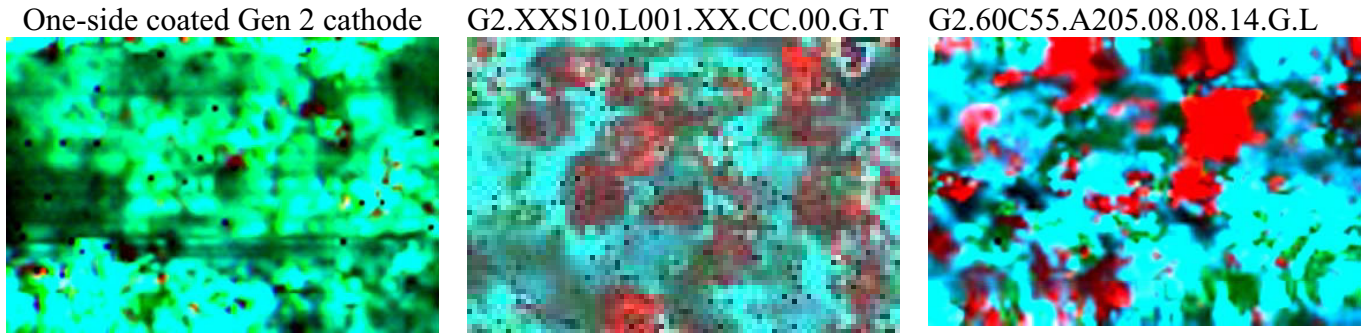
X-ray photoelectron spectroscopy (XPS) studies showed that the surfaces of fresh cathodes taken from both Gen 1 and Gen 2 cells were covered with PVDF and carbon, and no active material (Ni, Co) was observed before argon-ion sputtering of the cathode surface. This observation is consistent with LBNL’s Raman and AFM results (see above). Active material (Ni) does appear on the surfaces of cathodes taken from cells that were cycled/aged, the amount of which increases with increasing cell power fade. This observation appears to be consistent with the dissolution-deposition mechanism proposed earlier by LBNL (Kostecki and McLarnon). XPS also detected an organic film containing  $-\text{CH}_2-\text{O}-$  on both Gen 1 and Gen 2 cathode surfaces, which is possibly a solvent oxidation product. Figure 2 shows the XPS difference pattern between cell G2.60C55.A205.08.08.14.G.L (14% power fade) and a fresh cell (0% power fade), as compared with that between cell G2.60L25.I103.04.04.02.G.L (2% capacity fade) and the same fresh cell. Our analysis indicates that the thickness of this organic film increases in cells that display higher capacity fade. Surfaces of several tested Gen 2 cell anodes were studied using IR microscopy. A well-formed SEI layer with a peak at  $1650\text{ cm}^{-1}$ , possibly arising from the C=O stretching of Li alkyl carbonate, was observed on a fresh Gen 2 cell anode. This feature was also observed in four other tested Gen 2 cells, which indicates that the SEI layers on Gen 2 anodes remain mostly intact even after cells were cycled for up to 8 weeks and showed 14% power loss.

High-resolution transmission electron microscopy (HRTEM) and energy dispersive x-ray analysis (EDX) were used to investigate the crystallographic structure, particle morphology, and elemental composition of cathode active material ( $\text{LiNi}_{0.8}\text{Co}_{0.15}\text{Al}_{0.05}\text{O}_2$ ) from Gen2 cells. HRTEM of cathodes from cell G2.60C55.A205.08.08.14.G.L (aged at  $55^\circ\text{C}$  to 14% power fade) revealed no significant change in cathode crystal structure,

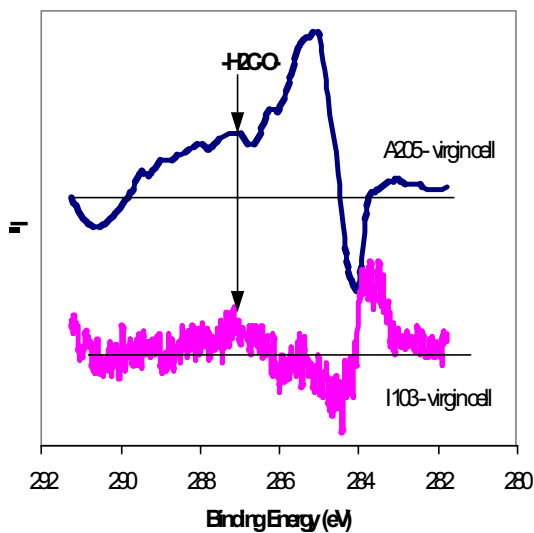
which was similar to that of as-received cathode powder. However, EDX revealed differences between the elemental composition near the surface and bulk of the cathode particles (typical data shown in Fig. 3). A thinner particle (Fig. 3a) appeared to be oxygen-rich near its surface, whereas the composition of a thicker particle (Fig. 3b) was uniform. These results can be interpreted by considering the distance over which the electron beam interacts with a specimen. For a thicker specimen, the elemental composition in its bulk contributes a greater fraction of the total signal that is detected. For a thinner specimen, the elemental composition of its surface layer contributes a greater fraction of the total signal, and the decreased distance of beam-specimen interaction yields improved analytical spatial resolution. Our EDX analysis suggests that the  $\text{LiNi}_{0.8}\text{Co}_{0.15}\text{Al}_{0.05}\text{O}_2$  undergoes only a small change in surface composition, *i.e.*, its bulk composition and crystal structure are unchanged, even after testing at 55°C. We have so far examined only a few Gen 2 cells using HRTEM and EDX. During FY 2002 we will characterize cells which will have been subjected to increased aging/cycling time, and we anticipate observing marked changes in the oxide structure and composition. The focus of this task will continue to involve HRTEM and EDX analyses of cathodes, because the cathode appears to play a major role in cell power fade.

The identification of reaction products in heated electrolyte samples has provided information on reaction pathways and possible effects on cell performance. Acid and base catalyzed transesterification products were observed in control experiments on electrolytes and in electrolytes

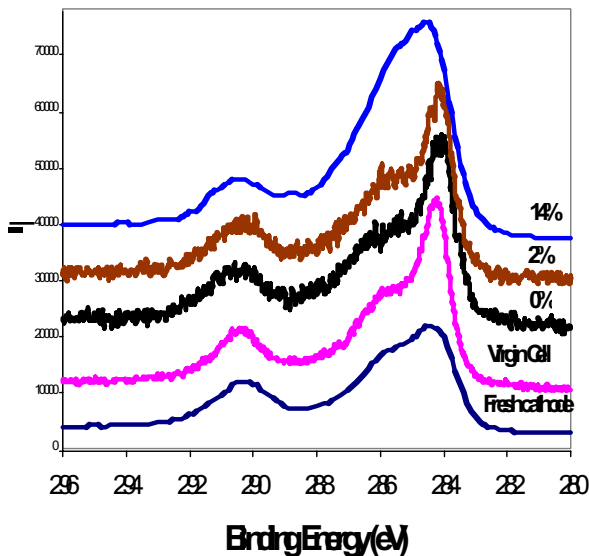
extracted from Gen 1 and Gen 2 cells. Scheme 1 shows the products of these reactions. Ring-opening of ethylene carbonate (EC) produces diethyl-2,5-dioxahexane carboxylate (DEDOHC) as shown in Scheme 2. In the Gen 2 electrolyte, EC-EMC, a mixture of products is formed which arises from the asymmetrical nature of EMC. All of these products are volatile and can be detected by gas chromatography. However, measurements of the rates of disappearance of EC and the appearance of the transesterification products as a function of temperature show that EC is much more reactive at ambient temperatures than the linear carbonates. The reactions of the linear carbonates may be accounted for by the transesterification products and the appearance of DEDOHC and its analogs, whereas the reaction of EC is not accounted for by volatile products. This observation can be explained by the formation of higher-molecular-weight products. Gel permeation chromatography of the electrolytes indicated the formation of polymers with molecular weights up to 15,000. The mechanism of polymer formation is suggested in Scheme 3, which also predicts the formation of  $\text{CO}_2$  (confirmed by measurements at Sandia National Laboratories). The  $\text{CO}_2$  can be reduced at anodes to form oxalate, formate (in the presence of water), carbonate, and CO (Scheme 4). We have detected these products in both Gen 1 and Gen 2 cells. The oxalate is soluble in the electrolyte and can migrate to the cathode where it is re-oxidized to  $\text{CO}_2$ , leading to cell self-discharge. A higher-molecular-weight product (18,000) was detected in a Gen 2 cell cathode that exhibited considerable power fade, a result which is consistent with a polymer coating the electrode. These mechanisms require further verification.



**Figure 1.** 60x40  $\mu\text{m}$  Raman microscope images Gen2 cathodes.  $\text{LiNi}_{0.8}\text{Co}_{0.15}\text{Al}_{0.05}\text{O}_2$ , carbon black, and graphite are represented by red, blue, and green, respectively



**Figure 2.** XPS spectra (upper panel) of Gen 2 cell cathodes show a weak peak at  $\sim 287$  eV, which is consistent with a  $-\text{CH}_2-\text{O}-$  moiety in a cathode surface film. The plot in the lower panel compares the XPS difference pattern between the cathode from cell G2.60C55.A205.08.08.14.G.L and a cathode from a fresh (virgin) cell with the cathode XPS difference pattern between cell G2.60L25.I103.04.04.02.G.L and the same fresh cell. These data indicate a trend of increasing cathode surface film thickness in cells with greater capacity fade.



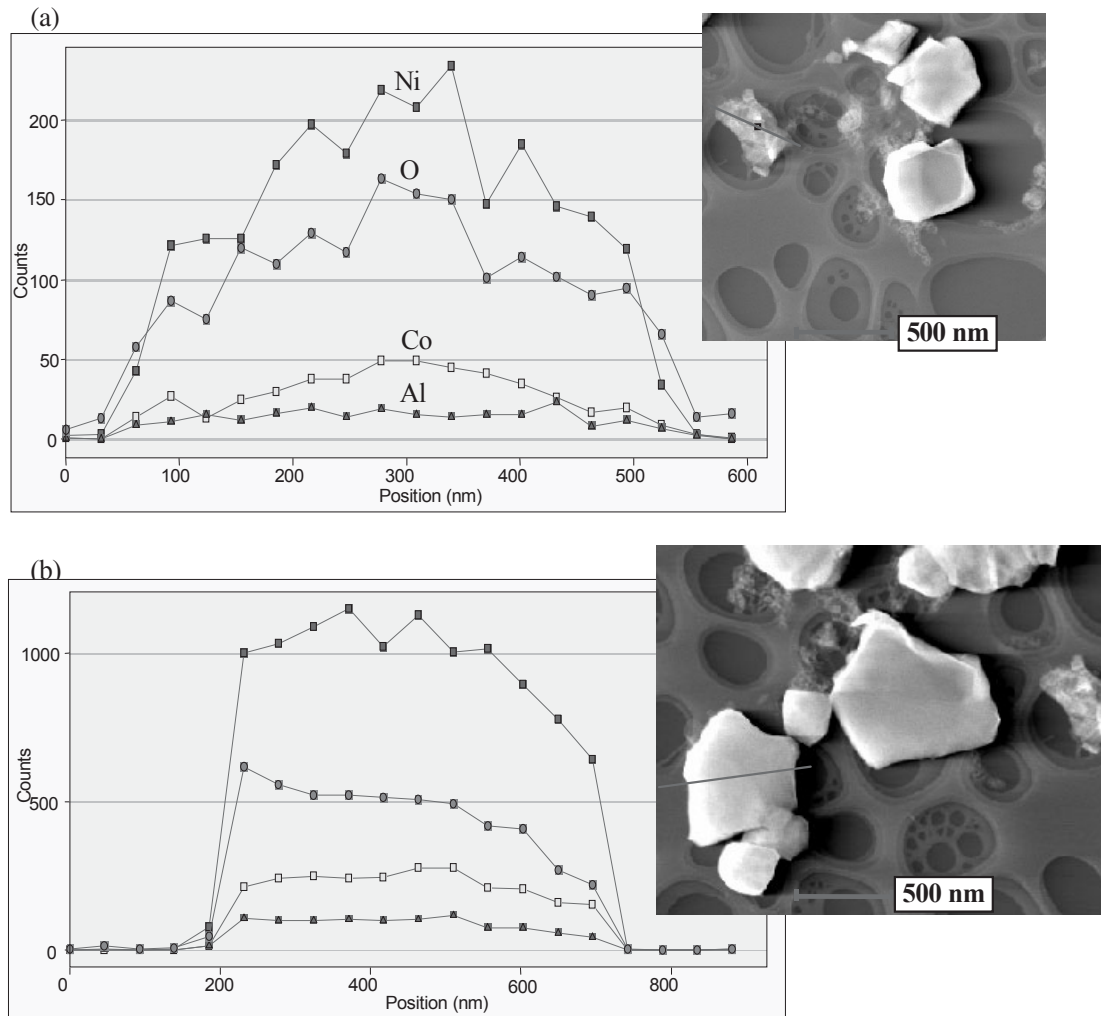
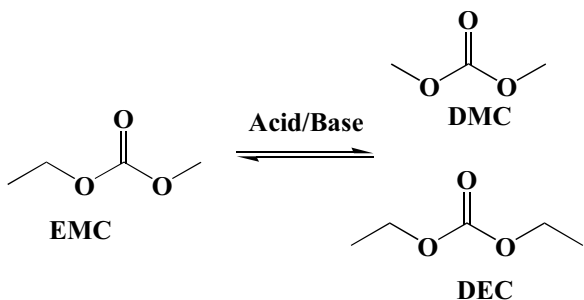
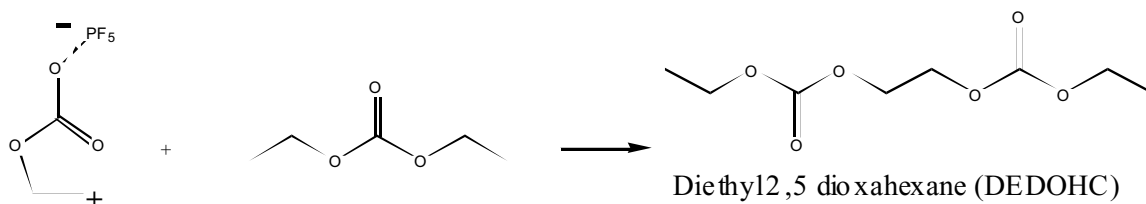


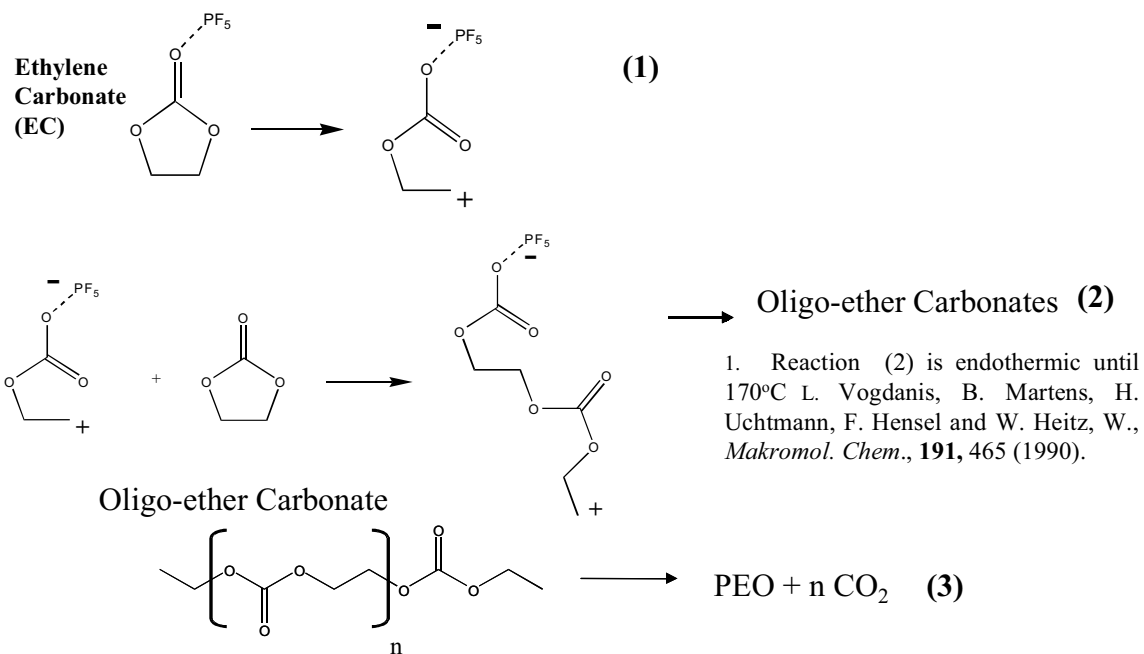
Figure 3. EDX analysis of negative electrodes. (a) thin specimen, (b) thick specimen.



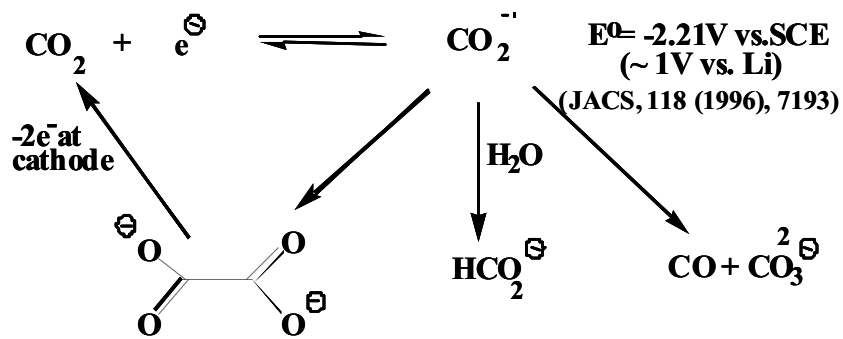
Scheme 1.



Scheme 2.



Scheme 3



Scheme 4.

## 5. Electrochemistry Improvement

*Khalil Amine, Jun Liu, Chenhua Chen, Christopher Johnson, and Jaekook Kim*

*Argonne National Laboratory, Argonne, IL 60439*

*(630) 252-3838; fax (630) 252-4176; e-mail: [amine@cmt.anl.gov](mailto:amine@cmt.anl.gov)*

*T. Richard Jow*

*Army Research Laboratory, Adelphi, MD 20783*

*(301) 394-0340; fax (303) 394-0273; e-mail: [rjow@arl.mil](mailto:rjow@arl.mil)*

*Jai Prakash*

*Illinois Institute of Technology, Chicago, IL 60616*

*(312) 567-3639; fax (312) 567-8874; email: [prakash@charlie.cns.iit.edu](mailto:prakash@charlie.cns.iit.edu)*

---

### Objectives

- Develop advanced materials that enhance the performance, calendar life, and inherent safety of high power Li-ion cell chemistries, while reducing cost.
- Develop an advanced high-power cell chemistry based on these materials that meets the PNGV hybrid electric vehicle battery goals.
- Verify the advanced high power cell chemistry in small hermetically sealed cells.
- Transfer the new cell materials and lab-scale processing technology to the Advanced Process Research project for industrial development.

### Approach

- Develop and thoroughly characterize an optimal multi-doped lithium nickel oxide positive electrode material that possesses the desired chemical, physical, and structural properties to survive for 15 years and exhibits the required performance and safety characteristics—solution-based processes are being investigated to accomplish this. Work will also be carried out to develop and characterize advanced lithium manganese oxide cathode materials.
- Screen a large number of advanced cathode, anode, electrolyte, and binder materials from industry and recommend the most promising materials to the industrial partners of PNGV.
- Develop and thoroughly characterize low-cost natural graphites and surface coating/ treatment processes that form stable pre-passivation films on the graphite particles.
- Develop and thoroughly characterize a low-cost advanced electrolyte system (preferably PC-based) that possesses enhanced stability to oxidation/reduction reactions at the electrodes, performs well at low temperature, and is less flammable than existing electrolyte systems—electrolyte additives as well as some of the new electrolyte salts will also be studied to retard the oxidation/reduction reactions and the flammability.
- Transfer the new materials and lab-scale processing to the *Advanced Process Research* project and subsequently to the industrial battery developers.
- Develop an improved cell chemistry using these optimal materials and transfer it to the industrial battery developers.

## Accomplishments

- Evaluated eight new graphite based materials and found the most promising materials for high power are the Mitsui GDR grade carbon-coated graphite, the Superior Graphite round-edge natural graphite, and the Hitachi boron-doped MAG graphite.
- Found that the particle morphology of the Mitsui GDR anode material did not change during the electrode pressing process nor exfoliate in PC electrolyte, both of which are common to most graphite materials.
- Developed a new low-cost titanium-doped lithium nickel oxide cathode material and found that it has excellent capacity, power, and calendar life.
- Refined the composition and processing of multi-doped lithium nickel-cobalt oxide cathode materials to achieve excellent power and calendar life.
- Demonstrated that the Tosoh lithium manganese oxide spinel cathode material has outstanding power and safety characteristics, as well as enhanced calendar life, when used with the new Merck LiFAP salt-based electrolytes.
- Identified and evaluated new electrolyte systems and electrolyte additives that enhance the safety and performance of lithium ion cells.

## Future Directions

- Continue the development and characterization of multi-doped lithium nickel oxide cathode materials.
- Continue the development and characterization of multi-doped lithium manganese oxide spinel and layered materials.
- Continue the development of two and three solvent electrolyte systems that use the LiPF<sub>6</sub> and LiFAP salt systems.
- Continue the development and characterization of electrolyte additives that provide passivation of the negative and positive electrodes that result in enhanced safety and calendar life.

## Publications

- The Effect of Tetravalent Titanium Substitution in LiNi<sub>1-x</sub>Ti<sub>x</sub>O<sub>2</sub> (0.025<x<0.2) System, J. Kim and K. Amine, *Electrochem. Commun.* 3, 52-55 (2001).
- Development of High-Power Lithium Ion Batteries for Hybrid Vehicle Application, K. Amine and J. Liu, *ITE Letters* 1(1), B39 (2000).

## Introduction

The Electrochemistry Improvement Project targets near-term improvements in life and abuse tolerance over the Gen 2 cell chemistry by identifying the best advanced materials under development by international chemical supply companies, as well as those being developed under this program at ANL. The objective of this project is to utilize information emanating from the Diagnostic Evaluation project to develop new advanced materials that are specifically tailored to

overcome the sources of life and abuse tolerance limitations, while keeping in mind the need for low-cost electrode materials; engineer the most-promising materials into electrodes; and develop a more optimal electrolyte system, including the new electrolyte salt [LiF<sub>3</sub>(C<sub>2</sub>F<sub>5</sub>)<sub>3</sub>, denoted LiFAP by Merck] for transfer to the *Advanced Process Research* project and to the industrial battery developers. Argonne National Laboratory (ANL) is carrying out this project in collaboration with the Army Research Laboratory (ARL), the Illinois

Institute of Technology (IIT), as well as several industrial collaborators.

In this project, ANL is focusing on the development of multi-doped lithium nickel oxide positive electrode materials. Opportunities exist to enhance the rate capability, as well as the chemical and structural stability of the positive electrode, while reducing its chemical reactivity with the electrolyte, via selective multi-doping of lithium nickel oxide at low levels. ANL is continuing to study various synthesis approaches to identify the best preparation method for producing multi-doped  $\text{LiNi}_x\text{Co}_y\text{Al}_w\text{Mg}_z\text{O}_2$  and  $\text{LiNi}_{(1-x)}\text{Ti}_x\text{O}_2$  materials that possess the desired product phase purity, morphology/particle size control, high chemical homogeneity, and, most importantly, the properly ordered structure. Solution-based processes continue to be pursued, because it is difficult to achieve high homogeneity when using high temperature solid-state reaction processes.

Additional efforts continue in the areas of pre-coated natural graphites, advanced electrolytes (including PC-based systems), and electrolyte additives that suppress oxidation and reduction reactions at the surface of electrodes, as well as gas and flame retardant additives. We continue to evaluate the newest advanced materials available from international material suppliers, as well as advanced materials that are developed under other DOE-sponsored projects, e.g. SBIR, STTR, CARAT, and GATE projects. Also, this project is the bridge to DOE's Batteries for Advanced Transportation Technologies (BATT) Program and any promising new materials developed on the BATT Program will be evaluated as candidate materials for the advanced cell chemistry system that meets the PNGV goals. Newly developed advanced materials, showing the most promise, will be transferred to the *Advanced Process Research* project for low-cost production-scale process development.

### **Positive Electrode Materials**

The objective of this work is to develop cathode materials with equivalent or better power and specific energy, longer life, enhanced safety, and lower cost. ANL's approach is to synthesize, characterize, and evaluate multi-doped lithium

nickel oxides and lithium manganese oxides that may incorporate one or more dopants to achieve: (1) a more ordered crystal structure for improved calendar life, (2) improved electronic conductivity for better power, and (3) greater oxidative stability for enhanced safety.

To prepare materials with a more ordered structure and to minimize the displacement of nickel into the lithium sites of the cathode material, one may (1) replace 15-18 percent of the nickel with cobalt, and 2-5 percent of it with aluminum and magnesium or (2) replace 5 percent of the nickel with titanium oxide. The safety characteristics of the cathode will be improved by adding a small amount of aluminum or titanium to reduce the oxygen activity of the cathode material at full charge. The magnesium is added to enhance its electronic conductivity by creating a mixed valence in the electrode structure. Consideration is also being given to the development of the lithium manganese oxide spinel materials, which have exceedingly high power characteristics.

Processes evaluated for the preparation of the cathode materials included, (1) solution combustion, (2) sol-gel, and (3) nickel-cobalt oxyhydroxide/ion-exchange. Each of these processes involves homogeneous reaction technology, unlike the high temperature solid-state reaction preparation methods, where in some cases it is difficult to get a well-defined homogeneous product. Many of the Japanese companies are currently using the high temperature solid-state reaction and spray drying techniques. Efforts at ANL indicate the sol-gel, the ion exchange, and the high temperature solid state reaction techniques can be used effectively to prepare highly ordered and doped lithium nickel oxide materials, as well as the manganese spinel materials.

Our cathode studies during the past year focused on the development and characterization of five different cathode materials. These included  $\text{LiNi}_{1-x-y}\text{Mg}_x\text{Al}_y\text{O}_2$ ,  $\text{LiNi}_{1-x-y-z}\text{Co}_x\text{Mg}_y\text{Al}_z\text{O}_2$ ,  $\text{LiNi}_{1-x}\text{Ti}_x\text{O}_2$ ,  $\text{LiNi}_{1-x-y}\text{Al}_x\text{Ti}_y\text{O}_2$  and  $\text{LiMn}_2\text{O}_4$  spinel. The cobalt, aluminum, and magnesium doped cathode materials were prepared by the sol-gel process, while the titanium doped cathode materials were prepared by solid-state reaction. Each additive in the cathode

materials plays an important role in enhancing the performance characteristics of the material. For example, magnesium enhances conductivity; aluminum enhances safety; cobalt tends to stabilize the layered structure; and titanium (like cobalt) stabilizes the structure but also enhances its conductivity and safety. Each of these cathode materials were prepared and evaluated. While they all performed very well, the most promising of these materials were the  $\text{LiNi}_{0.8}\text{Co}_{0.1}\text{Mg}_{0.05}\text{Al}_{0.05}\text{O}_2$  and  $\text{LiNi}_{0.95}\text{Ti}_{0.05}\text{O}_2$ . Another promising material is a partially-stabilized  $\text{LiMn}_2\text{O}_4$  spinel material, supplied by Tosoh.

The XRD, SEM, and performance characteristics of the  $\text{LiNi}_{0.8}\text{Co}_{0.1}\text{Mg}_{0.05}\text{Al}_{0.05}$  material are shown in Figures 1 and 2. They indicate a well structured layered material with excellent power characteristics. The cell aging characteristics of this material were found to be significantly better than that of the Gen 1 cathode. For example, accelerated aging tests at  $55^\circ\text{C}$  and a 90% SOC indicate that after 40 days the impedance of the Gen 1 cathode material was twice that of the  $\text{LiNi}_{0.8}\text{Co}_{0.1}\text{Mg}_{0.05}\text{Al}_{0.05}$  material. This material has been transferred to *Advanced Process Research* project for studying its low-cost production scale-up.

The  $\text{LiNi}_{0.95}\text{Ti}_{0.05}\text{O}_2$  cathode material was prepared by the solid-state reaction process. The concept here, of using  $\text{Ti}^{+4}$  as a dopant to stabilize the  $\text{LiNiO}_2$  layered structure, has several advantages over the cobalt, aluminum, and magnesium doped materials. The  $\text{Ti}^{+4}$  forms strong covalent bonds to the oxygen lattice and prevents the migration of  $\text{Ni}^{+2}$  ions into the lithium-ion lattice, see Figure 3, and the elimination of the cobalt additive results in a much less expensive material. The physical properties and performance characteristics of this material, presented in Figures 4 and 5, indicate a well-formed crystalline cathode material and a material with excellent power characteristics. This material has been transferred to *Advanced Process Research* project for studying its low-cost production scale-up.

Two new commercial cathode materials were also evaluated. The first was an aluminum doped  $\text{LiNi}_{1-x-y}\text{Co}_x\text{Al}_y\text{O}_2$  material, supplied by Seimi. This material is similar to our Gen 2 cathode material, but the aluminum concentration is graded within the particles, with a higher concentration near the

surface of the particles. They supplied three different materials, with average aluminum contents in the range of 1 to 5 wt %. The power characteristics of the materials with 1, 2 and 5-wt % were excellent, as were the safety characteristics. However, the aging characteristics of the materials varied with the Al content--the 5-wt % material being the best.

The second commercial cathode material evaluated was the Tosoh lithium manganese oxide spinel,  $\text{LiMn}_2\text{O}_4$ . The manganese spinel materials are a good alternative to the nickel oxide based cathode systems, exhibiting enhanced power and safety. The partially-stabilized Tosoh  $\text{Li}_{1.06}\text{Mn}_{1.94}\text{O}_2$  spinel material demonstrated very high power and fairly good life characteristics, see Figure 6. However, the capacity density of this material (at  $\sim 100$  mAh/g) is significantly lower than the Gen 1 and Gen 2 lithium nickel oxides cathode materials.

### **Negative Electrode Materials**

ANL obtained and evaluated eight new graphite electrode materials and identified the most promising materials for high power applications. The most promising materials are: GDR grade carbon-coated graphite from Mitsui, a round-edge natural graphite from Superior Graphite, and a boron-doped MAG grade graphite from Hitachi.

The GDR material has a spherical morphology with a soft carbon coating at the particle level. The material particles, when pressed to form an electrode, were essentially unchanged and tended to flow to form nearly a continuous mat, which results in excellent electronic conductivity characteristics. The GDR-AA-1 3 wt % carbon coated material exhibited excellent capacity (at  $>300$  mAh/g) and excellent efficiency as well as very good capacity retention when cycled against our Gen 2 cathode. The pulse power characteristics of this material are excellent, with little power fade even at 80% DOD. The estimated cost of this Mitsui material is \$16/kg, which is quite inexpensive when one considers its ability to function nicely in PC-based electrolytes, without exfoliation, and its spherical shape, which enhances its safety. However, it is still more expensive than desired for the PNGV application where the cost target is extremely aggressive.

The round-edge natural graphite, from Superior Graphite Company, was developed under the *Advanced Process Research* project. It possesses excellent capacity (>300 mAh/g) and safety characteristics (see Figure 7). Also, the power characteristics of the material, when used with our Gen 2 cathode, are also excellent. However, in order to function properly in electrolytes containing more than 30% PC, we found it needed to be coated or treated. The cost of this specially prepared round-edge natural graphite is projected to be <\$10/kg.

The third promising graphite anode material is from Hitachi Chemical Company. This graphite material (MAG-B) has its reactive edge surfaces treated with boron ( $B^{+3}$ ) to eliminate the unpaired electrons at its surfaces. The result is a graphite material which is much purer and less reactive toward the electrolyte, making it a safer anode. Also, the MAG-B graphite is stable in the PC-based electrolytes, where it exhibits a capacity density of about 320 mAh/g versus lithium. The cost of this material is higher than the other two graphite materials at \$20/kg.

### **Advanced Electrolytes**

This effort was directed toward: (1) developing a new ternary PC electrolyte for improved low temperature cell performance and safety, (2) developing electrolyte additives that passivate the anode and cathode materials for enhanced safety, as well as to protect against graphite exfoliation in PC electrolytes, and (3) evaluating new alternative electrolyte salts for enhanced cell safety and life. In efforts to develop a new ternary PC-based electrolyte solvent system, ANL selected the ternary EC-PC-EMC system. Next the Army Research Laboratory measured the liquidus temperature, ionic conductivity, and melting point of ternary compositions containing 1M  $LiPF_6$  salt. Next a partial phase diagram was prepared and conductivity maximums and melting point minimums were identified. Next the most promising compositions were identified; see Figure 8. From this it was

concluded that the EC:PC:EMC, 3:3:4 composition would be the best. It is the safest, least volatile and has adequate ionic conductivity at  $-32^\circ C$ . The EC:PC:EMC, 2:2:6 might also be an option, if appropriate electrolyte additives can be developed to enhance the safety of this electrolyte system.

In the area of electrolyte additives our efforts were focused on anode passivation and cell safety. Our approach for anode passivation is to form a stable film on the anode materials (graphite) during the first charge cycle at an electrode potential vs. lithium of 1.5 to 2.5 volts, long before the normal SEI is formed, which occurs at about 0.7 to 0.9 volts vs. lithium. The purpose of the film is two fold: (1) to reduce the reactivity of the anode material in the cell and (2) to eliminate graphite exfoliation in PC-based electrolytes. To identify additives for anode passivation, quantum calculations are being carried out to identify potential additives that are reduced in the voltage range of 1.5 to 2.5 volts vs. lithium. One of the most promising of the many additives evaluated in this effort is the vinyl ethylene carbonate (VEC), which is reduced at 2.20 volts vs. lithium. The passivation film formed with VEC prevents graphite exfoliation and enhances the safety of the cell.

During the past year, ANL evaluated a new salt based electrolyte 1M  $Li[PF_3(C_2F_5)_3]$  in EC:DEC (1:1), under an agreement with Merck. Relative to the  $LiPF_6$  salt, the new Merck salt (LiFAP) is stable in the presence of water. While the ionic conductivity of the LiFAP electrolytes are slightly lower than that of the  $LiPF_6$  electrolytes, the coulombic efficiency and utilization of cells using the LiFAP based electrolyte was slightly higher for cells that employ the Gen 1 anode and Gen 2 cathode. In accelerated aging tests, the cells with the 1 M LiFAP salt in the EC:DEC (1:1) solvent demonstrated better capacity retention than cells with the 1 M  $LiPF_6$  salt in the EC:DEC (1:1) solvent (see Figure 9). Similar results were obtained with cells that employed the Tosoh  $LiMn_2O_4$  spinel cathode, substituted for the Gen 2 cathode.

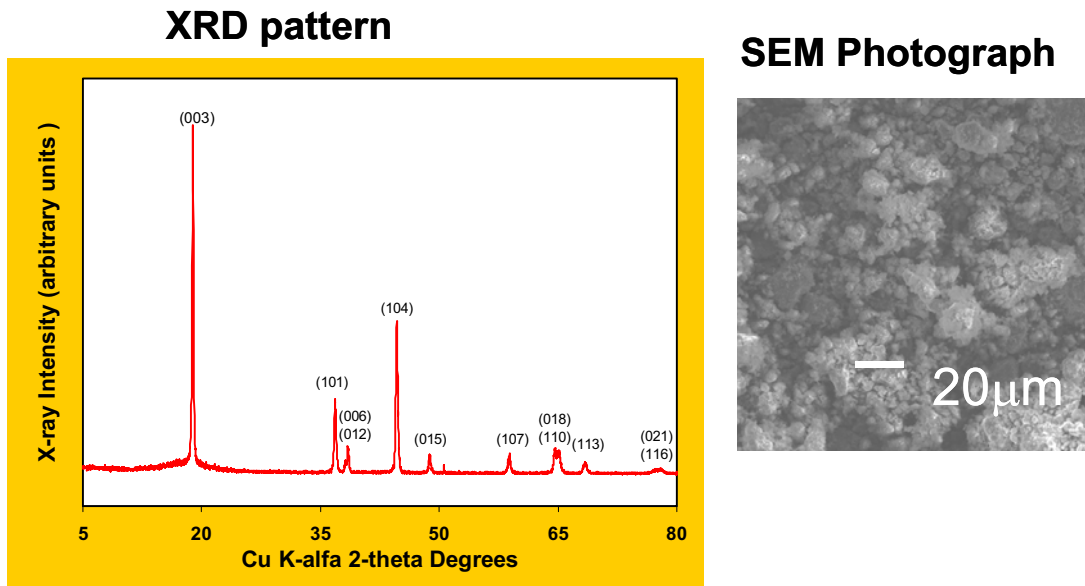


**Figure 1.** SEM and XRD of the  $\text{LiNi}_{0.8}\text{Co}_{0.1}\text{Mg}_{0.05}\text{Al}_{0.05}\text{O}_2$  cathode material prepared at ANL via lab-scale sol-gel process. It is a highly-ordered crystalline layered material with a spherical particle morphology.

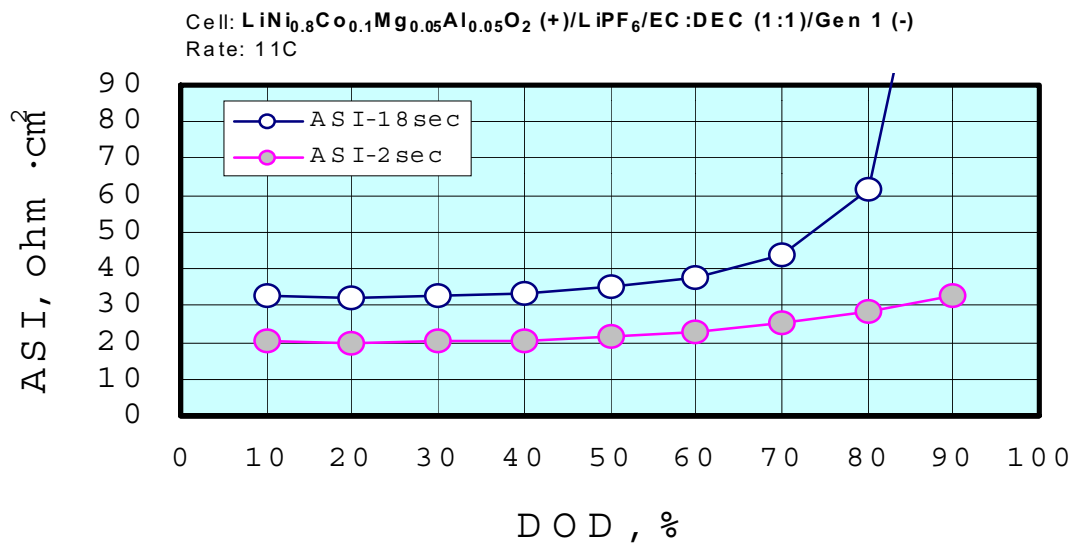


**Figure 2.** Area specific impedance (ASI) for a cell using ANL’s  $\text{LiNi}_{0.8}\text{Co}_{0.1}\text{Mg}_{0.05}\text{Al}_{0.05}\text{O}_2$  cathode material, the Gen 1 anode, and the Gen 1 electrolyte, as measured during HPPC tests. These low ASI values indicate very good power characteristics for this cell.

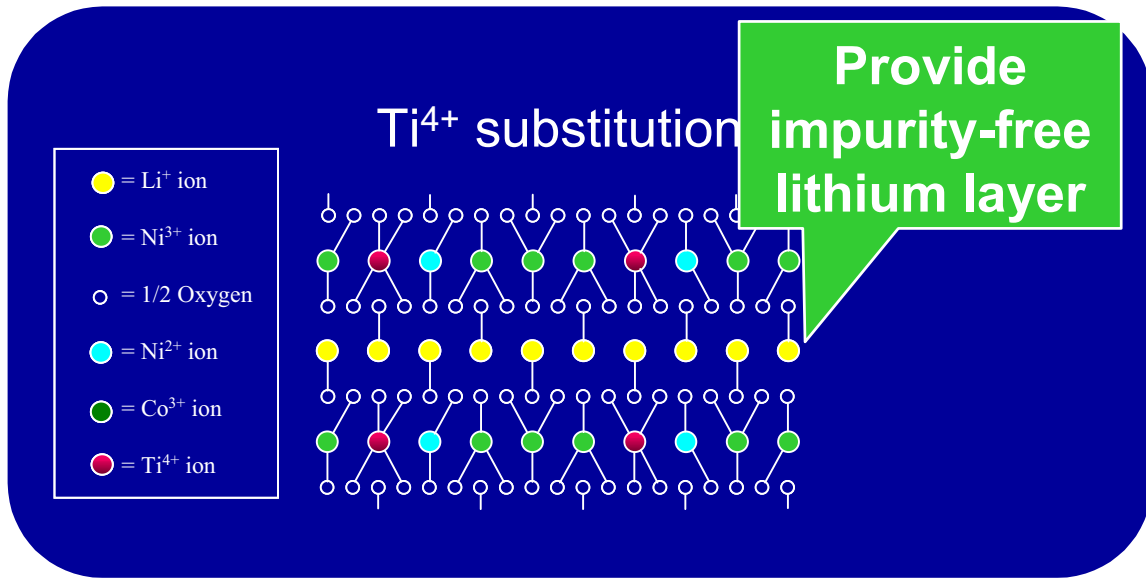


**Figure 3.** Schematic illustration of the concept of structural stability induced by tetravalent titanium doping of the  $\text{LiNiO}_2$  lattice. Tetravalent titanium ( $\text{Ti}^{4+}$ ) prevents  $\text{Ni}^{2+}$  displacement to the lithium sites in this layered structure. This stabilizes the reversible lithium capacity of the structure.

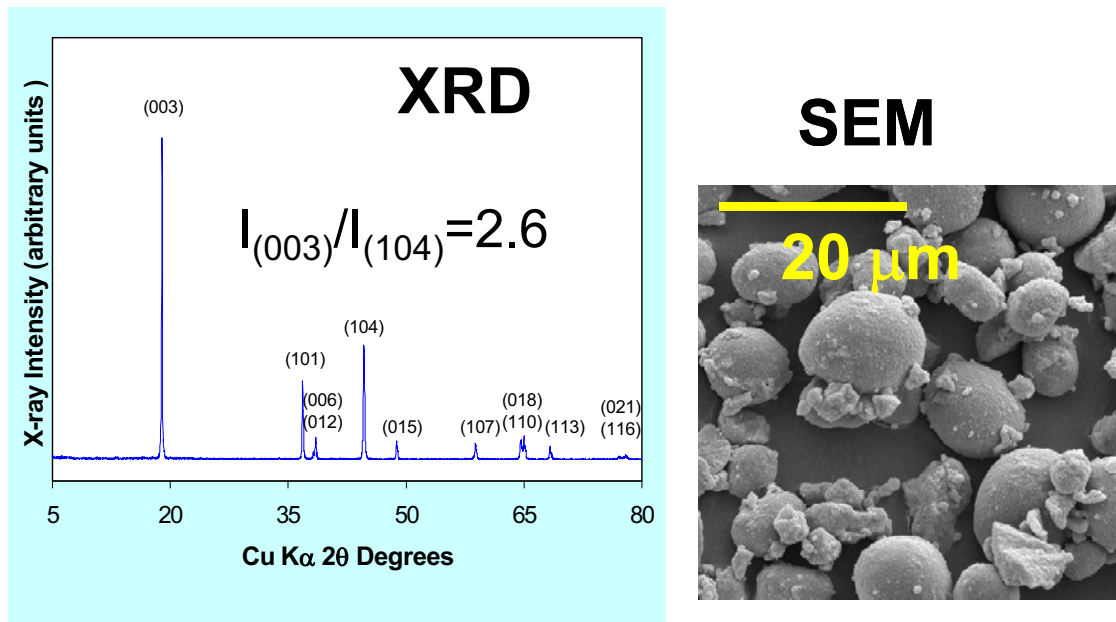


**Figure 4.** SEM and XRD of the  $\text{LiNi}_{0.95}\text{Ti}_{0.05}\text{O}_2$  cathode material prepared at ANL via lab-scale solid-state reaction process. It is a highly-ordered crystalline layered material with a spherical particle morphology.

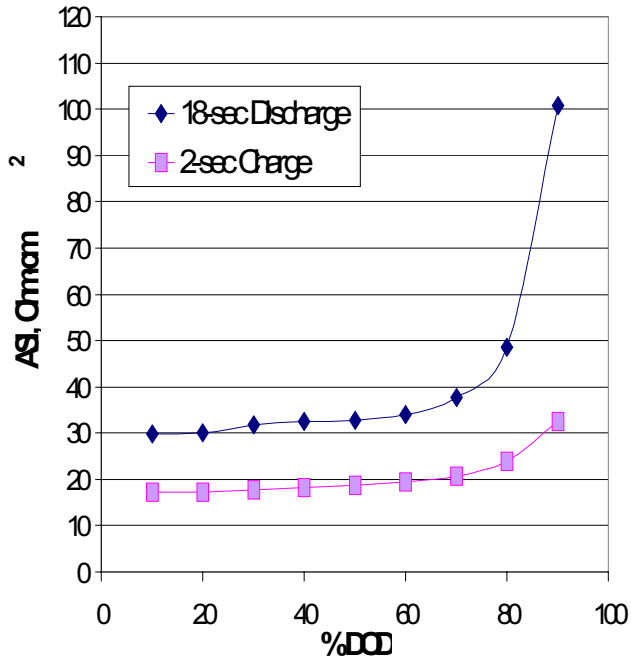


**Figure 5.** ASI values for a cell using ANL’s  $\text{LiNi}_{0.95}\text{Ti}_{0.05}\text{O}_2$  cathode material, the Gen 1 anode, and the Gen 1 electrolyte, as measured during HPPC tests with 10C current pulses. These low ASI values indicate very good power characteristics for this cell.

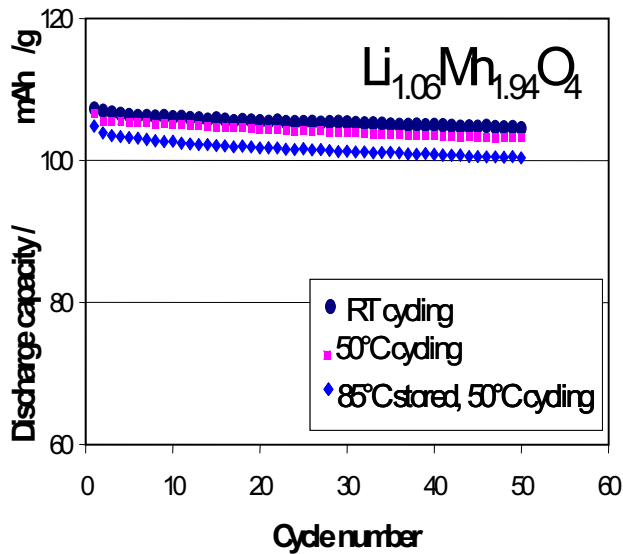
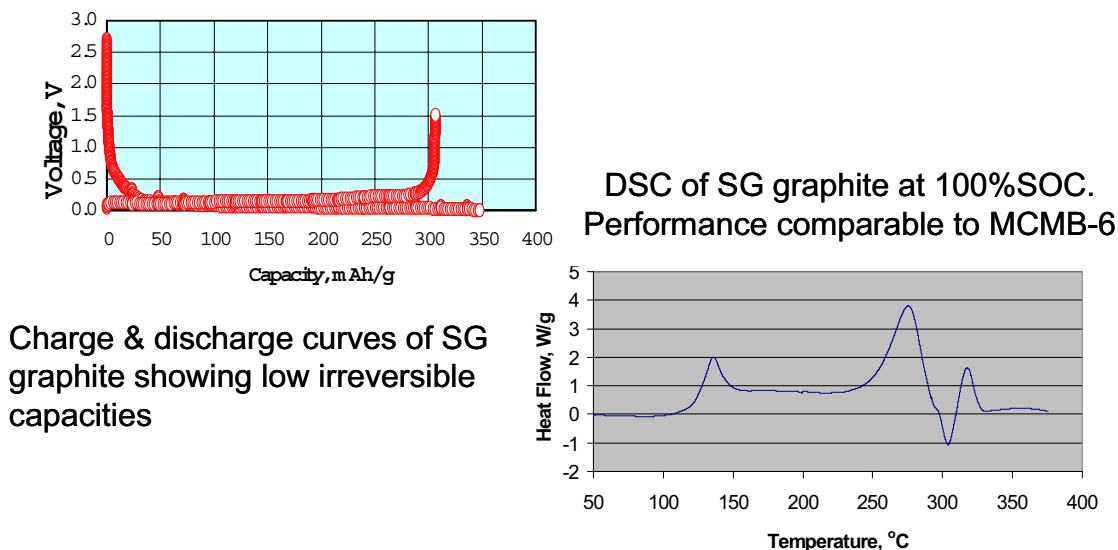


**Figure 6.** Discharge capacity density of cells using Tosoh’s partially-stabilized  $\text{Li}_{1.06}\text{Mn}_{1.94}\text{O}_4$  spinel cathode material, Gen 1 anodes, and the Gen 1 electrolyte during cycle testing. The stability looks good, even at 50°C.



Charge & discharge curves of SG graphite showing low irreversible capacities

**Figure 7.** A round-edge natural graphite, developed by Superior Graphite Company under the *Advanced Process Research* project, exhibits good reversible discharge capacity density (>300 mAh/g) and good safety characteristics in DSC tests at 100% SOC.

<b>Electrolyte</b>	<b>1 M LiPF<sub>6</sub>/EC-EMC (3:7)</b>	<b>1 M LiPF<sub>6</sub>/PC-EC-EMC (2:2:6)</b>	<b>1 M LiPF<sub>6</sub>/PC-EC-EMC (3:2:5)</b>	<b>1 M LiPF<sub>6</sub>/PC-EC-EMC (3:3:4)</b>
<b>Liquidus Temp., °C</b>	<b>-12.8</b>	<b>-40</b>	<b>-42</b>	<b>-32</b>
<b>σ (25 °C), mS/cm</b>	<b>8.77</b>	<b>9.71</b>	<b>9.01</b>	<b>9.4</b>
<b>σ (-30 °C), mS/cm</b>	<b>1.71</b>	<b>1.72</b>	<b>1.39</b>	<b>1.2</b>

**Figure 8.** Liquidus temperatures and conductivity data for three optimal EC/PC/EMC solvent mixtures containing 1 M LiPF<sub>6</sub> salt. All three have a lower liquidus temperature than our Gen 2 electrolyte, with comparable conductivities over the temperature range of -30 to 25°C.

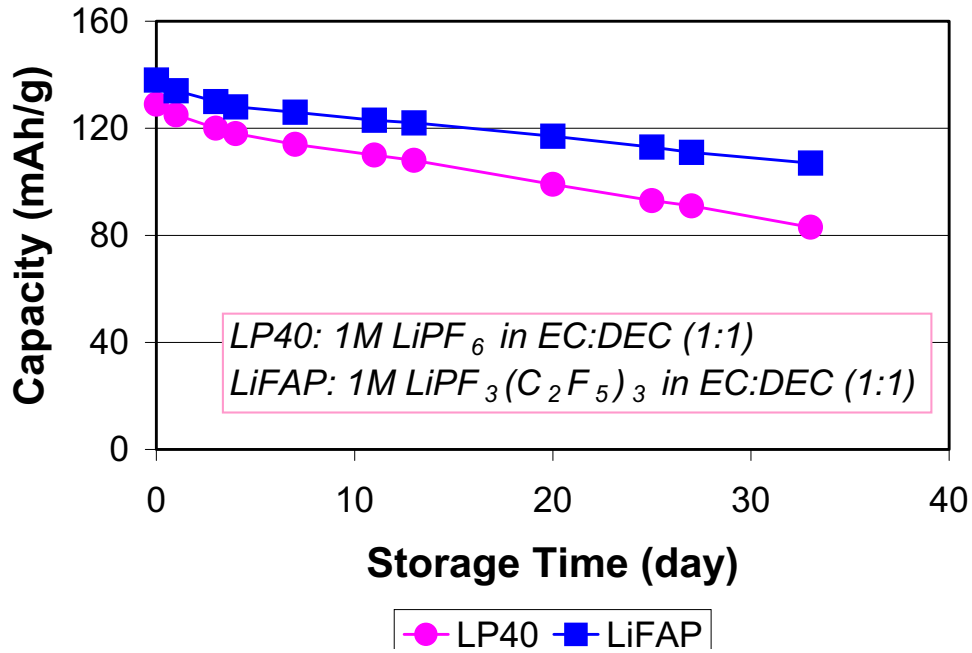


**Figure 9.** Cells that employed the Li[PF<sub>3</sub>(C<sub>2</sub>F<sub>5</sub>)<sub>3</sub>] salt in EC:DEC (1:1) electrolyte demonstrated less capacity fade than cells that employed the standard LiPF<sub>6</sub> salt in EC:DEC (1:1) electrolyte, when subjected to accelerated aging at 50°C

## 6. Low-Cost Cell Packaging

*Andrew Jansen, Khalil Amine, David Chaiko, Paul Nelson, and Don Vissers*  
Argonne National Laboratory, Argonne, IL 60439  
(630) 252-4261; fax (630) 972-4461; e-mail: [jansen@cmt.anl.gov](mailto:jansen@cmt.anl.gov)

---

### Objective

- Develop novel approaches for reducing the cost of cell packaging for high-power lithium-ion batteries.

### Approach

- Develop a flexible cell containment system based on a laminate that incorporates barriers for air, moisture, electrolyte, and HF.
- Develop a new flexible pouch design that limit permeation of electrolyte and moisture from the seal edges by means of pattern coating of absorbent near the seal areas.

### Accomplishments

- Received and evaluated five different laminate rolls that were previously contracted to an industrial vendor, Rollprint, for manufacture. These rolls became this program's 1<sup>st</sup> Generation of laminates.
- Determined from 1<sup>st</sup> Generation that the polyolefin class of polymers provides good moisture and electrolyte barrier properties.
- Determined from 1<sup>st</sup> Generation that adhesive compatibility with electrolyte is critical.
- Received four more modified laminate rolls from Rollprint. These rolls became this program's 2<sup>nd</sup> Generation of laminates. Evaluations are underway.
- Initiated investigations of organoclay composites with on-site expert who has novel approach of creating organoclay precursor.
- Received 350 lbs of spray-dried liquid crystal organoclay that was contracted to an outside vendor by ANL. This organoclay will become the basic ingredient that is compounded with select polymers.
- Used commercial vendor to compound previously identified moisture adsorbent into a selected polymer.
- Screened and performed permeation tests on candidate polymer films with the assistance of Mocon Controls, Inc.
- Conducted preliminary evaluations of permeation rates and extrapolated to 15 years for the 10 Ah flexible packaging design.

### Future Directions

- Evaluate the 2<sup>nd</sup> Generation of laminates from Rollprint for chemical resistance, mechanical properties, and barrier resistance to air, moisture, electrolyte, and HF.
  - Pursue the development of organoclay nanocomposites as an adhesive layer and as a barrier/sealant layer.
-

## **Introduction**

In order to meet the PNGV production cost target of \$300/battery (at the 100,000 units/year production rate) in a power-assist hybrid electric vehicle application, analyses indicate that the cost of a 10 Ah cell should be approximately \$5.50. Current costs are approximately \$30/cell. However, the industrial developers are projecting that they can reduce costs to approximately \$9/cell with design refinements and volume production. The objective of this project is to develop innovative methods for reducing cell packaging costs in order to meet the PNGV cost target. Argonne National Laboratory in collaboration with several industrial partners is working on low cost flexible packaging as an alternative to the packaging currently being used for lithium ion batteries. The goal is to propose innovative packaging approaches and to develop the air, moisture, electrolyte, and HF barrier layers, for use in flexible cell containers that have a lifetime of 15 years.

## **Low-Cost Flexible Packaging**

The ANL low-cost packaging approach consists of developing a low-cost flexible cell container based on plastic laminate technology. The concept is to fabricate a pouch-type container, consisting of a metal alloy foil, which forms the support base for applying polymeric coatings. The layers of the laminate work synergistically to create a cell packaging material that has chemical resistance, heat sealability, and good rupture strength. The required properties of this laminate are as follows:

- A moisture barrier, which prevents ambient moisture from penetrating into the cell and reacting with the electrolyte.
- An electrolyte barrier layer, which prevents electrolyte solvents from leaking out of the cell.
- An HF barrier layer, which prevents any HF present in the electrolyte from attacking the pouch support materials.
- A sealant layer, which provides the seal between the laminates and also seals the laminates to the current feedthroughs, via a simple and inexpensive hot pressing process.

The goal is to develop seals that will yield at the same pressure as the rupture disks in the present metal cans, which are a critical pressure relief safety component of the cells. Therefore, the pouch containment could eliminate the need for this expensive safety vent.

The loss of electrolyte solvent from the flexible cell package is one of the primary concerns for poor cell cycle life performance. This phenomenon could lead to cell starvation and performance degradation. The solvent potentially could exit the pouch by three means: (1) across the laminate, (2) through the edges where the two laminates are sealed together, and (3) at the feedthroughs where they seal to the pouch. In addition, the permeation of the solvent across the laminate could lead to the degradation of the adhesive layers that bond the barrier films together resulting in film delamination.

Another concern is the permeation of moisture into the packaging. Potential pathways for entry of the moisture are the same as those mentioned above for solvents exiting the pouch. The moisture permeation could cause degradation of the polymer sealant layer, the formation of HF due to the decomposition of the lithium hexafluorophosphate ( $\text{LiPF}_6$ ), and the reaction with the lithium from the electrodes to form hydrogen. The overall result is a degradation of cell life and performance.

This program's initial approach to laminate construction consisted of using typical aluminum foil and sealant films with the addition of a second foil layer to limit moisture permeation. This scheme employs four layers consisting of a tough polymer exterior barrier, typically oriented polyester, two 9-25  $\mu\text{m}$  thick aluminum foils, and a polyethylene sealant film. These layers are typically joined together using a solvent-based adhesive in which the solvents are driven off and the films joined together under pressure and temperature. The measurement of water transmission through a single 9  $\mu\text{m}$  thick aluminum foils, and a polyethylene sealant film. These layers are typically joined together using a solvent-based adhesive in which the solvents are driven off and the films joined together under pressure and

temperature. The measurement of water transmission through a single 9  $\mu\text{m}$  thick aluminum foil is 0.07 mg-mil/m<sup>2</sup>-24 hrs, while water transmission through a laminate of foil/adhesive/foil is 0.02 mg-mil/m<sup>2</sup>-24 hrs in a controlled humid environment. The transmission rate reduction by more than 3 times is attributed to a mismatch in pinholes between the two foils. Nevertheless, for a double foil laminate pouch measuring 10 cm by 20 cm, which is the general dimensions of a 10 Ah high-power cell, the calculated quantity of water entering the pouch is 2 grams over a fifteen-year period. Therefore, there is a need for further enhancing the barrier properties. In addition to material selection of laminate layers, adsorbents can be incorporated into the pouch design to limit the passage of moisture that enters into the cell. An appropriate adsorbent was determined in last year's effort and compounded into a selected polymer in this year's effort. Several methods of implementing this adsorbent were discussed last year.

An initial screening of polymer films was performed by measuring the weight loss of solvent filled pouches. The films to be investigated were made into pouches by heat sealing two sheets together on three sides, filling with the solvent, and sealing the final side. The pouches were stored at room temperature and their weights were measured as a function of time. Based on these screenings, efforts were centered on the following commercial films: polyethylene (high density-HDPE, medium density-MDPE, low density-LDPE, and linear low density-LLDPE), polypropylene (PP), polyethylene terephthalate (PET), ethyl vinyl alcohol (EVOH), Surlyn (an ionomer by Dupont), polyacrylonitrile (PAN), polyvinylidene fluoride (PVDF), and Nylon6 (a polyamide). These results were confirmed by an industrial vendor, Mocon, by film diffusion cell testing at various temperatures that were extrapolated to room temperature (Fig. 1).

A decision was made to have several multi-layer laminates manufactured by an industrial converter company, Rollprint Packaging Products Inc. Screening results indicated that PET was an excellent solvent barrier, however, due to its high crystallinity, it has poor sealant characteristics.

Thus, an additional layer of sealant film was necessary for the two rolls that contained PET; Surlyn and Forte PI was used in these cases. Two other rolls contained PP as the sealant/barrier layer. One of these was laminated onto a double Al foil (9  $\mu\text{m}$  each) substrate and the other onto a single thicker (25  $\mu\text{m}$ ) foil substrate. In this manner, a direct comparison of double versus single foil could be made. Only one of the five laminate rolls contained a double layer of 9  $\mu\text{m}$  Al foil; the rest were a single layer of 25  $\mu\text{m}$ . Oriented-PET was used as the outer protective film on the Al foil for one of the rolls; the rest used nylon.

A test matrix was established to evaluate the performance of each of the four laminates that consisted of filling 3" x 3" pouches with one of three liquids: water, EC/PC/EMC solvent, or 1M LiPF<sub>6</sub> in EC/PC/DEC/EMC electrolyte. The heat sealing of each pouch was performed at Rollprint. Weight loss analyses were performed for the water and solvent pouches at three temperatures: 37C, 50C, and 70C. These results are presented in Fig. 2. The polypropylene with two layers of aluminum foil was the best solvent barrier in this first generation of laminates. All had similar water barrier behavior.

A different approach was taken for analysis of the pouches filled with electrolyte. Several identical pouches were made of each laminate, placed in a 100% humidity environment at the same three temperatures, and periodically one pouch would be cut to extract the electrolyte within. This electrolyte was then titrated via Karl Fisher coulometric titration for water levels and buret titration for HF levels, the results are presented in Fig. 3. As expected, the HF levels were the lowest in the PP pouches. Many of the pouches ruptured within a few weeks due to the severity of the test conditions.

An anomaly was observed in the titration data in that the HF levels rose to significant levels while the water levels remained approximately constant (Fig. 3). This was investigated further by intentionally doping one electrolyte sample with a known amount of water and another electrolyte

sample with an amount of water ten times greater. Both samples underwent the Karl Fisher and HF titration procedures over time (Fig. 4). It became evident that the HF concentrations rose in direct proportion to the amount of water added as expected. However, the concentration of residual water decreased to approximately 500 ppm in both samples. It is uncertain if this background level is due to an equilibrium established with the electrolyte/HF or if it is an artifact of the Karl Fisher titration technique.

After analyzing the failure mechanism of the first generation of pouches, it was observed that nearly all of them suffered from delamination of the barrier film(s) from the Al foil. Such delamination would increase the permeation area by a factor of 1000 for a 10 Ah cell. Efforts were then directed to identifying better adhesives. Rollprint was able to send ANL five commercial adhesive samples applied to Al pans. Test strips were cut out from these adhesive samples and soaked in electrolyte at elevated temperatures to test their electrolyte-compatibility. The best of the five was selected for use in the second-generation laminates, while the search continues for a more optimal adhesive.

Rollprint manufactured the second generation of laminates, which incorporated information gained from the first generation. Namely, the double Al foil approach was adopted with a doubling of the Al thickness, the polyolefin class (PE, PP) of polymers was selected as a barrier/sealant film, and a different adhesive was selected. As with the first study, the second generation of laminates (four variant rolls) from Rollprint were made into 3" square pouches and filled with either water, solvent blend, or electrolyte blend. Weight loss studies at three temperatures (room temperature, 37° C, and 55° C) are on going.

The 50% increase in the PNGV calendar life goal to 15 years poses a significant challenge to the conventional flexible packaging approach. A new strategy must be enlisted. To this end, ANL has begun investigation into a novel

barrier material that is being developed within ANL under an unrelated program. This material is based on a unique method of combining natural clays with organic polymers to form organoclays (Fig. 5). The organoclays can then be compounded with traditional polymers to form barrier films. A preliminary lab-scale casting of an organoclay film showed tremendous reductions in oxygen permeation rates. Efforts are underway to determine if these materials can offer significant reductions in solvent/electrolyte permeation rates. Initial tests demonstrated that the organoclays appear to be compatible with our electrolytes.

*An outside vendor made 350 lbs of spray-dried liquid crystal hydrophilic organoclay under ANL's guidance which was then supplied to ANL in 12 large drums. This organoclay will become the basic ingredient that is compounded with polymers such as polyethylene and ethyl vinyl alcohol. Ideal weight ratios will be sought. Three of these drums were shipped to another vendor to be blended with selected polymers. ANL also received bench scale samples of a new organoclay composite from a vendor for investigation. These composites incorporate functional groups on the polymer chain to improve the adhesion between the aluminum foil and the clay composite. A number of organoclay samples were prepared for ANL using a total of six different surface chemistries based on montmorillonite and talc for use in bench-scale preparations of nanocomposites. Bench-scale composites were prepared in polyethylene, polypropylene, EVOH, and EAA using a Brabender mixer by an industrial vendor.*

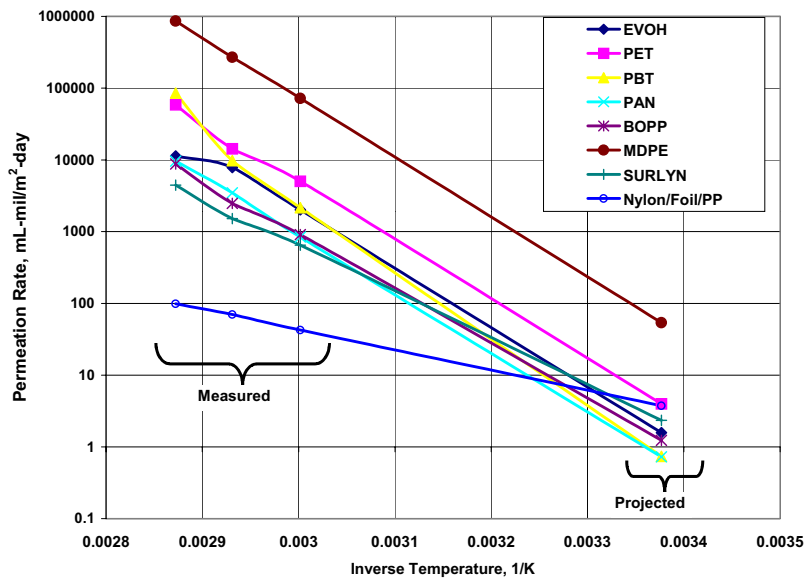


**Figure 1.** 1M LiPF<sub>6</sub> in EC/DEC/PC/EMC electrolyte vapor-permeation data from Mocon for selected single films and one 1<sup>st</sup> Generation laminate extrapolated to room temperature. Volume is vapor corrected to STP.

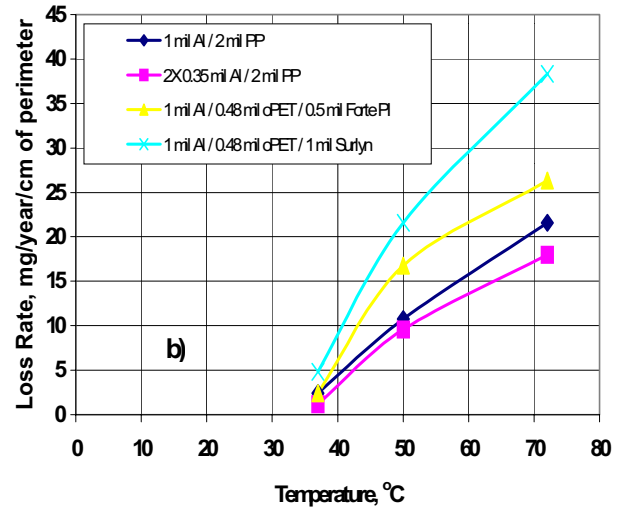
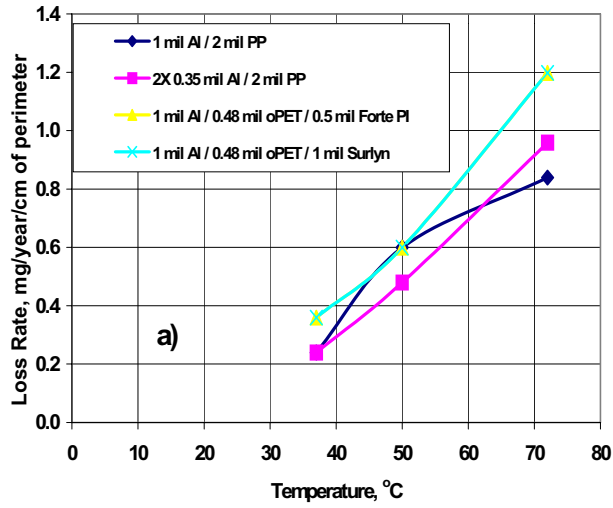


**Figure 2.** Summarized loss rates for 1<sup>st</sup> generation of laminates obtained from pouch weight loss tests for: a) water inside; and b) EC/PC/EMC inside.

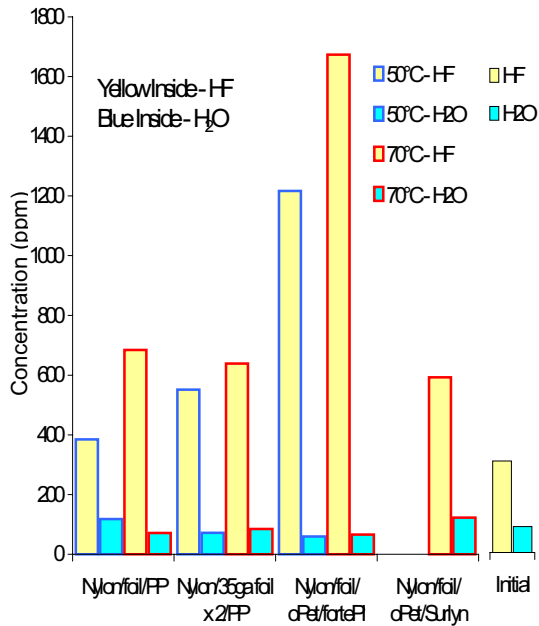


**Figure 3.** Water and HF concentration levels inside pouches filled with 1M LiPF<sub>6</sub> in EC/PC/DEC/EMC electrolyte after 2 weeks time for 1<sup>st</sup> generation of laminates

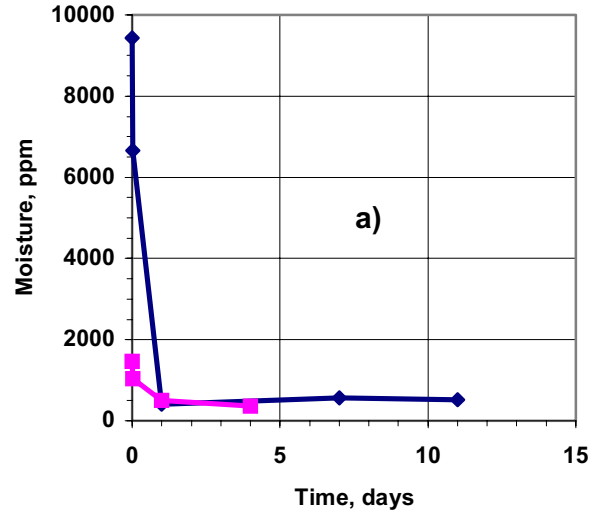
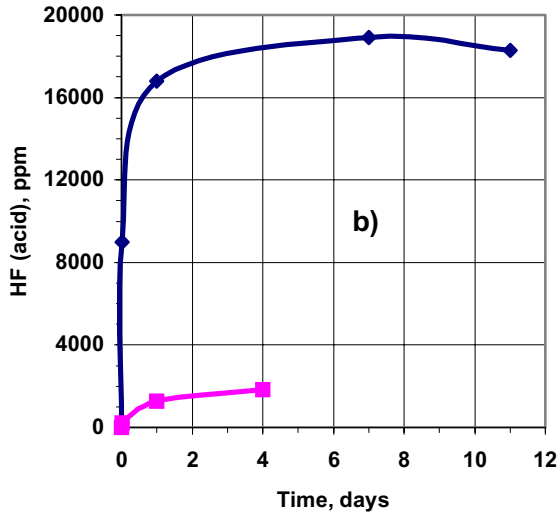


**Figure 4.** Moisture levels a), and HF levels b), resulting from intentional doping of electrolyte with 1,000 and 10,000 ppm of water. Note residual 500 ppm water.

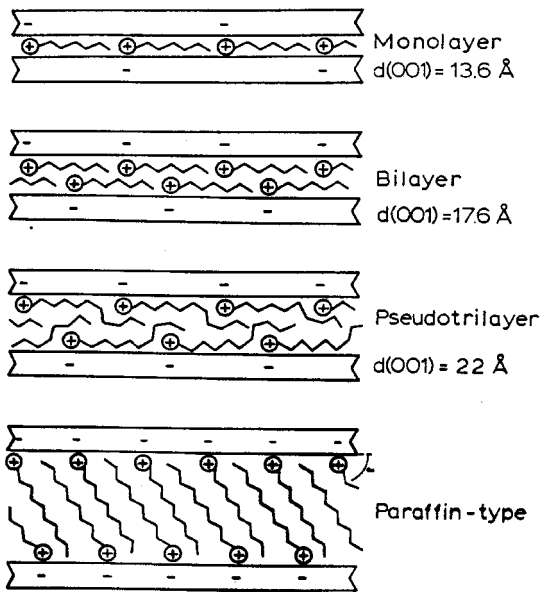


**Figure 5.** Pictorial of increasing amounts of organic between clay layers to form liquid crystal organoclays. These are then blended with polymers to form organoclay nanocomposites



## 7. Advanced Process Research

*Khalil Amine, Jaekook Kim, Chun-hua Chen, Jun Liu, and Gary Henriksen*

*Argonne National Laboratory, Argonne, IL 60439*

*(630) 252-3838; fax (630) 252-4176; e-mail: [amine@cmt.anl.gov](mailto:amine@cmt.anl.gov)*

Major Industrial Collaborators: *FMC Corporation, OMG Americas, Fuji Chemical Industry Co., LTD., Quallion, LLC, and Superior Graphite Co.*

---

### Objectives

- Establish collaborations with industrial firms that facilitate the development of low-cost processes for manufacturing optimal advanced materials.
- Provide guidance to industrial collaborators on the optimal chemical and physical characteristics for the electrode and electrolyte materials.
- Work with industrial collaborators to develop low-cost production-scalable processes for making optimal materials.

### Approach

- In the area of optimal positive electrode materials, ANL develops lab-scale processes for making multi-doped lithium nickel oxide materials that possess the chemical, physical, and structural properties needed to achieve acceptable performance with enhanced life and safety, as part of the Electrochemistry Improvement project. In this project, ANL establishes collaborations with industrial firms to study production-scale processes for making these materials and to develop cost estimates.
- In the area of optimal negative electrode materials, ANL collaborates with industrial firms to develop and characterize a round-edge low-cost natural graphite. This new material is being used as the starting material to study coating/treatment processes that form stable pre-passivation films on the graphite particles.
- In the area of advanced electrolytes, ANL works with the Army Research Laboratory to develop advanced PC-based electrolyte systems, as part of the Electrochemistry Improvement project. In this project, ANL establishes collaborations with industrial firms to produce pilot-scale quantities of this electrolyte and study the cost associated with producing it on an industrial scale. These electrolyte systems could incorporate additives that are being developed as part of the Electrochemistry Improvement project.

### Accomplishments

- ANL established collaborations with FMC, OMG, and Fuji to study industrial-scale processes that can be used to manufacture multi-doped lithium nickel oxide positive electrode materials. FMC produced pilot-scale samples and performed manufacturing cost studies on a solid-state process, while OMG and Fuji produced pilot-scale quantities of material using two different solution-based processes.
- ANL established a collaboration with Superior Graphite to develop and characterize a rounded-edge low-cost natural graphite. This material has a reversible capacity density >300 mAh/g, possesses safety characteristics similar to the expensive MCMB synthetic graphite, can be used in 30% PC-based electrolytes (w/o exfoliating), and is projected to cost <\$10/kg. This material is being used as the starting material to study coating/treatment processes that form stable pre-passivation films on the graphite particles.
- ANL established a collaboration with Quallion, LLC, to produce pilot-scale quantities of an advanced PC-based 3-solvent electrolyte system (1.2M LiPF<sub>6</sub>/EC:PC:EMC [3:3:4]). Under agreements with ANL, Merck and Ube have both agreed to make larger quantities of this electrolyte, with and without ANL-specified additives.
- ANL used its spreadsheet battery design model to conduct material cost comparisons for the Gen 1, Gen 2, and advanced cell chemistries.

## Future Directions

- Continue working with FMC, OMG, and Fuji to develop the lowest cost process for the industrial-scale production of an optimal multi-doped lithium nickel oxide positive electrode material.
- Continue collaborations with Quallion, Merck, and Ube to scale-up a low-cost optimal electrolyte system for high-power long-life lithium-ion batteries.

## Introduction

The Electrochemistry Improvement project targets the development and/or identification of advanced materials and cell chemistries that offer equivalent or better performance, longer life, and enhanced safety at a cost that is lower than the ATD Gen 1 and Gen 2 cell chemistries. Information obtained from diagnostic studies on aged Gen 1 and Gen 2 cells is helping to guide the development of these advanced materials. Many of these advanced materials, which are tailored to provide these improvements in life and safety, are not yet commercially available. Therefore, this Advanced Process Research project was created to study the industrial-scale manufacturing of these materials, with a focus on the development of low-cost processing. In order to conduct this project in a meaningful way, it was necessary to establish numerous collaborations with industrial organizations; primarily with firms having operations in the USA. Table 1 lists ANL's industrial collaborators during this reporting period.

**Table 1.** ANL's Industrial Collaborators

Company	Positive Electrode	Negative Electrode	Electrolyte
Fluid Air		X	
FMC	X		
Fuji	X		
INCO		X	
Merck			X
OMG	X		
Quallion	X		X
Superior Graphite		X	
Ube			X

## Process Scale-Up of Positive Electrode Materials

The objective of this work is to develop low-cost processes for the production-scale processing of positive electrode materials, based on multi-doped lithium nickel oxide positive electrode materials that ANL synthesized (at the laboratory scale), characterized, and evaluated in lab cells. These materials incorporate up to 4 dopants to achieve: (1) a more ordered crystal structure for improved calendar life, (2) a material with improved electronic conductivity for better power, and (3) a material with greater oxidative stability for enhanced safety. The power performance and stability of this material is related to the particle homogeneity and the structural order which are dependent on the preparation process. Therefore, the production-scale process needs to be low-cost and produce material with the proper chemical, physical, and structural properties.

During the last year, efforts focused on the following types of multi-doped lithium nickel oxide materials: a)  $\text{LiNi}_{1-x-y}\text{Mg}_x\text{Al}_y\text{O}_2$ , b)  $\text{LiNi}_{1-x-y-z}\text{Co}_x\text{Mg}_y\text{Al}_z\text{O}_2$ , c)  $\text{LiNi}_{1-x}\text{Ti}_x\text{O}_2$ , and d)  $\text{LiNi}_{1-x-y}\text{Al}_x\text{Ti}_y\text{O}_2$ . In the first two materials, Co and Al strengthen the covalency of the layers, thereby preventing structural transitions during cycling; Mg enhances the electronic conductivity; and Al enhances the safety and stability of the material. Solution-based processes are being considered for making these materials, as mixing on the molecular level enhances the chemical homogeneity of the product. For the other two materials, Ti could play three roles: 1) Strengthen the covalency of the layers to prevent structural transitions during cycling, 2) enhance electronic conductivity by introducing mixed valence, and 3) enhance safety and stability of the material. Solid-state reaction processing is needed when Ti is the dopant.

Several types of solution-based processes were evaluated for making the Co, Mg, & Al doped materials:

- Sol-gel and co-precipitation processes (studied by FMC)
- Oxyhydroxide/ion-exchange process (studied by OMG)
- Spray drying process (studied by Fuji)
- Solid-liquid reaction process (studied by Quallion)

Although the sol-gel process produces highly ordered structures, even without Co present, (as illustrated in Fig. 1), FMC determined that the industrial scale processing costs would be too great for this process. Prior to reaching this conclusion, numerous process changes were recommended by FMC and evaluated by ANL (on the lab-scale). These recommended changes are listed below:

- Replace acetic acid by less expensive acid or water
- Consider using air instead of oxygen
- Optimize thermal conditions to minimize time at elevated temperature, i.e. use higher temperature for shorter duration
- Eliminate process steps, where possible

ANL was able to successfully implement most of these changes at the lab-scale, but the resulting cost reductions (via FMC's analyses) were insufficient to render this a viable low-cost process for making industrial-scale quantities of these materials.

Toward the end of the reporting period, OMG provided ANL with oxyhydroxide precursor materials that they prepared at the pilot-scale, using their solution-based process. Using these precursor materials, ANL was able to prepare high-quality final product by ion exchange. These materials are currently being characterized and evaluated by ANL.

ANL established a non-disclosure agreement (NDA) with Fuji to produce these materials by their spray drying process. Samples of material from Fuji have been received and ANL is

currently characterizing and evaluating these materials.

Quallion, in conjunction with its partner, prepared samples via their solid-liquid reaction process, using pilot scale processing equipment. ANL characterized and evaluated these materials and they did not perform as well as ANL's lab-scale materials. Quallion is making a second batch of material samples for ANL's evaluation.

Solid-state processing was used for making the Ti doped materials. FMC Corporation has industrial-scale solid-state processing facilities for making lithium cobalt oxide material. Under a contract with ANL, they prepared pilot-scale samples of ANL's Ti-doped lithium nickel oxide materials and supplied those materials to ANL for characterization and evaluation. Figure 2 shows an X-ray pattern of the  $\text{LiNi}_{0.95}\text{Ti}_{0.05}\text{O}_2$  material produced by FMC. The X-ray pattern shows that it is a highly-ordered, layered, crystalline material. Figure 3 compares SEM photomicrographs of the FMC and ANL produced materials. The spherical shape of the ANL material is preferred for safety reasons and FMC is altering their process conditions to achieve the spherical shape and proper particle size.

FMC conducted a cost study on the 500,000 kg/year industrial-scale processing of the  $\text{LiNi}_{0.95}\text{Ti}_{0.05}\text{O}_2$  material, using their process. The procedure they used is listed below:

- Establish process steps and equipment
- Size the equipment
- Obtain raw material costs
- Obtain equipment purchase costs from vendor quotes
- Estimate utility costs
- Estimate labor cost and "other costs"
- Estimate invested capital for installed equipment + working capital
- Estimate overhead costs and depreciation & capital recovery
- Estimated product cost is sum of raw material, labor, utilities, overheads, depreciation, and capital recovery

FMC estimates a selling price of \$26/kg (with a range of \$22-30/kg) for material produced in this quantity with their industrial-scale process.

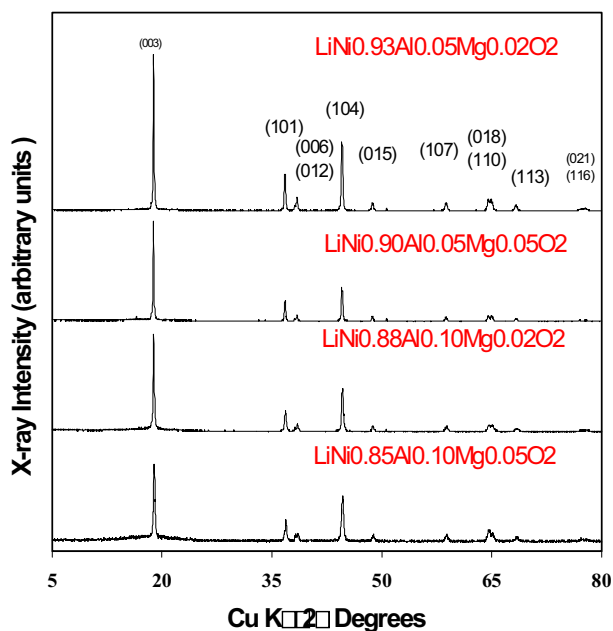
### Process Scale-Up of Negative Electrode Materials

The objective of this work is to develop low-cost processes for the production-scale processing of optimal negative electrode materials for this high-power application. Our approach was to work with one or more industrial firms to develop a low-cost natural graphite particulate material with the desired properties. Using this as a starting material, we evaluated different processes for coating the natural graphite particles with a thin layer of metal. The concept is to protect the natural graphite from exfoliation in a PC-based electrolyte and to produce a more stable SEI layer on the surface of the negative electrode. The low-cost natural graphite starting material was also evaluated in its original state in PC-based electrolytes, with and without additives, which could protect the graphite from exfoliation in PC-based electrolytes.

ANL contracted with Superior Graphite Company to develop a round-edge natural graphite with the desired particle size distribution. During this reporting period Superior Graphite developed low-cost processes for manufacturing a round-edge material. Figure 4 shows the particle size distribution and an SEM photomicroph of this material. Superior Graphite still needs to refine their processing to achieve a more desirable particle distribution. However, this material possesses a reversible discharge capacity density of >300 mAh/gm, good high-power characteristics, and safety characteristics that are comparable to the more expensive MCMB synthetic graphite. Additionally, this material does not exfoliate when used in a 30% PC-based electrolyte. Superior Graphite projects that this material will have selling price of <\$10/kg, when produced in large volume.

Several processes were evaluated for coating graphite particles with a thin layer of metal, via collaborations with Fluid Air, Illinois Institute of Technology (IIT), and INCO. For most of this work, we used MAG-10 graphite (our Gen 2 cell

negative electrode material) as the starting material for coating. Fluid Air used their fluidized bed reactor, IIT used electroless plating, and INCO used their nickel carbonyl process. We studied nickel and copper for use as the metal coatings. Without a protective coating, the MAG-10 graphite exfoliates in PC-based electrolytes containing only minimal PC. Copper coated MAG-10 appeared to be quite good. Figure 5 shows that the copper coating on the MAG-10 graphite protects it from exfoliation in a 30% PC-based electrolyte. When the Superior Graphite round-edge natural graphite became available, we initiated coating trials with this new natural graphite material. It was successfully coated with nickel, using the nickel carbonyl process. The nickel coating appears to enhance its high-power performance.

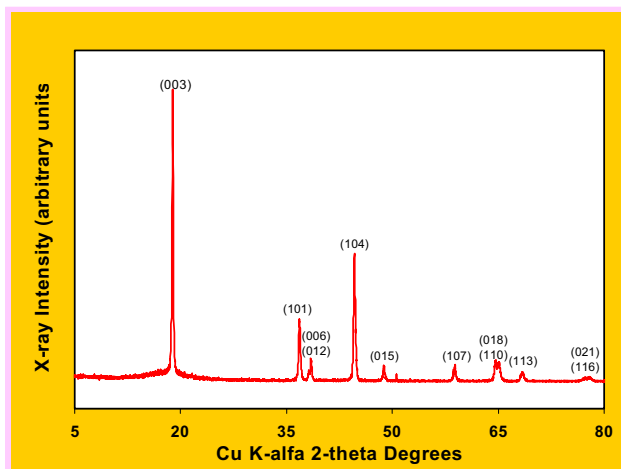


### Scale-Up of Advanced Electrolytes

Under the Electrochemistry Improvement project, ANL is working with the Army Research Laboratory to develop multi-solvent advanced electrolyte systems. A new PC-based 3-solvent electrolyte system was successfully developed. Also, ANL is developing electrolyte additives under that project. The objective of this portion of the project is to establish working relationships with industrial firms that can produce pilot-scale

and production-scale quantities of these advanced electrolyte systems.

During this reporting period, ANL established collaborations with Quallion, Merck, and Ube. Quallion has facilities for producing pilot-scale quantities of electrolytes in a tightly controlled environment. They produced sufficient quantities of our new 1.2M LiPF<sub>6</sub>/ EC:PC:EMC (3:3:4) electrolyte system, with and without additives, for evaluations in sealed cells. This new electrolyte system possesses a low melting point, high ionic conductivity, a low flame propagation rate, reduced cost, and enhanced aging stability. Additional details are provided in the Electrochemistry Improvement section of this report. Merck and Ube have both agreed to produce larger quantities of this and other advanced electrolytes that are developed as part of our ATD program.



### Cu K-alfa 2-theta Degrees

**Figure 1.** XRD patterns for doped lithium nickel oxide cathode materials, produced by ANL's lab-scale sol-gel process, show highly-ordered crystalline layered structures.

**FMC's**

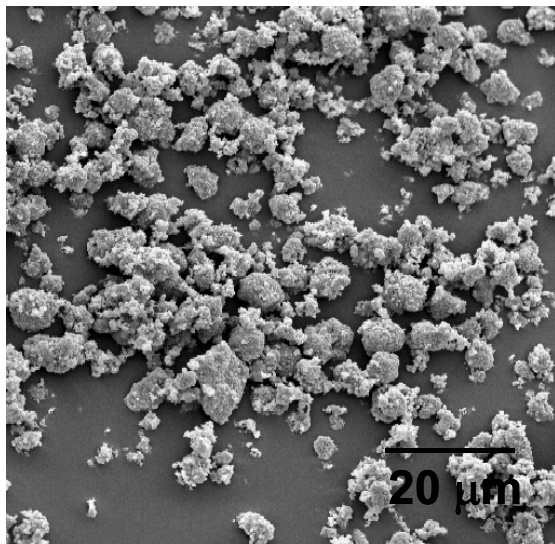


**Figure 2.** XRD pattern of  $\text{LiNi}_{0.95}\text{Ti}_{0.05}\text{O}_2$  material, produced by FMC's pilot-scale solid-state reaction process, shows a highly-ordered crystalline layered structure.

**ANL's**

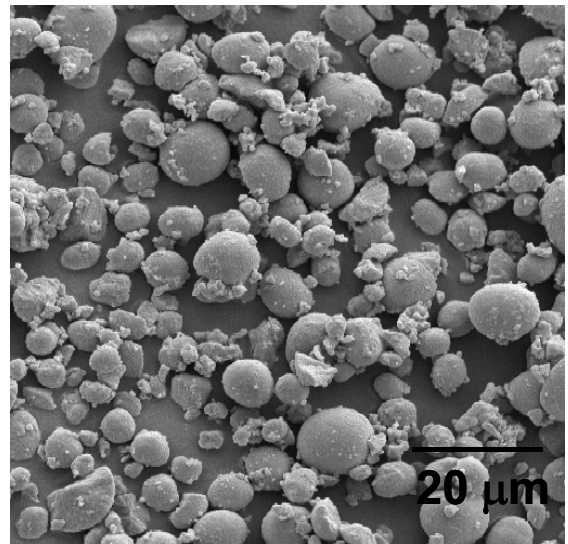


**Figure 3.** SEM photomicrographs of  $\text{LiNi}_{0.95}\text{Ti}_{0.05}\text{O}_2$  powders produced by FMC and ANL. The material produced by ANL's lab-scale process possesses the desired spherical shaping and narrow particle size distribution.

**Particle Size Distribution**

<b>90% (<math>D_{90}</math>) passing</b>	<b>38 µm</b>
<b>50% (<math>D_{50}</math>) passing</b>	<b>22 µm</b>
<b>10% (<math>D_{10}</math>) passing</b>	<b>13 µm</b>
<b>100 % particles pass 325 US mesh sieve (45 micron opening)</b>	

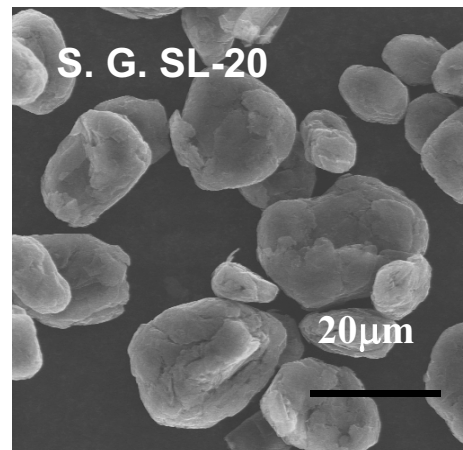


**Figure 4.** Particle size distribution and SEM photomicrograph of the round-edge natural graphite developed and produced by Superior Graphite Company.

First 20 Cycles at 50°C in electrolyte containing 30% PC

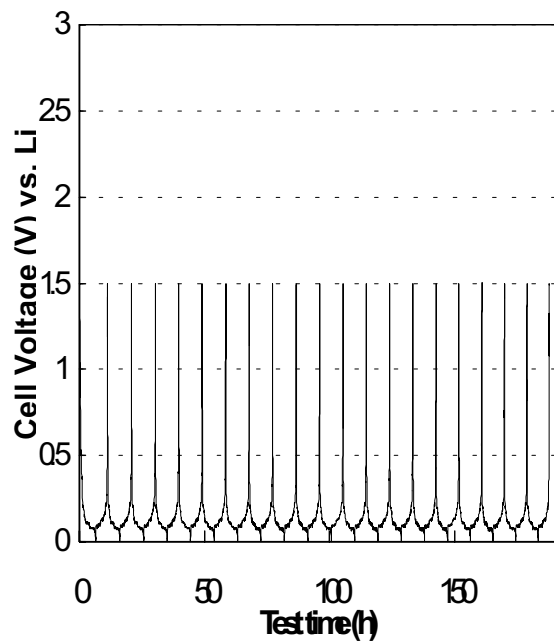


**Figure 5.** Cycling behavior of copper coated MAG-10 shows that the copper coating adequately protects the graphite and allows it to be used in PC-based electrolytes without exfoliating.

This document highlights work sponsored by agencies of the U.S. Government. Neither the U.S. Government nor any agency thereof, nor any of their employees, makes any warranty, express or implied, or assumes any legal liability or responsibility for the accuracy, completeness, or usefulness of any information, apparatus, product, or process disclosed, or represents that its use would not infringe privately owned rights. Reference herein to any specific commercial product, process, or service by trade name, trademark, manufacturer, or otherwise does not necessarily constitute or imply its endorsement, recommendation, or favoring by the U.S. Government or any agency thereof. The views and opinions of authors expressed herein do not necessarily state or reflect those of the U.S. Government or any agency thereof.



Printed on recycled paper

## Office of Transportation Technologies Series of 2001 Annual Progress Reports

- Office of Advanced Automotive Technologies FY 2001 Program Highlights
- Vehicle Propulsion and Ancillary Subsystems
- Automotive Lightweighting Materials
- Automotive Propulsion Materials
- Fuels for Advanced CIDI Engines and Fuel Cells
- Spark Ignition, Direct Injection Engine R&D
- Combustion and Emission Control for Advanced CIDI Engines
- Fuel Cells for Transportation
- Advanced Technology Development (High-Power Battery)
- Batteries for Advanced Transportation Technologies (High-Energy Battery)
- Vehicle Power Electronics and Electric Machines
- Vehicle High-Power Energy Storage
- Electric Vehicle Batteries R&D



[www.carttech.doe.gov](http://www.carttech.doe.gov)

DOE/EERE/OTT/OAAT - 2001/009